BeFo

STIFTELSEN BERGTEKNISK FORSKNING
ROCK ENGINEERING RESEARCH FOUNDATION

MULTICOMPONENT DIGITAL-BASED SEISMIC LANDSTREAMER AND BOATTOWED RMT SYSTEMS FOR URBAN UNDERGROUND INFRASTRUCTURE PLANNING

Alireza Malehmir

Cover photo: (left) Seismic landstreamer when tested at the Vinsta access ramp (Förbifart Stockholm) during its early stage of development (the first test in 2013) and (right) the boat-towed RTM when tested over the Äspö HRL facility (2015).

STIFTELSEN BERGTEKNISK FORSKNING
ROCK ENGINEERING RESEARCH FOUNDATION

MULTICOMPONENT DIGITAL-BASED SEISMIC LANDSTREAMER AND BOAT-TOWED RMT SYSTEMS FOR URBAN UNDERGROUND INFRASTRUCTURE PLANNING

Digital seismisk multikomponentlandstreamer och båtbogserat RMT-system för bergundersökning vid planering av infrastruktur i stadsmiljö

Alireza Malehmir, Uppsala University

BeFo Report170
Stockholm 2024
ISSN 1104 – 1773
ISRN BEFO-R-170-SE

PREFACE

Urban environment poses by far a different challenge to most geophysical surveys than those of other places. Given the logistic challenges, space limitation, mixed land and water bodies, various type of noise, source and receiver coupling, and urban underground complexities, new and refined ways to better tackle these issues are necessary. In the frame of an industry-academia consortium (TRUST: TRansparent Underground STructures), a digital, MEMS-based, 3C seismic landstreamer and a boat-towed radio-magnetotelluric (RMT) system that can partly overcome some of these challenges in the urban environment has been developed; tested at several sites and studied for their applications for urban underground infrastructure planning projects. It is demonstrated that the seismic streamer is free of electromagnetic-electric noise; it allows high-resolution broadband data recording, and it is by far superior to its geophone-type predecessors when it comes to its full spectrum of applications. The boat-towed RMT system combined with additional low-frequency controlled sources makes the method quite cost-effective and is reliable for bedrock mapping and fracture delineation.

The project reference group has consisted of Robert Sturk (Skanska), André Pugin (Geological Survey of Canada), Andreas Aspmo Pfaffhuber (NGI), Christer Andersson (Ramboll), Nils Rydén (PEAB), Cecilia Montelius (NCC), Per Tengborg (BeFo).

The project was co-financed with major grants from Formas, SBUF, Skanska, SGU, FQM and NGI. Several case studies have been carried out with the help of funding from external parties.

Stockholm,

Patrik Vidstrand

FÖRORD

Urbana stadsmiljöer utgör i många aspekter större utmaningar för geofysiska mätningar än andra miljöer. Det är därför nödvändigt att utveckla nya och förbättrade metoder för att kunna hantera logistiska utmaningar, bristen på utrymme, kombinationen av både land- och vattenytor, olika typer av brus, sensorernas och källans koppling till marken, samt komplexa förhållanden i underjorden. Inom ramarna för ett samarbete mellan industrin och akademin (TRUST: Transparent Underground STructures) har en seismisk landstreamer med digitala MEMS-baserade 3-komponentsensorer och ett system för radiomagnetotelluriska (RMT) mätningar som bogseras efter en båt utvecklats. Dessa system kan i viss utsträckning övervinna flera av utmaningarna i urbana miljöer. Ett flertal tester vid olika platser har genomförts och teknikens användbarhet för planeringen av underjordiska infrastrukturprojekt har bedömts. Det är demonstrerat att den seismiska landstreamern möjliggör insamling av högupplöst bredbandsdata utan att påverkas av elektromagnetiskt brus och att den är, när det gäller hela dess breda spektrum av användningsområde, helt överlägsen de sensorer av geofon-typ som länge varit standard. Det båt-bogserade RMT systemet i kombination med en kontrollerad källa för lågfrekventa signaler har visat sig vara både jämförelsevis snabbt och pålitligt vid kartläggning av berggrunden och sprickzoner.

Projektets referensgrupp har bestått av Robert Sturk (Skanska), André Pugin (Geological Survey of Canada), Andreas Aspmo Pfaffhuber (NGI), Christer Andersson (Ramboll), Nils Rydén (PEAB), Cecilia Montelius (NCC), Per Tengborg (BeFo).

Projektet var samfinansierat med större bidrag från Formas, SBUF, Skanska, SGU, FQM och NGI. Ett flertal fallstudier har genomförts med hjälp av finansiering från externa parter.

Stockholm,

Patrik Vidstrand

SUMMARY

Over the past few years, the demand for urban infrastructures has continuously increased worldwide and in particular, in Sweden. However, there is a lack of knowledge about subsurface geology and structures in the urban environment. Occasionally, information about former or hidden outcrops exists or is available from, for example, municipalities, consultants, and construction companies. Accurate knowledge about the bedrock depth and condition is important for planning a trench or a tunnel because it may imply what kind of excavation and rock reinforcement methods should be used. The urban environment is, however, challenging for most geophysical methods due to the multiple sources of noise (e.g., ground vibrations caused by vehicles and electromagnetic noise from power lines) and spatial and temporal restrictions imposed on geophysical surveys by infrastructure. The geophysical survey equipment used needs to be flexible and versatile, and highly insensitive to electromagnetic noise. In this project, we have developed a multicomponent broadband seismic landstreamer system based on digital sensors and particularly suitable for noisy environments and areas in which high-resolution images of the subsurface are desired. We have evaluated results, interpretations, and approaches using the streamer in the planning of several underground infrastructure projects in Sweden, Norway and Finland. We have also developed a new data acquisition system and technique to measure the radio magnetotelluric (RMT) signals from distant radio transmitters with the objective of mapping and modeling electric resistivity structures below a river or lake. A boat tows the acquisition system; therefore, we refer to it as boat-towed RMT. The data acquisition is fast with a production rate of approximately 1 km/hr using a nominal sampling spacing of 10–15 m. Owing to the ample number of radio transmitters available in most parts of the world, the method can be used for near-surface studies of various targets. We have developed boat-towed RMT measurements on Lake Mälaren near the city of Stockholm in Sweden and at the Äspö Hard Rock Laboratory to determine the feasibility of the method. The boat-towed RMT technique is well suited for water bodies with moderate electric resistivity such as in brackish and freshwater environments. The project has served research materials for three PhD students (expected to defend by the end of 2017), one post-doc and several short-term researches.

SAMMANFATTNING

Under de senaste åren har efterfrågan och krav på urban infrastruktur ökat över hela världen och då inte minst i Sverige. Även om viss information om berggrunden från platser som idag inte är tillgängliga ibland kan ha bevarats av t.ex. kommuner, konsult- och byggföretag, så saknas dock oftast kunskap och förståelse om rådande geologi och strukturer under ytan i stadsmiljöer. En detaljerad kunskap om förhållanden i berggrunden är väldigt viktig vid planeringen av till exempel diken, kulvertar och tunnlar eftersom det kan avgöra vilka metoder som bör användas vid när man gräver eller förstärker.

Geofysiska mätningar i en dynamisk stadsmiljö är däremot i de flesta fall förknippat med en mängd svårigheter relaterat till begränsningar i utrymme och tid samt den stora mängden av signalstörningar (t.ex. markvibrationer från fordon eller elektromagnetiska störningar från kraftledningar). Därför ställs det höga krav på att den geofysiska mätutrustningen måste vara flexibel och anpassningsbar för en mängd olika situationer med minimal påverkan på omgivningen. Men samtidigt får den inte heller påverkas av t.ex. elektromagnetiskt brus.

Som en första del i detta projekt har vi utvecklat ett seismiskt landstreamer-system med digitala multikomponent-sensorer som är känsliga över ett brett frekvensspektrum. Detta har visat sig särskilt lämpligt när man är i behov av högupplöst information i omgivningar med starkt störande miljöer. Både tekniken och metoder för datainsamling med den seismiska landstreamern, samt resultat och tolkningar av insamlad data har utvärderats vid ett flertal planeringsprojekt för underjordisk infrastruktur i både Sverige, Finland och Norge.

För att möjliggöra kartläggning och modellering av elektriskt resistiva strukturer i berggrund som täcks av sjöar eller vattendrag har vi dessutom utvecklat helt ny utrustning och en ny metod för mätning av radiomagnetotelluriska (RMT) signaler från avlägsna radiosändare. Detta system bogseras på vattenytan av en båt och metoden har därför getts namnet båt-bogserad RMT. Datainsamlingen har visat sig kunna göras förhållandevis snabbt vid till exempel profilmätningar med en hastighet på ungefär 1 km per timme om mätvärden tas med 10 – 15 meters mellanrum. Tack vare det stora antalet aktiva radiosändare som finns över hela världen så kan metoden användas för många olika typer av studier. Den båt-bogserade RMT metoden har testats och utvärderats genom mätningar vid Mälaren i närheten av Stockholm och vid det underjordiska Äspö Hard Rock Laboratory. Den båt-bogserade RMT metoden lämpar sig särskilt bra på vatten med måttlig resistivitet, såsom bräckt vatten eller färskvatten. Hittills har forskningen inom projektet sysselsatt tre doktorander (som förväntas disputera mot slutet av 2017), en post-doktor och ett flertal korttidsanställda forskare.

Table of content

PREFACE ..... **i**

FÖRORD ..... **iii**

SUMMARY ..... **v**

SAMMANFATTNING ..... **vii**

1. INTRODUCTION **1**
1.1 Scope and objectives 1
1.1.1 Project structure and advisory board *2*
1.1.2 Sponsors and industry participants *2*
1.1.3 Educational aspects and cross collaborations *3*
1.2 State-of-the-art and success measures 4
1.2.1 Beyond TRUST 2.2-GeoInfra project *4*

2 INSTRUMENT SET-UP **5**
2.1 Seismic landstreamer 5
2.2 Boat-towed RMT 7

3. EXAMPLES OF FIELD DATA AND RESULTS **9**
3.1 Vinsta Stockholm Bypass access ramp (Förbifart) 9
3.2 Varberg double-track train tunnel 11
3.3 Bollnäs post-glacial fault 12
3.4 Äspö Hard Rock Laboratory 13
3.4.1 Tunnel-surface-tunnel seismics *13*
3.4.2 boat-towed RMT *17*
3.5 Lake Mälaren (Förbifart Stockholm) 18

4. EXAMPLES OF SPIN-OFF PROJECTS **21**
4.1 Dalby energy storage site 21
4.2 Oslo E18 underground tunnel planning 21
4.3 Turku esker water management 22
4.4 Siilinjärvi open-pit apatite mine 22
4.5 Blötberget mining area 23

5.OUTREACH **25**

6. DISCUSSION **27**

7. CONCLUSIONS **27**

8. ACKNOWLEDGMENTS **27**

9. PEER-REVIEWED JOURNAL PUBLICATIONS **29**

10. PEER-REVIEWED CONFERNCE PUBLICATIONS **31**

11. Appendixes **33**

1. INTRODUCTION

Over the past few years, the demand for urban infrastructures has continuously increased worldwide and in particular, in Sweden. However, there is a lack of knowledge about subsurface geology and structures in the urban environment. Occasionally, information about former or hidden outcrops exists or is available from, for example, municipalities, consultants, and construction companies. Accurate knowledge about near-surface geology and rock quality is important for planning of underground infrastructures because it implies what kind of excavation and rock reinforcement methods should be used. The urban environment is, however, challenging for most geophysical methods due to the multiple sources of noise (e.g., ground vibrations caused by vehicles and electromagnetic noise from power lines) and spatial and temporal restrictions imposed on geophysical surveys by infrastructure. The geophysical survey equipment used needs to be flexible and versatile, and highly insensitive to electromagnetic noise. Geophysical systems and methods have to also be developed top tackle water-bodies covering 7-8% of Swedish land where the need to develop infrastructures in these areas is highly.

1.1 Scope and objectives

To overcome issues with the electromagnetic noise and also to provide sensors that are of higher amplitude dynamic compared with common geophones, we developed a multicomponent broadband seismic landstreamer (Figure 1) based on the micro-electromechanical systems (MEMS) sensors and tested and employed it during the course of the project for planning of several major urban underground infrastructures inside and outside Sweden. A boat-towed RMT system (Figure 1) was also developed and used at several test sites in Sweden to show case its potential for delineating structures that are crucial for planning of under-water tunnels or facilities. Along the equipment developments, several methods and algorithms were developed to extract rock quality information and proxies that can be directly linked to tunneling design or compared with parameters obtained using static tests.

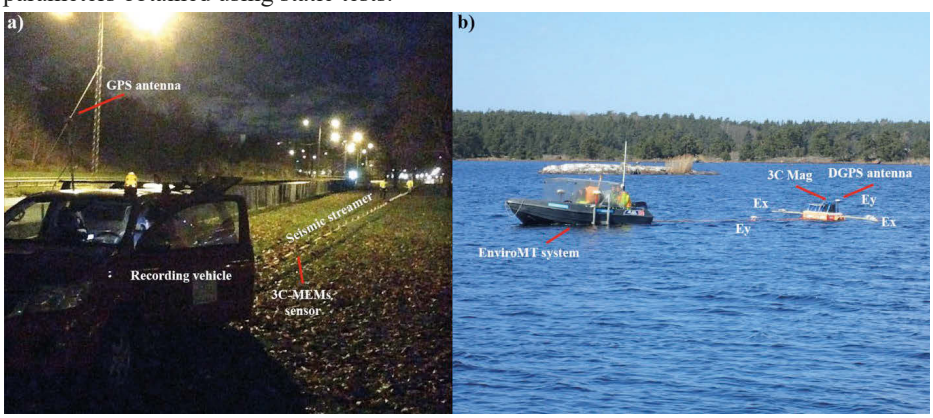

***Figure 1**. (left) Seismic landstreamer when tested at the Vinsta access ramp (Förbifart Stockholm) during its early stage of development (the first test in 2013) and (right) the boat-towed RTM when tested over the Äspö HRL facility (2015).*

The project comprised of 4 main steps:

- Brainstorming and backyard tests on instrumentations
- Small-scale tests and quality control against known targets
- Larger-scale surveys and becoming involved in major running urban underground infrastructure projects
- Developing algorithms and methodologies to maximize the results and their impacts with a particular focus on either extracting dynamic mechanical properties or quantifying uncertainty in the results.

The working team had two separate objectives: (i) development of the seismic landstreamer and boat-towed RMT and also (ii) met, discussed and provided ways to integrate the two methods with each other also other type of data. TRUST 2.2 (*Development of modern seismic and electromagnetic methods for pre-investigation for underground infrastructure facilities in urban environment*) also provided support and input to other projects; for example collaborated with TRUST 2.1 (*Geoelectric mapping as a tool for pre-investigation for underground infrastructure facilities in urban environment*), TRUST 3.3 (*Real time monitoring of grouting need using the RTGC-method*) and TRUST 4.2 (*Integrated use and interpretation of geophysical and non-geophysical data in pre-investigations for underground infrastructure facilities*).

1.1.1 Project structure and advisory board

The core institutions worked actively on the project were Uppsala University and the Geological Survey of Sweden. The project however benefited from additional experts and advisors who provided feedbacks and supports but also organized sites and knowledge to improve data acquisition and methods used in the project. The core research team consisted of:

Uppsala University: Alireza Malehmir, Christopher Juhlin, Laust B. Pedersen, Lars Dynesius, Bojan Brodic (PhD student), Suman Mehta (PhD student), Shunguo Wang (PhD student), Joachim Place (post-doc), Mahdieh Dehghannejad (short-term researcher), Magnus Andersson (short-term researcher), Emil Lundberg (short-term researcher).

SGU: Mehrdad Bastani, Lena Persson, Philip Curtis, Sverker Olsson.

Support and advisory team: Robert Sturk (Skanska), Per Tengborg (BeFo)
Andre Pugin (Geological Survey of Canada), Mats Svensson (Tyréns), Chris Wijns (FQM, Australia), Andreas Aspmo Pfaffhuber and Sara Bazin (NGI), Roger Wisén and Christer Andersson (Ramboll), Nils Rydén (PEAB), Antti Pasanen (GTK), Ulrich Polom (LIAG), Cecilia Montelius (NCC).

1.1.2 Sponsors and industry participants

These organizations provided direct funding to TRUST 2.2:

Formas: The main funding sponsor of the project.
Uppsala University: A major in-kind supporter of the project.
Geological Survey of Sweden (SGU): Co-financed the project through sponsoring their staff and funding for boat-towed RMT surveys.
BeFo: Co-financed the project for 4 years through the support of the PhD students and their field activities.

SBUF-Skanska: Co-financed the project for 4 years through the support of the PhD students and their field activities. Skanska was also providing advice and support to the activities of TRUST 2.2.
Norwegian Geotechnical Institute (NGI): Co-financed the project through sponsoring their staff and provided funding to employ the streamer for the planning of E18-Oslo underground tunnel.
First Quantum Minerals Ltd. (FQM): A small co-financing through their staff and consulting during the course of the project.
Boliden: A small co-financing through a test site at Laisvall. Boliden pulled out during the second year of the project.
Tyréns: Became a major supporter of the project by providing test sites at Varberg and Kristianstad.
Nova FoU-SKB: Sponsored the tunnel-surface-tunnel seismic experiment and the boat-towed RMT at Äspö HRL. SKB also sponsored the Bollnäs geophysical investigations.

Project progress and example case studies were presented at two major Swedish related conferences:

- Malehmir, A., Lundberg, E., Dehgahnnejad, M., Zhang, F., Friberg, O., Brodic, B., Döse, C., Place, J., Svensson, M., and Möller, H., 2015. Varberg: Developing urban geophysical instruments and methods – Pushing the boundaries. **Grundläggningsdag** (Foundation Day), Stockholm, Sweden, 15 pages.
- Malehmir, A., Lundberg, E., Dehgahnnejad, M., Zhang, F., Friberg, O., Brodic, B., Döse, C., Place, J., Svensson, M., and Möller, H., 2015. Seismic landstreamer for planning of infrastructure projects – A case study from Varberg. **Bergmekanikdagen** (Rock Mechanic Day), Stockholm, Sweden, 15 pages.

1.1.3 Educational aspects and cross collaborations

TRUST 2.2 had a major component in supporting three PhD studies. Two licentiates by Bojan Brodic and Suman Mehta were produced during December 2015. Three PhD theses are planned for September (Shunguo Wang), October (Suman Mehta) and December (Bojan Brodic) of 2017, respectively at which the project formally terminates.

- Licentiate thesis of Bojan Brodic can be found here:

http://uu.diva-portal.org/smash/get/diva2:873173/FULLTEXT01.pdf

- Licentiate thesis of Suman Mehta can be found here:

http://uu.diva-portal.org/smash/get/diva2:875252/FULLTEXT01.pdf

During the course of the project we also collaborated with TRUST 3.3 to monitor grouting in artificial fractures using ultrasonic waves and sensors (Place et al., 2016).

The collaboration has also been fruitful with TRUSTs 2.1 and 4.2 at Äspö HRL, Lake Mälaren, Varberg and Dalby.

1.2 State-of-the-art and success measures

TRUST 2.2 had a late start due to missing co-financing issues but quickly managed to recover when the potentials of the instrumentations and ideas became clear to several partners inside and outside of the project team. The landstreamer system for example has been and is being used in various projects hence meeting the main objective of the call by Formas on being truly innovative. The application fields are enormous as listed in the following where we have contributed with the instrumentations and methods:

Sweden:

- Laisvall (October 2014): Mineral exploration and geological mapping
- Stockholm (November 2013): Förbifart Stockholm, site characterization and equipment quality control
- Kristianstad (April 2014): Contaminated site and test work
- Varberg (May 2014): Planning of a double-track train tunnel
- Bollnäs (October 2014): Post-glacial fault imaging
- Äspö (April 2015): Tunnel-surface-tunnel seismics and boat-towed RMT for fracture mapping and rock quality estimations
- Ludvika (October 2015): Mineral exploration and geological mapping
- Mora (October 2015): Geological mapping
- Malmberget (Nov 2015): Mine planning
- Varberg (June 2017): Contaminated site prior in the planning of the tunneling project

Norway:

- Oslo (June 2015): Planning of E18-Oslo tunnel

Finland:

- Turku (July 2014): Esker structures and water management
- Siilinjärvi (July 2014): Mineral exploration/mine planning

Denmark:

- Stevns chalk group May 2016, PhD school

More than 15 peer-reviewed publications, 30 conference abstracts, 30 oral presentations (including keynotes) nationally and internationally, contribution to popular science publications and promotional videos, two-licentiate theses and several reports have come out of TRUST 2.2 project. Examples are provided in the publication list.

1.2.1 Beyond TRUST 2.2-GeoInfra project

TRUST 2.2 will continue employing the methods and instruments developed within the project beyond the TRUST project. Examples include:

- High-resolution landstreamer seismic studies prior to the COSC2 deep drilling (sponsored by SGU to Peter Hedin et al.): planned for August 2017.
- High-resolution in-mine landstreamer seismics similar to the Äspö HRL surface-tunnel-surface test sponsored by EIT KIC Raw Materials to be used at Garpenberg mine: planned for 2018.
- Planned activities and further developments in an up-coming H2020 project.

2 INSTRUMENT SET-UP

2.1 Seismic landstreamer

Similar to marine seismic surveys, the idea of having a portable receiver array that can be towed along the surface has been intriguing researchers working on shallow subsurface characterization using seismic methods on land as well. In the 1970s, this led to the development of the concept of a seismic landstreamer. Landstreamer is defined as an array of seismic receivers that can be dragged along the surface without the need for 'planting'. The concept was first applied in the form of a snow-streamer and since this pioneering work, seismic landstreamers of various kinds have proven their value and potential. This is particularly true for near-surface mapping and characterization in urban areas, especially on asphalt and/or paved surfaces (see Brodic et al., 2015 and references therein). Published studies involving landstreamers for acquiring seismic data have used various types of geophones, mostly single geophones on a sled (vertical or horizontal), two geophones per sled (one vertical and one horizontal), or in our case even single 3C accelerometers (see Brodic et al., 2015 and references therein). In contrast to the mentioned studies, the Uppsala University landstreamer (Figure 2) is built with digital 3C, MEMS-based sensors, making this landstreamer a unique system to date. Compared to geophones that are widespread and conventionally used, the MEMS-based sensors are digital accelerometers designed to work below their resonance frequency (e.g., 1 kHz).

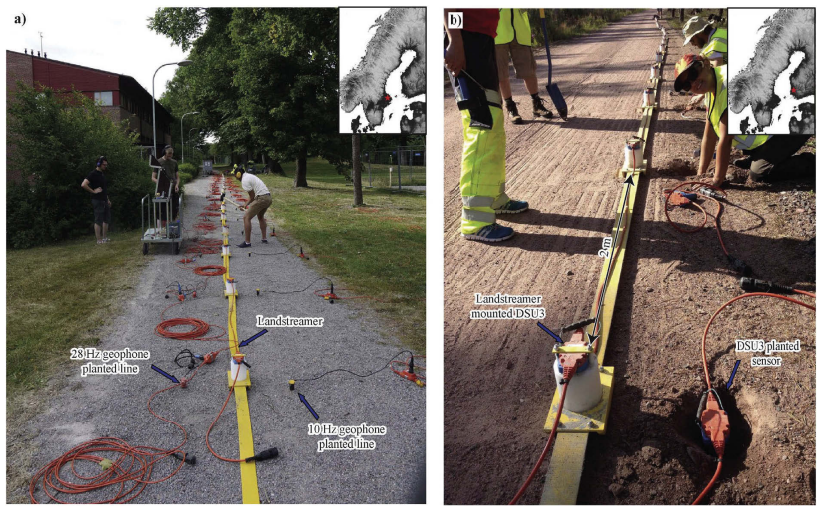

Figure 2. *Photos showing details of the landstreamer versus planted geophones tested at the early stage of the development of the streamer. (a) Landstreamer was located in the middle of two planted geophone-type (10 Hz on the right-hand and 28 Hz on the left-hand side) lines. Note the difference in cabling involved for the planted lines and the streamer-mounted units. A sledgehammer was used as the seismic source in this study. (b) Side-by-side comparison between planted and streamer mounted 3C (DSU3, MEMS-based) sensors. This test was done to study different characteristics of the seismic wavefield registered on the streamer mounted sensors and if the sleds have some noticeable effects on the wavefield especially the horizontal components.*

Advantages of MEMS over geophones include their broadband linear amplitude and phase response (0-800 Hz), tilt angle measurements up to high angles and insensitivity to contamination from electric or EM noise sources (Figure 3). The landstreamer is based on Sercel Lite technology and Sercel DSU3 (MEMS-based) sensors. The sensors are mounted on sleds (receiver holders), and the sleds fixed firmly to a non-stretchable woven belt used in the aircraft industry (Figure 2). The system was designed to support both DSU3 sensors and geophones and can be combined with wireless units for complementary acquisition if longer offsets are necessary (Figure 2). Technical details of the developed system can be found in Table 1.

Table 1. *Technical details of the system developed in this study.*

Parameters	**UU Seismic Landstreamer**
Sensors	3C MEMS
Frequency bandwidth	0 - 800 Hz
Tilt angle	Recorded in the header
Acquisition system	Sercel Lite (MEMS + geophones)
Max number of channels	2000
Present configuration	100 sensors on 5 segments each 20 units and spaced 2 m, 20 units spaced 4 m
Cable connection	Sensors on a single cable
Data transmission	Digital
Data format	SEGD
GPS time of the record	Recorded in the header

The present-day configuration of the streamer consists of five segments with each of the segments having 20 sensors mounted. The segments are interconnected by small carriages carrying line-powering units (Figure 2). Four of the segments contain 20 units spaced 2 m, while the fifth one has 20 units spaced at 4 m. The spacing can be reduced to 25 cm, if required. The entire five segments long spread connected by small trolleys was designed to be as light as possible and easily pulled by a 2WD or 4WD vehicle. With a team of 3 to 4 persons for the set-up, data acquisition rates vary from 600 m to 1200 m of seismic line in a day using a source spacing of 2 m to 4 m. A summary of the key landstreamer properties can be found in Table 2.

Table 2. *Summary of the important characteristics of the developed landstreamer.*

Technical advantages of the developed seismic landstreamer
1. Less sensitivity to tilting or can be easily estimated and corrected for it using built in tilt test
2. Full digital data transmission avoids any pick-up noise, crosstalk and sensitivity to leakage
3. It is lighter and requires less number of batteries compared to the existing and comparable technology available on the market
4. No need for sensor planting, an issue in big cities, mines, etc.
5. High-resolution imaging using densely spaced sensors
6. Covering large areas relatively fast
7. Easily combined with wireless units to extend the line or extending offset
8. It can be towed in series (2D surveys) or parallel (3D surveys)
9. It can be used for both passive (ReMi, MASW) and active data recording

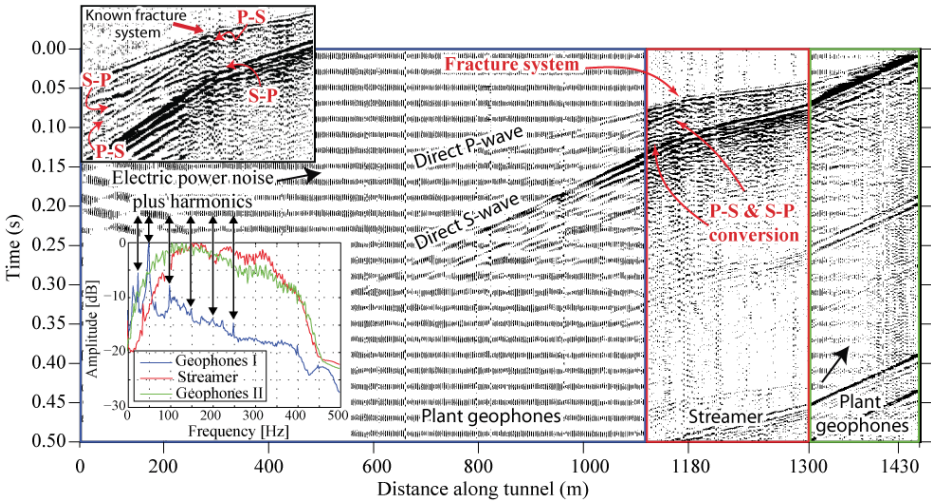

Figure 3. *Example shot gather acquired from the tunnel experiment at Äspö HRL showing the quality of streamer data in comparison with the plant geophones. Note the 50 Hz noise contaminations and its harmonic sequence in the geophone data that are totally absent in the streamer data. A major fracture system inside the tunnel was the target of this study producing strong wave-mode conversions (P-S and S-P) that are better noticeable in the streamer data (see the inset on the top).*

2.2 Boat-towed RMT

The boat-towed RMT system is developed for shallow fresh water surveys to support the planning phase of underground infrastructure developments in the city of Stockholm (Bastani et al., 2015) and evolved from the EnviroMT acquisition system (Bastani, 2001) that has been traditionally used for land surveying. The RMT method uses distant radio-transmitters in the very low frequency range (VLF, 15–30 kHz) and low-frequency range (30-300 kHz) as the EM source. Compared with traditional VLF measurements, RMT covers a wider frequency range and the data are used to model the variations of the electrical resistivity in the subsurface.

The boat-towed RMT system remains the same as for the land surveys, with the difference of the analog part of the equipment being mounted on a floating platform made of wood and Styrofoam and towed by a boat (Figure 4). The analog parts include a 3C magnetic field sensor (MFS), steel electrodes, analog filter (AF) box and other electronics. Three components of the Earth's magnetic field are measured by the MFS on the platform. Measurement of the two components of the electric field is enabled by two pairs of steel electrodes (with buffer amplifiers used to minimize capacitive leakage in the cables) fixed on a pair of five-meter-long arms (Figure 4, marked by '1' and '2'). The floating platform is towed at a distance of 10 m behind the boat and connected to an additional arm carrying the cable used to transfer the analog signal to the digital part of the system that is positioned inside the boat (Figure 4, central processing unit). The measurements with the boat-towed RMT system are carried out while the boat is moving,

making the data acquisition much more efficient and faster compared to the land surveys.

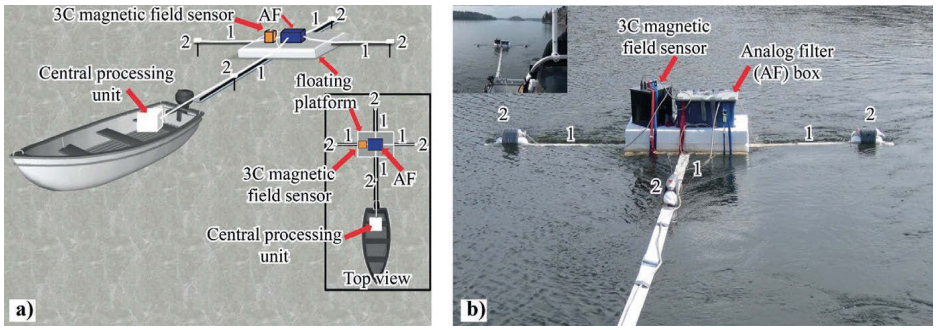

Figure 4. *Boat-towed RMT acquisition system schematic (a) and a photo of the actual look of the system with inset showing it dragged behind the boat (b). Arms and cables for electric field measurements are marked with '1', while '2' marks 4 steel electrodes with buffer amplifiers. From Bastani et al. (2015).*

3. EXAMPLES OF FIELD DATA AND RESULTS

3.1 Vinsta Stockholm Bypass access ramp (Förbifart)

This survey was carried out at the early stage of the system development and for checking the potential of the landstreamer system in urban environment. Stockholm Bypass (also known as Förbifart Stockholm) was chosen, which is a planned underground highway (8 lanes) approximately 21 km long of which more than 17 km is to be tunnel through crystalline bedrock (www.trafikverket.se/forbifartstockholm). It will pass under 3 water bodies, with the deepest point reaching approximately 85 m below sea level. A test site where an access ramp for the tunneling will start, "Vinsta", located in the northern part of Stockholm city was chosen for the streamer test (Figure 5).

Motivation to carry out the test at this site was a priori knowledge about a potential weak zone identified by a number of geotechnical boreholes suggesting poor rock quality (geotechnical Q-value below one) close to where the two seismic lines were designed to intersect each other (Figure 5). The geophysical objectives of the study were to evaluate the potential of the landstreamer in such a noisy environment, combination of the streamer with wireless units, obtaining information about depth to the bedrock and velocity information that may be linked to the rock quality, especially where the poor quality rocks were inferred to be present.

During November 2013, we acquired two seismic lines (Lines 1 and 2; Figure 5) at the site. Due to the urban nature of the site, after a reconnaissance, a decision was made to conduct the whole survey at night to avoid heavy traffic and, most importantly, trams passing next to one of the seismic lines (Line 2). Although we managed to avoid "rush hours", there was still significant traffic during the whole survey time, including trams passing every few minutes up until midnight and heavy trucks passing due to accessibility to the city during the night hours. The trams stopped for four hours during the nights for maintenance between 1 a.m. and 5 a.m., thus allowing a time slot to conduct the survey.

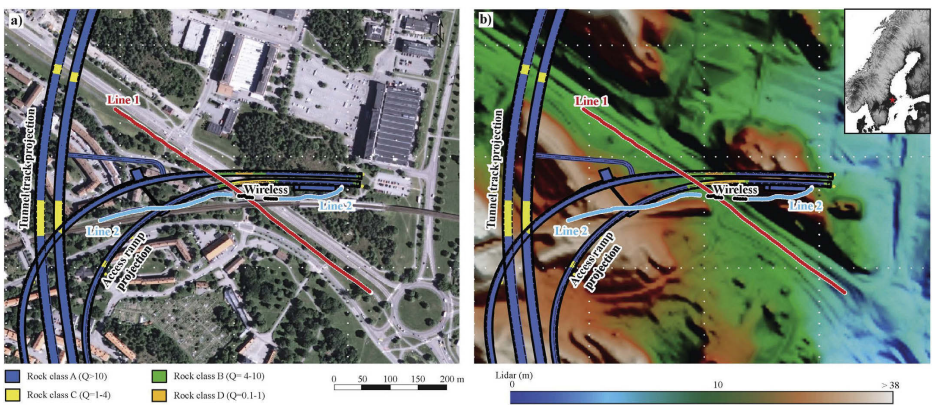

Figure 5. *Location of seismic lines (Lines 1 and 2) with respect to the planned access ramp and the main tunnel projected to the surface (a) aerial photo and (b) LiDAR (elevation) map. Colors*

on the tunnel track and access ramps show different rock classes identified from geotechnical boreholes. Twelve MEMS-based wireless recorders, six on each side of the road, are marked with the black points. Geotechnical data were kindly provided by the Swedish Transport Administration (Trafikverket). From Brodic et al. (2015).

Tomography results along Line 1 (Figure 6) suggest that the bedrock deepens towards the southeastern side of the line, but with sharp changes in elevation where the poor quality rocks are observed. The sudden change in the bedrock topography may be an indication of fracturing or faulting, hence the poor quality of rocks at this location. Bedrock in the northwestern side of the line is as shallow as a couple of meters. The tomography results along Line 2 suggest an undulating bedrock surface with its deepest point where the road is located (Figure 6). At almost every location where velocities more than 5000 m/s are observed near the surface there is bedrock outcropping (our observations), supporting the tomography results and further showing the potential of the streamer for this type of application. This test survey was encouraging to use the streamer for more real applications with no known or little known subsurface geology.

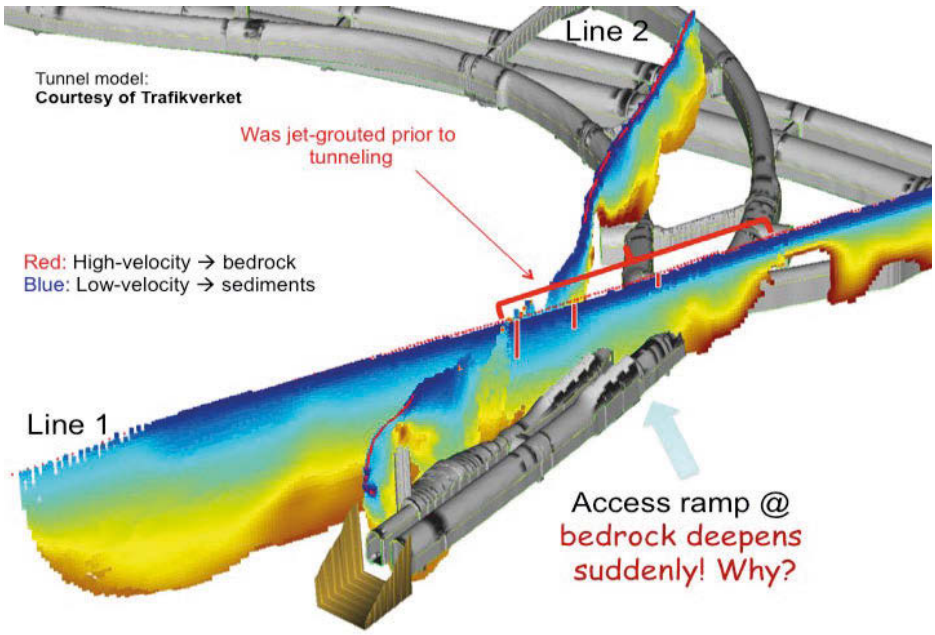

Figure 6. *3D view showing visualization of the first-break traveltime tomography results with the model of the planned tunnel and the access ramp. It indicates a low-velocity zone where the bedrock deepens and where rocks have poor quality. This area was jet grouted prior to the excavation. The tunnel model was kindly provided by the Swedish Transport Administration (Trafikverket). Modified from Brodic et al. (2015).*

This study showing the development of the landstreamer was published by Brodic et al. (2015) for the Journal of Applied Geophysics.

3.2 Varberg double-track train tunnel

As an example, the streamer was used for the planning of an underground double-track train tunnel in the city of Varberg in southwest Sweden during May 2014. Targets were depth to bedrock and weakness zones (e.g., fracture zones) in it. More than 7 km of high-resolution seismic data, 25 profiles, were acquired using 2-4 m source and receiver spacing and an accelerated weight-drop (ESS100) source. At places where placing the streamer was not possible (e.g., at road crossings), wireless recorders were deployed (Figure 7); these data were later merged with the streamer data using the GPS time of the active shots recorded on the streamer data. Details of the data acquisition and results can be found in Malehmir et al. (2015).

Figure 7. *Field photos showing the acquisition conditions in the city of Varberg. (a) Combined seismic streamer and wireless recorders (often about 4 m apart) were used to acquire the data (along line 2 and parts of line 3; see Figure 1). (b and c) Ground conditions and (d) use of a sledgehammer for some of the lines in downtown Varberg. From Dehghannejad et al. (2017).*

As an example we present first-break tomography results (Figure 8) from the city center area and their correlations with borehole data (bedrock depth) provided to us for this study. A good correspondence can be observed in most places illustrating the success of the streamer in this project.

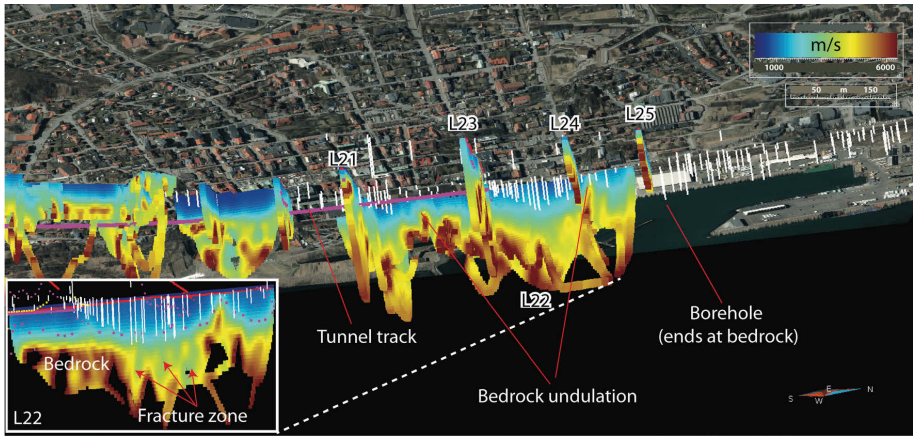

Figure 8. *3D view (from below) showing first-break tomography results in the city center (about 12 profiles are shown) and available borehole data (until May 2016). The planned tunnel is shown using purple line. A close up of the results along profile 22 where several fracture systems are speculated is shown as an inset. Modified from Malehmir et al. (2015) and Dehghannejad et al. (2017).*

Varberg seismic studies were published in Geophysics by Malehmir et al. (2015) and Near Surface Geophysics by Dehghannejad et al. (2017).

3.3 Bollnäs post-glacial fault

We were asked by SKB if we could use our newly developed systems for delineating a speculated post-glacial fault near the city of Bollnäs, central Sweden. Glacially induced intraplate faults are conspicuous in Fennoscandia where they reach trace lengths of up to 155 km with estimated magnitudes up to 8 for the associated earthquakes. While they are typically found in northern parts of Fennoscandia, there are a number of published accounts claiming their existence further south and even in northern central Europe. This study focused on a prominent scarp discovered recently in LiDAR (light detection and ranging) imagery hypothesized to be from a post-glacial fault and located about 250 km north of Stockholm near the town of Bollnäs. The Bollnäs scarp strikes approximately north–south for about 12 km. The maximum vertical offset in the sediments across the scarp is 4–5 m with the western block being elevated relative to the eastern block. To investigate potential displacement in the bedrock and identify structures in it that are related to the scarp, we conducted a multidisciplinary geophysical investigation that included gravity and magnetic measurements, high-resolution landstreamer seismics, land RMT, electrical resistivity tomography (ERT) and ground-penetrating radar (GPR).

Results of the investigations (Figure 9) suggest a zone of low-velocity and high-conductivity in the bedrock associated with a magnetic lineament that is offset horizontally about 50 m to the west of the scarp. The top of the bedrock is found 10 m below the surface on the eastern side of the scarp and about 20 m below on its western side. This difference is due to the different thicknesses of the overlying sediments

accounting for the surface topography, while the bedrock surface is likely to be more or less at the same topographic level on both sides of the scarp; else the difference is not resolvable by the methods used. To explain the difference in the sediment covers, we suggest that the Bollnäs scarp is associated with an earlier deformation zone, within a wide (> 150 m), highly fractured, water-bearing zone that became active as a reverse fault after the latest Weichselian deglaciation.

This work was published in the journal of Solid Earth by Malehmir et al. (2016).

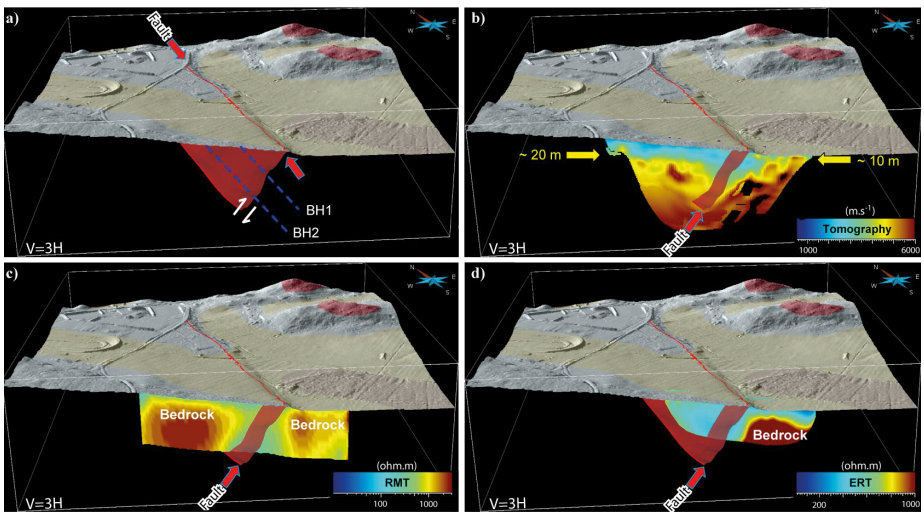

Figure 9. *Boat 3-D visualization of the geophysical results along profile 1. (a) Surface geology projected onto the lidar data with a hypothetical shape of the Bollnäs fault plane (assumed to be reversed) generated using the magnetic lineament observed in our own data, (b) travel time tomography, (c) RMT and (d) ERT models. Future plans should aim at drilling (e.g. BH1 and BH2) the weak zone that is interpreted to be a deformation zone hosting the Bollnäs postglacial fault and defining the bedrock level along profile 1. A better estimation of the throw may be then estimated and downhole logging would be conducted to verify the geophysical results presented here. From Malehmir et al. (2016).*

3.4 Äspö Hard Rock Laboratory

TRUST 2.2 employed both landstreamer and boat-towed RMT at the Äspö HRL site. It also combined with other works carried out by TRUSTs 2.1 and 4.2.

3.4.1 Tunnel-surface-tunnel seismics

A surface-tunnel-surface seismic experiment was conducted at the Äspö Hard Rock Laboratory to study the seismic response of major fracture systems intersecting the tunnel. A newly developed three-component micro-electro-mechanical sensor-based seismic landstreamer was deployed inside the noisy tunnel (Figure 10) along with conventional seismic receivers. In addition to these, wireless recorders were placed on the surface. This combination enabled simultaneous recording of the seismic wavefield both

inside the tunnel and on the surface. The landstreamer was positioned between two geophone-based line segments, along the interval where known fracture systems intersect the tunnel.

Figure 10. *Photo showing the deployment of the landstreamer in the Äspö tunnel intersecting the NE1 fracture system. The experiment was done using a tunnel-surface-tunnel seismic experiment.*

First arrival tomography produced a velocity model of the rock mass between the tunnel and the surface with anomalous low-velocity zones correlating well with locations of known fracture systems (Figure 11). Prominent wave mode converted direct and reflected signals, P-S and S-P waves, were observed in numerous source gathers recorded inside the tunnel. Forward travel time and 2-D finite difference elastic modeling, based on the known geometry of the fracture systems, show that the converted waves are generated at these systems.

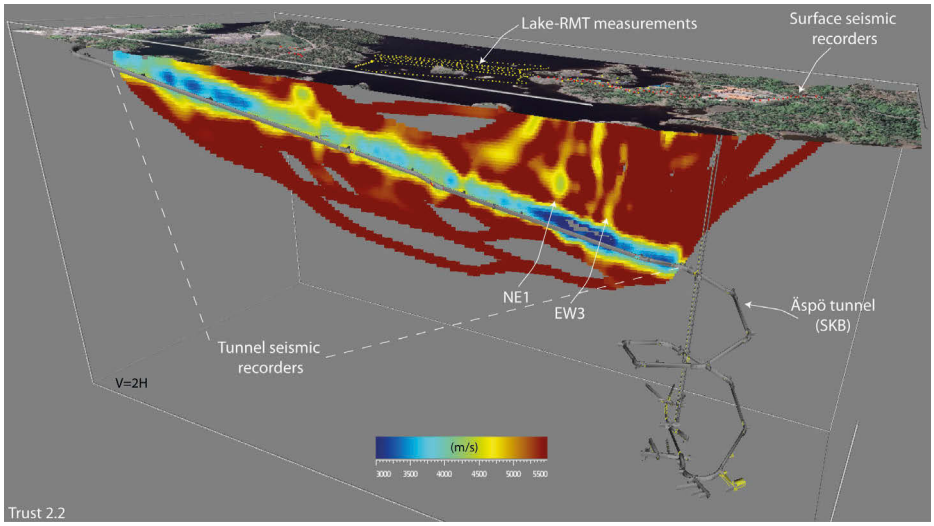

Figure 11. *The 3D of the final P-wave velocity model obtained from joint P- and S-wave tomography inversion. P-wave velocity model with aerial photo projected on top of the LiDAR surface, tunnel model, surface projections of the fracture systems, and their intersection with the tunnel, along with location of seismic receivers both in the tunnel and on the surface shown by red dots. Note how NE1 and EW3 are clearly delineated in this study. From Brodic et al. (2017).*

Additionally, the landstreamer data were used to estimate Vp/Vs, Poisson's ratio, and seismic attenuation factors (Qp and Qs) over fracture sets that have different hydraulic conductivities (Figure 12). The low-conductivity fracture sets have greater reductions in P wave velocities and Poisson's ratio and are more attenuating than the highly hydraulically conductive fracture set. Our investigations contribute to fracture zone characterization on a scale corresponding to seismic exploration wavelengths.

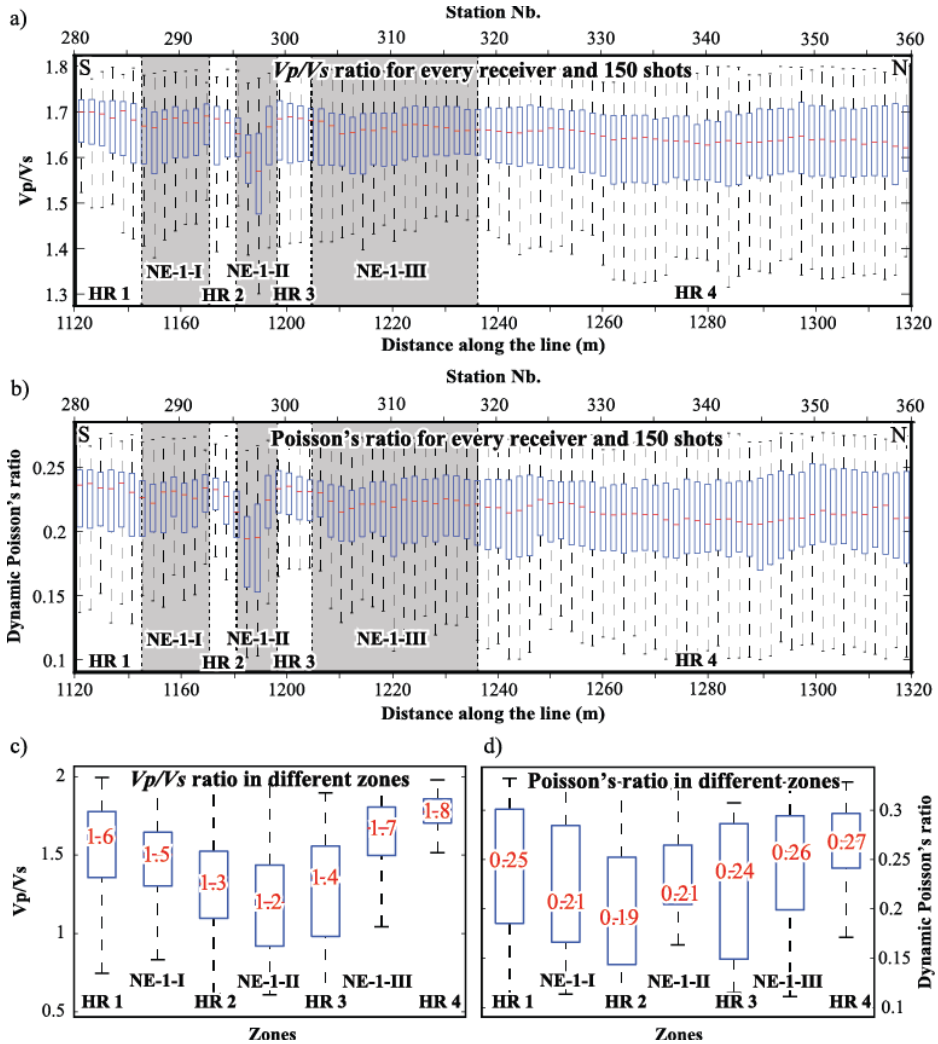

Figure 12. *Variations of dynamic elastic properties in the zone of the NE-1 fracture system calculated using two different approaches. (a) Vp/Vs ratio variation and (b) Poisson's ratio variation based on the ratio of picked first arrivals of the S- and P-waves from 150 sources along a portion of the seismic line in the tunnel. (c) Vp/Vs ratio variation and (d) Poisson's ratio variation within seven different zones as shown in Figure 9 and velocities obtained from regression analysis. HR represents host rock before and after NE-1 (HR 1 and 4) and between its different sets (HR 2 and 3). From Brodic et al. (2017).*

This study was published in the Journal of Geophysical Research-Solid Earth by Brodic et al. (2017).

3.4.2 boat-towed RMT

The ERT method provides moderately good constraints for both conductive and resistive structures while the RMT method is well suited to constrain conductive structures. Additionally, RMT and ERT data may have different target coverage and are differently affected by various type of noise. Thus, joint inversion of RMT and ERT datasets may better constrain the resultant model compared with single inversion. In this study, joint inversion of boat-towed RMT (TRUST 2.2) and lake-floor ERT (TRUST 2.1) data was for the first time formulated and implemented. A synthetic test together with a case study from the Äspö HRL was used to illustrate the implementation of the joint inversion approach. A 790-m-long profile comprising lake-floor ERT, boat-towed RMT data, and partial land RMT data was used in the field application (Figure 13).

Figure 13. *Photos showing the deployment of the boat-towed RMT system during the Äspö experiment.*

With or without weighting (applied to different datasets, vertical and horizontal model smoothness) and constraint of bathymetry data and water resistivity measurements, joint inversion were performed and compared. A major north-easterly directed fracture system, NE-1, observed in the HRL facility and boreholes together with a previously uncertain weak zone EW-5 are inferred in this study (Figure 14).

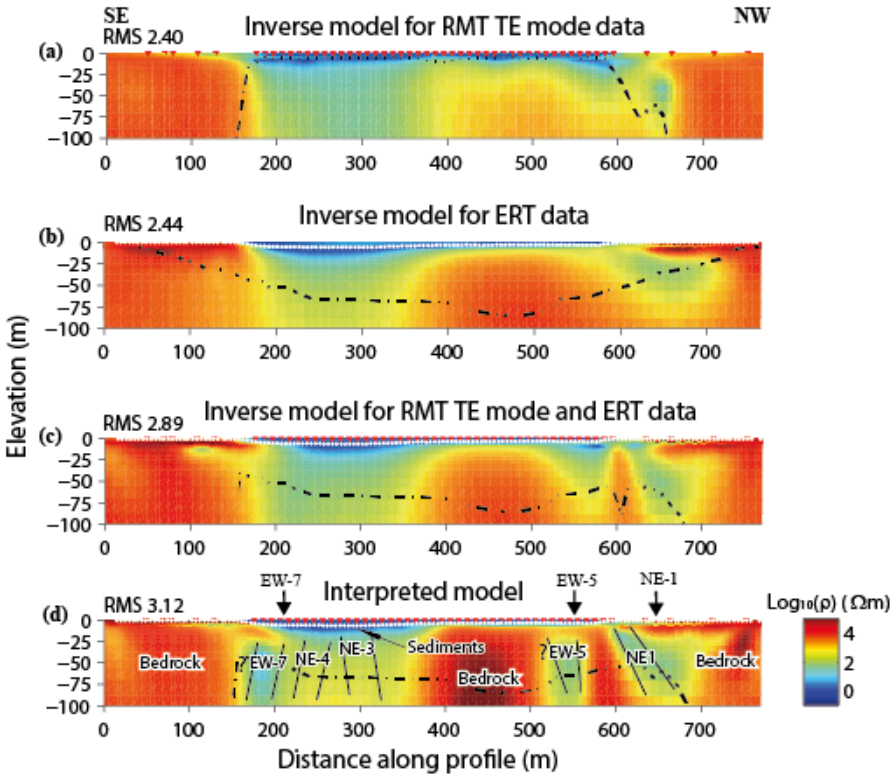

Figure 14. *(a) Inversion model for RMT TE-mode data. (b) Inversion model for ERT data. (c) Joint inversion model for RMT TE-mode and ERT data. Total RMS is 2.89 (RMS of RMT is 3.36 and RMS of ERT is 2.69). (d) Joint inversion model constrained with bathymetrical data and water resistivity measurement. Total RMS is 3.12 (RMS of RMT is 4.28 and RMS of ERT is 2.56). Separate RMS values from joint inversion are slightly higher than those of the single inversions. However, the model fits both datasets with an acceptable RMS. From Wang et al. (2017).*

This study is under revision in Geophysical Journal International by Wang et al. (2017).

3.5 Lake Mälaren (Förbifart Stockholm)

To illustrate the potential of the boat-towed RMT system, an RMT survey was conducted in the city of Stockholm where one of the largest underground infrastructures in Sweden is being built, a 21-km-long multi-lane bypass-tunnel (Förbifart Stockholm).
Several RMT profiles were acquired in the lake Mälaren to determine the depth to bedrock and investigate possible fracture zones that were geotechnically inferred at one location. The tunnel will pass beneath three water passages and the deepest point will reach about -80 m (or 65 m below sea level). Here, we will focus on one of the three water passages, Kungshatt-Löven (Figure 15).

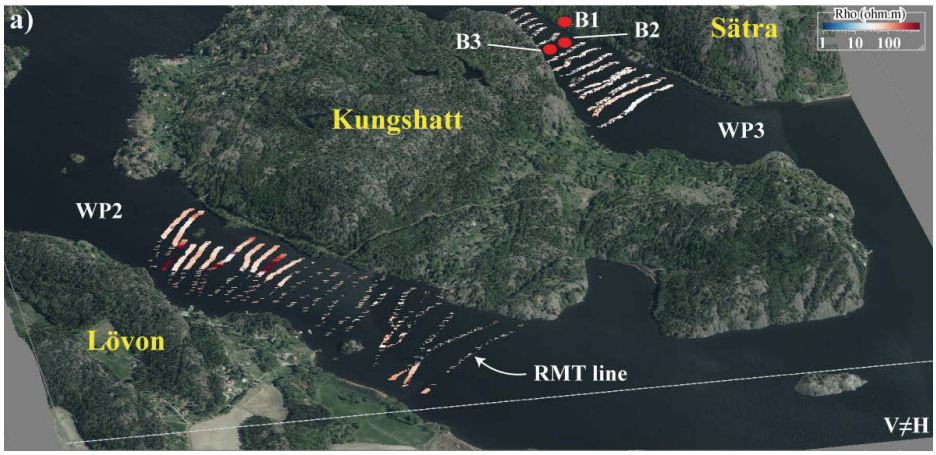

Figure 15. *3D views showing (a) RMT lines from the two of the three water passages where measurements were conducted, and (b) resistivity models and interpretations of features observed. From Mehta et al. (2017).*

The tunneling is planned with two separate tunnels, each with three lanes. The longest part of the tunnel is 16.5 km between the Kungens kurva and Lunda access ramps. Construction began in early 2015 and is expected to take ten years to complete. When up and running, 140,000 vehicles per day are expected to use the bypass. Approximately 15 km of RMT profiles, with 15 m average spacing, were surveyed during three days, 3-5 hours each day between Löven and Kungshatt islands (Figure 15). Compared to traditional RMT land surveys, under normal field conditions (0.5 km long profile per day with 10 m station spacing), the new system is around 10 times faster.

Figure 16 shows 3D views from the 2D modeling of the RMT data together with information from an inclined well, B4, along with the model of the planned tunnel trace. Fracture systems found during the core analyses are marked as K1-K5. Some cores analyzed showed clays, graphite, salt and sulphide minerals within them likely contributing to the low-resistivity features seen in the models. The top of the bedrock is well resolved near the shorelines, but not as clearly in the middle of the water passages owing to the diffusive behavior of EM signals, making the direct interpretation of the fractured bedrock ambiguous. A small island visible on the aerial photo is clearly resolved by the RMT models. The top resistive layer is interpreted to be the fresh water in Figure 16b, particularly note the resistive fresh water, with conductive sediments and resistive bedrock near the small island on the Löven side of the profiles. These models show the reliability and potential of this prototype boat-towed RMT system in shallow water conditions with it being both cost effective and efficient. Thus, it has encouraged us to build a more robust and sophisticated acquisition system for future use. One of the drawbacks of RMT is the limited depth of penetration. Acquisition of lower frequencies using a controlled source is planned in the future.

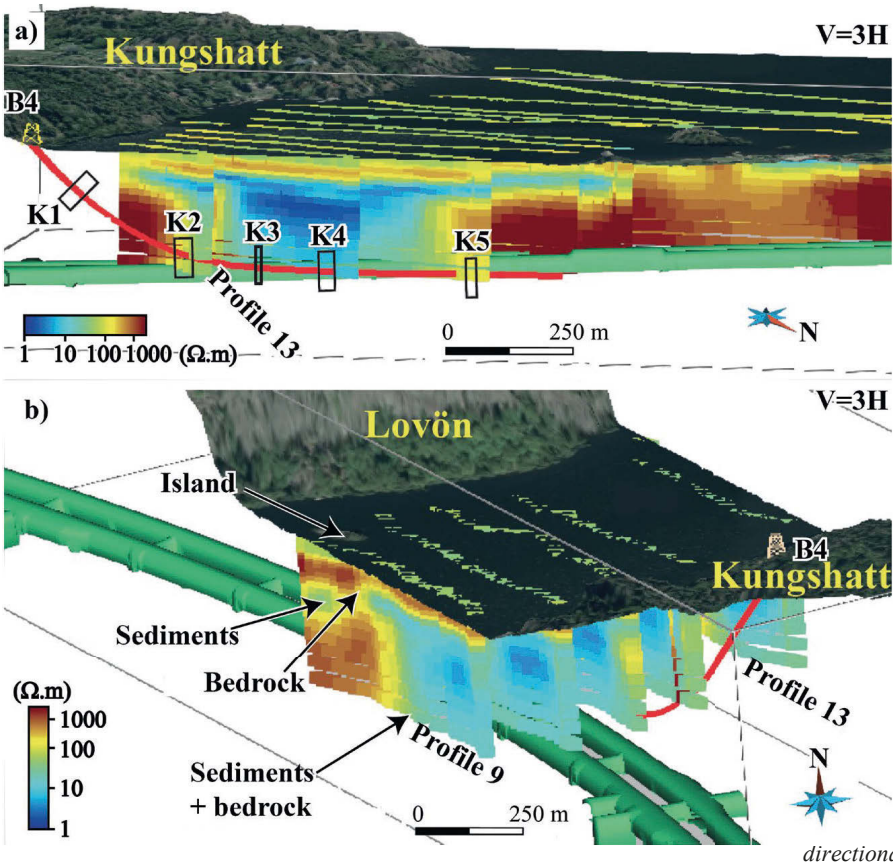

re 3D ving the directional

borehole, B4, along with the RMT inverted models and tunnel model shown in green. Five major fracture systems and their widths were mapped in the cores from B4; four (K2–K5) are likely to be contributing to the conductivity zone in the middle of the water passage. (b) A small island at the site and its response observed in the RMT model. Note that the RMT data resolve the water column, lake sediments and the underlying bedrock clearly in this part of the model. From Mehta et al. (2017).

Details of the data acquisition and processing work can be found in Bastani et al. (2015). Details concerning resolution and a sensitivity analysis can be found in Mehta et al. (2017).

4. EXAMPLES OF SPIN-OFF PROJECTS

We provide short summary for a selection of spin-off projects here where the seismic landstreamer or methods developed in the project were used for relevant projects.

4.1 Dalby energy storage site

This study was conducted in collaboration with Skanska, Sweco and Lund University:

Three high-resolution refraction and reflection seismic profiles for the planning of a major underground thermal-energy-storage site within the Tornquist suture zone of Scania in southwest of Sweden were acquired during August 2015. Combined cabled- and wireless recorders were used to provide continuity on both side of a major road running in the middle of the study area. First arrivals are clear in most shot gathers allowing them to be used for traditional refraction seismic data analysis and also for more advanced traveltime tomography. Bedrock depressions are clearly observed in the tomograms suggesting the possibility of weakness zones, highly fractured and/or weathered, in the bedrock and confirmed in several places by boreholes. Signs of reflections in raw shot gathers were encouraging and motivated to process the reflection component of the data. Several steeply dipping reflections were imaged down to 400 m depth. The origins of the reflections are unclear right now ranging from amphibolite sheets to diabase dykes as well as faults within the gneissic rocks, and each of this implies a different geological scenario at where the site will be developed. This study however illustrates the potential of the combined refraction and reflection imaging for underground energy-storage-site characterizations.

An extended abstract presentation was given at the EAGE-NSG 2017, Malmö.

4.2 Oslo E18 underground tunnel planning

This study was conducted in collaboration with NGI:

Oslo municipality is presently planning bus and car tunnels to facilitate its accessibility and increase traffic efficiency. Urban environment is usually a challenge for geophysical pre-investigations because of the various sources of noise, vibrations and restriction both in time and space. These technical challenges were overcome with the use of a newly developed seismic streamer specifically designed for noisy urban areas, from an industry-academia partnership. A total of 3.5 km long seismic data along 14 profiles were acquired for the tunnels pre-investigation with the main goals of (1) obtaining information about depth to bedrock, (2) detecting potential weakness zones, and (3) optimizing the number of drillings and their locations for a follow-up study. In addition, six electrical resistivity tomography profiles were acquired near the planned tunnel alignments. Inversion of first breaks and electrical resistivity data provides a seamless depth to bedrock interface that is in most places in good agreement with the nearby geotechnical soundings. In addition, the geophysical sections reveal the bedrock undulation character and provide some indication of weakness zones. This case study also illustrates that if the pre-investigation had been based only on boreholes, it would have overseen a potential difficulty during excavation.

An extended abstract presentation was given at the EAGE-NSG 2016, Barcelona.

4.3 Turku esker water management

This study was conducted in collaboration with GTK, Turku Water Management Company and University of Turku:

A novel high-resolution (2–4 m source and receiver spacing) reflection and refraction seismic survey was carried out for aquifer characterization and to confirm the existing depositional model of the interlobate esker of Virttaankangas, which is part of the Säkylänharju-Virttaankangas glaciofluvial esker-chain complex in southwest Finland. The interlobate esker complex hosting the managed aquifer recharge (MAR) plant is the source of the entire water supply for the city of Turku and its surrounding municipalities. An accurate delineation of the aquifer is therefore critical for long-term MAR planning and sustainable use of the esker resources. Moreover, an additional target was to resolve the poorly known stratigraphy of the 70–100-m-thick glacial deposits overlying a zone of fractured bedrock. Bedrock surface as well as fracture zones were confirmed through combined reflection seismic and refraction tomography results and further validated against existing borehole information. The high-resolution seismic data proved successful in accurately delineating the esker cores and revealing complex stratigraphy from fan lobes to kettle holes, providing valuable information for potential new pumping wells. This study illustrates the potential of geophysical methods for fast and cost-effective esker studies, in particular the digital-based landstreamer and its combination with geophone-based wireless recorders, where the cover sediments are reasonably thick.

A follow-up RMT survey was also conducted at one of the two sites surveyed in Turku area, however, results are not yet ready for presentations.

A peer-reviewed article is already published by Maries et al. (2017). Several extended abstract presentations given at for example the EAGE-NSG 2016, Barcelona.

4.4 Siilinjärvi open-pit apatite mine

This study was conducted within ERA-MIN1 StartGeoDelineation (sponsored by Vinnova, SGU, Tekes, Yara and NIO) and in collaboration with GTK and Yara for open-pit mine planning purposes:

We tested the applicability of a newly developed broadband (0–800 Hz) digital-based seismic landstreamer for open-pit mine planning in the apatite-bearing Siilinjärvi mine in central Finland. Four seismic profiles, in total approximately 2.5 km long (2–4 m source and landstreamer receiver spacing), two inside the pit and two on its margins, were acquired in combination with wireless recorders connected to 10 Hz geophones and fixed at every 10 m spacing along the seismic profiles while the streamer data were being acquired. Downhole logging and laboratory physical property measurements on core and rock samples were carried out to not only support the seismic interpretations but also to provide information about the possible geophysical signature of these unique types of deposits. In spite of a highly noisy mining environment, seismic data of high quality were acquired; however, reflection processing and interpretations were challenged by the

geologic complexities of several generations of basic and carbonatite dikes. To complement the reflection data imaging and to account for the steep elevation changes and crookedness of some of the seismic profiles, 3D first-arrival traveltime tomography and 3D swath reflection imaging were also carried out. Clear refracted arrivals from the open-pit profiles suggest the possibility of low-velocity zones associated with either blasting or several shear zones intersecting the seismic profiles. In terms of reflectivity, reflections have a different appearance from short and flat to longer and steep ones. The downhole- and borehole logging data suggest that some of these reflections are associated with diabase dikes and some are likely from zones of weaknesses in the alkaline-carbonatite complex. We determine the potential of using seismic streamers for cost- and time-effective open-pit mine planning and encourage further testing in simpler geologic settings to be established.

A peer-reviewed article is already published by Malehmir et al. (2017).

4.5 Blötberget mining area

This study was conducted within ERA-MIN1 StartGeoDelineation project (sponsored by Vinnova, SGU, Tekes, Yara and NIO) and in collaboration with Nordic Iron Ore where the potential of the streamer for deep mineral exploration was tested:

To be fully embraced into mineral exploration, seismic data require to be acquired fast, cheaper and with minimum environmental impacts addressing also the often brown-field highly noisy environment where these surveys are employed. Since 2013 and through a number of case studies, we have been testing a newly developed for urban environment, digital-based 240 m long, seismic landstreamer for mine planning and mineral exploration purposes. Here, we present a pilot study examining the potential of the streamer for deep targeting a known, down to approximately 850 m depth, iron-oxide mineralization in the historical Blötberget-Ludvika mining area of Bergslagen mineral district of central Sweden. Combined streamer (100-3C-MEMS (micro-electromechanical system), 2-4 m spacing) and 75 wireless recorders (mixed 10 Hz and MEMS, 10 m spacing) were used. A Bobcat-mounted drophammer, 500 kg, was used to generate the seismic signal. Within 4 days, approximately 3.5 km of seismic data using 2-10 m source and receiver spacing were acquired. Reflection data processing results clearly image the mineralization as a set of strong high-amplitude reflections and likely slightly extending beyond the known 850 m depth. This is encouraging and suggests such a cost-effective exploration method can be used in the area and elsewhere to delineate similar depth range iron-oxide deposits.

A peer-reviewed article is submitted for publication by Malehmir et al. (2017).

5. OUTREACH

TRUST 2.2 took part or even contributed to several outreach activities. Participated actively in all the workshops organized by the management team, those by Trafikverket, SGU, Boliden, GTK, SBUF and Skanska. Figure 17 shows an example popular science article published by NyTeknik where our developments have a clear presence in the article.

16 NY TEKNIK · 20 JANUARI 2016 · NR 3

Fokus • Underjordens hemligheter synas

Fler metoder samtidigt ger billigare tunnel

Det gäller att veta hur berggrunden ser ut när stora tunnlar ska byggas. Därför utvärderar svenska experter elektriska och seismiska mätmetoder för att kunna se under markytan.

Inför ett stort infrastrukturbygge brukar man alltid göra provborningar och ta djupa jordprover, så kallade jordsonderingar, för att ta reda på vad som döljer sig under markytan.

Men det är inte alltid som seismiska eller elektriska mätningar görs.

– Vi tycker att sådana här undersökningar ska göras som standard i ett tidigt stadium i komplicerade projekt, säger Maria Ask, professor i tillämpad geofysik vid Luleå tekniska universitet.

Maria Ask.

Hon leder det svenska projektet Trust, Transparent Underground Structure, som förenar forskare, företag och myndigheter. Syftet är bland annat att utveckla metoder som ska ge ett bättre underlag för tunnelbyggen.

– Det som är unikt med vårt projekt är att vi använder flera mätmetoder. När du lägger ihop dem ökas kunskapen, du får säkrare tolkning och bättre kvalitet på dina undersökningar, säger Maria Ask.

– Till exempel kan sprickzoner i berget och förorenade jordlager upptäckas, som kan skapa kostsamma problem i bygget om de dyker upp som överraskningar.

Elektriska, elektromagnetiska och seismiska mätningar har hittills gjorts på flera ställen i landet, främst vid Aspölaboratoriet i Oskarshamn, Västergötatunneln och Förbifart Stockholm.

Den seismiska mätmetoden innebär att sensorer mäter hur snabbt vågor rör sig genom marken efter ett hammarslag eller en dynamitsprängning. Inom Trust-projektet utvärderas nya sensorer som kan hämta av markens olikheter i flera olika riktningar.

– Resultatet är en snabb mätmetod där man ser allt tydligare och med bättre upplösning. Det är som när man får på sig nya glasögon, säger Maria Ask.

Genom att sätta sensorerna på en 240 meter lång kabel har forskarna utvecklat ett nytt mätinstrument. Det kallas för landstreamer och innebär att man släpper det tidskrävande arbetet att gräva ner sensorerna i marken.

– Vi har utvecklat ett unikt seismiskt mätsystem, som inte är så känsligt för elektrisk brus, för att kunna utföra seismiska mätningar i städer där det finns mycket sen störe, säger Alireza Malehmir, lektor i geofysik vid Uppsala universitet och ledare för ett av delprojekten i Trust.

Även radiovågor används inom Trustprojektet för att ta reda på hur berggrunden ser ut. Via reflexioner från hål har forskarna också kunnat avgöra hur berget ser ut under grunda vattendrag.

– De har till exempel sett en sprickzon i Mälaren, det är viktigt när man ska dra tunneln till Förbifart Stockholm där, säger Maria Ask.

LINDA NOHRSTEDT

Uppsalaforskare med den nya landstreamern, som består av en ny typ av sensorer (i vita plastboxar med gult band). Resultatet jämförs med traditionella sensorer (till höger i bild, sammanbundna av en orange slang) som grävs ned i marken. I mitten är Peter Hedin redo att slå till metallplattan som ska generera seismiska vågor.

Seismiska mätningar i Varberg. Forskaren Joachim Place med hammaren som genererar vågor i marken.

Radiovågor används för att undersöka hur berggrunden ser ut under vattendrag. Här görs så kallade RMT-mätningar vid Oskarshamn. Längst fram i båten syns Lundaforskaren Roger Wiklén.

Så ser Trustforskarna under markytan

Resistivitetsmätning: En elektrisk ström sänds genom två elektroder för att mäta markens elektriska motstånd, resistiviteten. Metoden kan användas för att se jordlager, berggavelhet och förorenade områden.

Inducerad polarisation: Elektrisk ström skickas ned i marken och sedan mäts hur fort den uppladdade spänningen avtar med tiden. Metoden används för att se berggrunden med olika typer av mineraler från varandra.

Seismiska mätningar: Sensorer mäter hur snabbt seismiska vågor rör sig i marken efter ett hammarslag eller dynamitladdning. På så sätt kan man upptäcka sprickor och olika typer av material i marken.

Radiomagnetotellurik: Mäter hur elektromagnetiska signaler i frekvensbandet 10–250 kHz påverkas av att passera genom marken. Metoden kan användas för att avgöra hur djup berggrunden är och se om berget har sprickor.

Figure 17. *A scan copy of the NyTeknik article published in the January of 2016 dedicated to the activities of the TRUST with clear presence of our development as illustrated in the pictures.*

Other outreach activities included short videos and here a couple of links to some of the short videos produced during the course of the project:

- TRUST 2.2 general ideas and Varberg seismic survey:

https://www.youtube.com/watch?v=xjK8EhkGpEc

- Our advisory member, Maria Ask and PhD student Bojan Brodic:

https://www.youtube.com/watch?v=yOTkbqzXWco

- TRUST – GeoBIM-metodik och nyutvecklade geofysiska metoder:

https://www.youtube.com/watch?v=NmXicev0coQ

- Pilot tests at Laisvall and Förbifart Stockholm using the seismic landstreamer:

https://www.youtube.com/watch?v=TClV3ie8FVY

- Äspö HRL surveys:

https://www.youtube.com/watch?v=X3YE2A0RDFA

Several short news and information activities were also produced by various organizations. Figure 18 shows an example from SKB in connection with the Bollnäs surveys.

Geofysiker med fokus på jordens ytskikt

Hur kan geofysiker göra världen till en bättre plats? Efter att ha förfinat metoder, algoritmer och mätutrustning i över hundra år är det dags att göra skillnad på riktigt, tycker professor Alireza Malehmir, som installerades som ny professor i november.

– Geofysiker studerar jordens inre med hjälp av fysikens lagar och matematiska tricks. Vi använder oss av vibrationer, magnetism, seismik, gravitation och elektromagnetiska vågor, som hjälper oss att avläsa innehållet i marken, säger Alireza Malehmir, en av alla nya professorer som installerades i november.

Tack vare geofysiken så vet vi i dag ungefär hur planeten ser ut ända ned till jordens mittpunkt, trots att det fortfarande är praktiskt taget omöjligt att borra djupare än tre kilometer ned i jordskorpan.

FOTO: LASSE MODIN, SKB

Alireza Malehmir avläser innehållet i marken under våra fötter. Här undersöker han en så kallad förkastningslinje i Bollnäs.

ALIREZA MALEHMIRS FORSKARGRUPP HAR

de senaste åren jobbat med att undersöka mer marknära fenomen.

– Utan geofysiken skulle vi bokstavligen talat bara skrapa på ytan i vår förståelse av planeten. Den "djupa" geofysiken är viktigt, men vi får inte glömma bort att det som händer i det översta skiktet har störst betydelse för oss människor. Det är där vi gräver våra tunnlar, bygger hus och vägar och hittar våra naturresurser. Det är helt enkelt i jordens ytskikt som vi geofysiker har möjlighet att göra störst skillnad, förklarar Alireza Malehmir.

– Jag ser det som vår uppgift att bli mer aktiva i samhället och samhällsbyggandet. I över hundra år har vi förfinat våra metoder och vår mätutrustning, och nu har vi verkligen möjligheter att vara till hjälp.

Dessa nya mätmetoder har forskargruppen använt i planeringen av projektet Förbifart Stockholm, där forskarna kunde peka ut den bästa och säkraste placeringen av vägtunnlar. De undersöker också marken för att se om det finns risk för till exempel jordskred.

– Nu är det dags för oss geofysiker att visa att vi kan göra världen till en bättre plats, säger Alireza Malehmir.

Börje Dahrén

Figure 18. *Promotion news by SKB in connection with the Bollnäs surveys. Seismic landstreamer is shown in the background.*

6. DISCUSSION

Two modern geophysical systems have been developed and employed for various near-surface applications with a particular focus on urban underground infrastructure planning projects. Data acquired by the systems show excellent quality allowing high-resolution imaging of the subsurface structures. While there are rooms for improvements, they are currently being used in several infrastructure-planning projects inside and outside Sweden illustrating their potentials.

Future developments will include exploiting the broadband frequency nature of the streamer data and development of a 3C source that can generate broad frequency data that the streamer sensors are capable of recording. Boat-towed RMT system will require new hardware and software developments. A DGPS system was recently linked to the system to provide high-precision geodetic surveying of the acquisition points, which proved to be important for this type of survey.

7. CONCLUSIONS

Two modern geophysical systems have been developed with a particular focus on urban underground infrastructure planning projects and that can be used for various near-surface applications. Data acquired by the two systems show excellent quality, allowing high-resolution imaging of the subsurface structures in urban environments. The two systems are currently being used in several infrastructure-planning projects and there is still space for improvements based on the feedback from their application. Future developments will include exploiting the broadband frequency nature of the streamer data and development of a 3C source that can generate broad frequency range signals that the streamer sensors are capable of recording. The boat-towed RMT system will require new hardware and software developments. A DGPS system was recently linked to the system to provide high-precision geodetic surveying of the acquisition points, which is essential for this type of survey. The boat-towed RMT works quite efficiently, e.g., 5 km line-data per day, and shows high reliability for bedrock mapping and fracture zone delineation, particularly over shallow water bodies. The signal penetration depth of the boat-towed RMT system can also be enhanced using additional lower frequency controlled source (controlled-source RMT).

The boat-towed RMT case study from the Förbifart Stockholm also shows the potential of this method for bedrock topography and fracture zone mapping in a time- and cost-effective manner on fresh or brackish water bodies. This is particularly important and can provide important information for where detailed drilling and geotechnical investigations should be carried out. The two systems have been used in several related studies in Sweden, Finland, Norway and Denmark, which encourages us to improve them further.

8. ACKNOWLEDGMENTS

This work was conducted within the framework of TRUST 2.2 (TRUST-GeoInfra; http://www.TRUST-geoinfra.se,) sponsored by Formas (project number: 252-2012-

1907), SGU (363-26512013), BeFo (BeFo 340), SBUF, Skanska, Tyréns, FQM and NGI. We thank all our sponsors and those who contributed to our project from Lund University, KTH, FQM, GTK, University of Turku, SKB, and Nova FoU. We thank the TRUST management team (TRUST 1) in particular Maria Ask, Mats Svensson and Håkan Rosqvist among others for stimulating discussions and generating new initiatives during a number of workshops organized during the course of the project. We also thank all our collaborators in particular researchers from SGU, Skanska, KTH, Lund University, and University of Turku for their fruitful research and joint project collaborations. The Swedish Transport Administration (Trafikverket) provided access to some of the sites and also models of the planned tunnels for which we are grateful.

9. PEER-REVIEWED JOURNAL PUBLICATIONS

Here we list in a chronological order peer-reviewed journal publications where TRUST 2.2 was involved:

Mehta, S., Pedersen, L.B., Kamm, J., Bastani, M., and Malehmir, A., 2017. Enhanced model resolution from inversion of RMT data by preserving the identity of radio transmitters. *Submitted.*

Wang, S., Kalscheuer, T., Bastani, M., Malehmir, A., Pedersen, L.B., Dahlin, T., and Meqbel, N., 2017. Joint inversion of lake-floor direct current resistivity and on-lake radio-magnetotelluric data and an example application from the Äspö Hard Rock Laboratory site, Sweden. *Geophysical Journal International*, in revision.

Brodic, B., Malehmir, A., and Juhlin, C., 2017. Delineating fracture zones using surface-tunnel-surface seismic data, P-S and S-P mode conversions. *Journal of Geophysical Research Solid Earth,* 122. http://dx.doi.org/10.1002/2017JB014304.

Brodic, B., Malehmir, A., Bastani, M., Mehta, S., Juhlin, C., Lundberg, E., and Wang, S., 2017. Multi-component digital-based seismic landstreamer and boat-towed radio-magnetotelluric acquisition systems for improved subsurface characterization in the urban environment. *First Break*, 35(8), 41–47.

Dehgahnnejad, M., Malehmir, A., Svensson, M., Lindén, M., and Möller, H., 2017. High-resolution reflection seismic imaging for the planning of a double-train-track tunnel in the city of Varberg, southwest Sweden. *Near Surface Geophysics,* 15(3), 226–240.

Malehmir, A., Heinonen, S., Dehgahnnejad, M., Heino, P., Maries, G., Karell, F., Suikkanen, M., and Salo, A., 2017. Landstreamer seismics and physical property measurements in the Siilinjärvi open-pit apatite (phosphate) mine, central Finland. *Geophysics,* 82*,* B29–B48.

Mehta, S., Bastani, M., Malehmir, A., and Pedersen, L.B., 2017. Resolution and sensitivity of boat-towed RMT data to delineate fracture zones — Example of the Stockholm bypass multi-lane tunnel. *Journal of Applied Geophysics*, 139*,* 131–143.

Maries, G., Ahokangas, E., Mäkinen, J., Pasanen, A., and Malehmir, A., 2017. Interlobate esker architecture and related hydrogeological features derived from a combination of high-resolution reflection seismics and refraction tomography, Virttaankangas, SW-Finland. *Hydrogeology Journal,* 25*,* 829–845.

Malehmir, A., Socco, L.V., Bastani, M., Krawczyk, C.M., Pfaffhuber, A.A., Miller, R.D., Maurer, H., Frauenfelder, R., Suto, K., Bazin, S., Merz, K., and Dahlin, T., 2016. Near-surface geophysical characterization of areas prone to natural hazards: A review of the current and perspective on the future. In L. Nielsen (Ed.), *Advances in Geophysics,* 57, 51–146. http://dx.doi.org/10.1016/bs.agph. ISBN: 9780128095331

Place, J.A.P., Nejad Ghafar, A., Malehmir, A., Draganovic, A., Larsson, S., 2016. On using the thin fluid-layer approach at ultrasonic frequencies for characterising grout propagation in an artificial fracture. *International Journal of Rock Mechanics & Mining Sciences,* 89, 68–74.

Wang, S., Malehmir, A., and Bastani, M., 2016. Geophysical characterization of areas prone to quick-clay landslides using radio-magnetotelluric and seismic methods. *Tectonophysics*, 677-678, 248–260.

Malehmir, A., Andersson, M., Mehta, S., Brodic, B., Munier, R., Place, J., Maries, G., Smith, C., Kamm, J., Bastani, M., Mikko, H., and Lund, B., 2016. Post-glacial reactivation of the Bollnäs fault, central Sweden - a multidisciplinary geophysical investigation. *Solid Earth*, 7, 509–527.

Brodic, B., Malehmir, A., Juhlin, C., Dynesius, L., Bastani, M., and Palm, H., 2015. Multicomponent broadband digital-based seismic landstreamer for near surface applications. *Journal of Applied Geophysics,* 123, 227–241.

Malehmir, A., Zhang, F., Dehgahnnejad, M., Lundberg, E., Döse, C., Friberg, O., Brodic, B., Place, J., Svensson, M., and Möller, H., 2015. Planning of urban underground infrastructure using a broadband seismic landstreamer—Tomography results and uncertainty quantifications from a case study in southwest of Sweden. *Geophysics,* 80, B177–B192.

Bastani, M., Persson, L., Mehta, S., and Malehmir, A., 2015. Boat-towed radio-magnetotellurics (RMT)—a new technique and case study from the city of Stockholm. *Geophysics,* 80, B193–B202.

Abbaszadeh Shahri, A., Malehmir, A., and Juhlin, C., 2015. Soil classification analysis based on piezocone penetration test data — A case study from a quick-clay landslide site in southwestern of Sweden. *Engineering Geology,* 189, 32–47.

Malehmir, A., Wang, S., Lamminen, J., Brodic, B., Bastani, M., Vaittinen, K., Juhlin, C., and Place, J., 2015. Delineating structures controlling sandstone-hosted base-metal deposits using high-resolution multicomponent seismic and radio-magnetotelluric methods: a case study from Northern Sweden. *Geophysical Prospecting,* 63, 774–797.

10. PEER-REVIEWED CONFERNCE PUBLICATIONS

Brodic, B., Malehmir, A., Maries, G., 2017. SH- and surface-wave imaging potential of a 3C-digital-based seismic landstreamer illustrated at an esker site in SW Finland. EAGE Near Surface Geoscience, workshop on Geophysics in infrastructure planning, Malmö-Sweden, September 2017.

Malehmir, A., 2017. Geohazards and how geophysics can help. Geosciences applied to solve humanitarian problems all over the world, Belgrade-Serbia, May 2017.

Brodic, B., Lundberg, E., and Malehmir, A., 2017. Subsurface characterization of a cancerogenic contaminated site seismic methods in an urban setting in southwest Sweden. Geosciences applied to solve humanitarian problems all over the world, Belgrade-Serbia, May 2017.

Ronczk, M., Olsson, P.-I., Rossi, M., Malehmir, A., and Dahlin, T., 2017. Geophysical site investigation at Dalby-Önneslov using joint inversion. EAGE Near Surface Geoscience, Malmö-Sweden, September 2017.

Malehmir, A., Bergman, B., Andersson, B., Sturk, R., and Johansson, M., 2017. High-resolution seismic investigations of a geological energy-storage site: Dalby (Tornquist Zone), southwest Sweden. EAGE Near Surface Geoscience, Malmö-Sweden, September 2017.

Kammann, J., Bækgaard, J., Albrechtsen, C., Malehmir, A., and Nielsen, L., 2017.Seismic shear-wave acquisition parameters for characterization of chalk reservoir analogues. EAGE Near Surface Geoscience, Malmö-Sweden, September 2017.

Lähivaara, T., Pasanen, A., Malehmir, A., and Kaipio, J.P., 2017. Full-waveform seismic inversion for estimating aquifer dimensions and hydrologic parameters. EAGE Near Surface Geoscience, Malmö-Sweden, September 2017.

Brodic, B., and Malehmir, A., and Juhlin, C., 2017. Bedrock and fracture zone delineation using different near-surface seismic sources. EAGE Near Surface Geoscience, Malmö-Sweden, September 2017.

Mehta, S., Bastani, M., Malehmir, A., and Pedersen, L.B., 2017. CSRMT survey on frozen lake – A new technique with an example from the Stockholm bypass tunnel. EAGE Near Surface Geoscience, Malmö-Sweden, September 2017.

Malehmir, A., Maries, G., Bäckström, E., Schon, M., and Marsden, P., 2017. Deep targeting an iron-oxide ore body using a seismic landstreamer and a 500-kg drop hammer source. EAGE annual conference, Paris-France, June 2017.

Wang, S., Bastani, M., Kalscheuer, T., Malehmir, A., and Dynesius, L., 2017. Controlled source boat-towed radio-magnetotellurics for site investigation at Äspö Hard Rock Laboratory, southeastern Sweden. EAGE annual conference, Paris-France, June 2017.

Malehmir, A., Tryggvason, A., Wijns, C., Koivisto, E., Lindqvist, T., Skyttä, P., and Montonen, M., 2016. November 2016. Why 3D seismic data are an asset for both exploration and mine planning? Example of Kevitsa Ni-Cu-PGE, Finland. Lithosphere symposium, Helsinki-Finland, November 2016.

Brodic, B., Malehmir, A., and Juhlin, C., 2016. Rock mass and fracture characterization at Äspö HRL using tunnel-surface seismics. The underground space challenge, Kalmar, Sweden, October 2016.

Malehmir, A., Bastani, M., Brodic, B., Mehta, S., and Wang, S., 2016. Development and applications of a MEMs-based seismic landstreamer and a boat-towed radio-magnetotelluric system–tackling the urban environment. EAGE workshop on Urban Geophysics, Barcelona, Spain, September 2016.

Wang, S., Kalscheuer, T., Bastani, M., Malehmir, A., Pedersen, L.B., Dahlin, T., and Meqbel, N., 2016. Joint inversion of on-lake radio-magnetotelluric and lake-floor direct current

resistivity data and its applications. 23rd Electromagnetic Induction in the Earth Workshop, Chiang Mai, Thailand, August 2016.

Dehghannejad, M., Malehmir, A., Lundberg, E., Möller, H., and Svensson, M., 2016. High-resolution reflection imaging for the planning of a double train-track tunnel in the city of Varberg, Sweden. EAGE workshop on Near Surface Seismology, Vienna, Austria, May 2016.

Bazin, S., Sauvin, G., Dehghannejad, M., Lundberg, E., Lysdahl, A.K., Malehmir, A., Kveldsvik, V., Boge, K., and Pfaffhuber, A.A., 2016. Seismic and electrical resistivity investigations for the planning of a tunnel in Oslo outskirts. EAGE Near Surface Geoscience, Barcelona, Spain, September 2016.

Malehmir, A., Tryggvason, A., Wijns, C., Lindqvist, T., Skyttä, P., Koivisto, E., and Montonen, M., 2016. 3D traveltime tomography and reflection imaging for mine planning and exploration in the Kevitsa Ni-Cu-PGE mine, Finland. EAGE Near Surface Geoscience, Geophysics on Mineral Exploration and Mining, Barcelona, Spain, September 2016.

Salas-Romero, S., Malehmir, A., and Snowball I., 2016. Combined land and river high-resolution reflection seismic imaging of an area prone to quick-clay landslides in Sweden. EAGE Near Surface Geoscience, Barcelona, Spain, September 2016.

Ahokangas, E., Maries, G., Mäkinen, J., Pasanen, A., and Malehmir, A., 2016. Seismic imaging of esker sediments within the Satakunta sandstone depression in Köyliö, SW Finland. EAGE Near Surface Geoscience, Barcelona, Spain, September 2016.

Bastani, M., Wang, S., and Malehmir, A., 2016. Boat-towed RMT measurements on the water surface over the Äspö Hard Rock Tunnel in Sweden. EAGE Near Surface Geoscience, Barcelona, Spain, September 2016.

Brodic, B., and Malehmir, A., and Juhlin, C., 2016. Fracture system characterization using wave-mode conversions and tunnel-surface seismics. EAGE Near Surface Geoscience, Geophysics on Mineral Exploration and Mining, Barcelona, Spain, September 2016.

Malehmir, A., Brodic, B., Dehgahnnejad, M., Juhlin, C., and Lundberg, E., 2016. A state-of-the-art MEMs-based 3C seismic landstreamer for various near-surface applications. EAGE workshop on Near Surface Seismology, Vienna, Austria, May 2016.

Place, J., and Malehmir, A., 2016. Using Super-virtual First Arrivals for Improving the Seismic Imaging of Deep Deposits - Well Worth the Effort. DGG-EAGE workshop on Deep Mineral exploration: chasing both land and sea deposits, Münster, Germany, March 2016.

Malehmir, A., Lundberg, E., Dehgahnnejad, M., Zhang, F., Friberg, O., Brodic, B., Döse, C., Place, J., Svensson, M., and Möller, H., 2015. Varberg: Developing urban geophysical instruments and methods – Pushing the boundaries. Grundläggningsdag (Foundation Day), Stockholm, Sweden, 15 pages.

Malehmir, A., Lundberg, E., Dehgahnnejad, M., Zhang, F., Friberg, O., Brodic, B., Döse, C., Place, J., Svensson, M., and Möller, H., 2015. Seismic landstreamer for planning of infrastructure projects – A case study from Varberg. Bergmekanikdagen (Rock Mechanic Day), Stockholm, Sweden, 15 pages.

Bastani, M., Malehmir, A., Saavaidis, 2015. Combined use of controlled-source and radio-magnetotelluric methods for near surface studies. Expanded abstract, 4 pages, ASEG 2015. Perth, Australia.

Wang, S., Bastani, M., Malehmir, A., 2014. Integrated use of Radio-Magnetotelluric and High-Resolution Reflection Seismic data to delineate near surface structures – two case studies from Sweden. 22nd EM Induction workshop, Weimar, Germany.

Malehmir, A., Wang, S., Lamminen, J., Bastani, M., Juhlin, C., Vaittinen, K., Dynesius, L., and Palm, H., 2014. High-resolution multicomponent hardrock seismic imaging of mineral deposits and their host rock structures. Expanded abstract, 3 pages, *EAGE 2014*, Amsterdam, Netherlands.

11. Appendixes

All the publications are available upon request. Write your requests for the publications and data sharing to alireza.malehmir@geo.uu.se. These publications are attached to this report:

- SBUF flyer (mid-project), NR 16:24.
- Brodic, B., Malehmir, A., and Juhlin, C., 2017. Delineating fracture zones using surface-tunnel-surface seismic data, P-S and S-P mode conversions. *Journal of Geophysical Research Solid Earth,* 122. http://dx.doi.org/10.1002/2017JB014304.
- Brodic, B., Malehmir, A., Bastani, M., Mehta, S., Juhlin, C., Lundberg, E., and Wang, S., 2017. Multi-component digital-based seismic landstreamer and boat-towed radio-magnetotelluric acquisition systems for improved subsurface characterization in the urban environment. *First Break*, 35(8), 41–47.
- Brodic, B., Malehmir, A., Juhlin, C., Dynesius, L., Bastani, M., and Palm, H., 2015. Multicomponent broadband digital-based seismic landstreamer for near surface applications. *Journal of Applied Geophysics,* 123, 227–241.

Landstreamer-system för seismiska markundersökningar i urbana miljöer

En landstreamer har utvecklats av Uppsala Universitet med syfte att förbättra seismiska mätningar i utmanande miljöer såsom städer, tunnlar och gruvor där elektriskt brus och logistiska utmaningar är vanligt förekommande. Landstreamern har testats vid flera infrastrukturprojekt och i tunnel- och gruvmiljöer. Resultaten visar att metoden har stor potential och att landstreamerns sensorer är mindre känsliga för elektriskt brus. I kombination med trådlösa enheter kan landstreamern användas på ett effektivt sätt också i komplicerade situationer.

Bakgrund

Seismiska metoder ger högupplösta bilder av jordens inre. Seismiskt data tillhandahåller geometrisk information om geologiska strukturer, men också om fysikaliska egenskaper. I vanliga seismiska mätningar måste sensorerna placeras fast i marken. Detta är ofta en av de mest tidskrävande delarna av en fältmätning. Detta gäller särskilt om sensorerna måste flyttas flera gånger under mätningarna, vilket ofta är fallet. I stadsmiljöer är fast placering av sensorer besvärlig på grund av att markunderlaget ofta består av asfalt. Dessutom kan det vara logistiskt utmanande att mäta profiler över stora vägkorsningar eller järnvägsspår.

Syfte

Ett ökat behov av markundersökningar i urbana miljöer har kommit tack vare stora satsningar på avancerade infrastrukturprojekt såsom till exempel omfattande tunnelbyggen. För att överkomma svårigheter vid seismiska mätningar i urbana miljöer har en modern landstreamer utvecklats vid Uppsala Universitet. En seismisk landstreamer är en array av sensorer monterade på slädar som sitter ihop. Dessa behöver inte placeras fast i marken och kan därför dras, till exempel efter en bil, och kan därmed flyttas snabbt och effektivt (Fig. 1).

Den nuvarande konfigurationen av landstreamern på Uppsala Universitet består av fem segment med sammanlagt 100 trekomponents-sensorer placerade på 2-4 meters avstånd och med en total längd på 240 meter. Sensorerna är baserade på så kallad MEMS-teknik (Mikroelektromekaniska system) vilket gör dem mindre känsliga för elektriskt brus. Landstreamern kan också användas tillsammans med trådlösa enheter. Detta ger stor flexibilitet där svårpasserade glapp kan överbryggas (till exempel stora vägkorsningar eller järnvägsspår). Landstreamern tillsammans med de trådlösa enheterna har stora fördelar i stadsmiljöer tack vare (i) låg känslighet för elektriskt brus (ii) ingen fast placering av sensorer i marken (iii) flexibilitet i utmanande trafikmiljöer.

Figur 1. Landstreamern dras av en bil längs en grusväg och trådlösa enheter är placerade vid sidan av vägen.

SVENSKA BYGGBRANSCHENS UTVECKLINGSFOND
The Development Fund of the Swedish Construction Industry

Besök: Storgatan 19
Postadress: Box 5501, SE114 85 Stockholm
Tel: +46 8 783 81 00
Internet: www.sbuf.se, Email: info@sbuf.se

Genomförande

Med stöd från SBUF och andra samarbetspartners inom TRUST (Transparent Underground STructure) har landstreamern testats på flera platser och i olika miljöer i både Sverige, Norge och Finland. Dessutom har flera tester gjorts hemmavid för att utveckla och testa olika seismiska källor. De skarpa projekten där landstreamern har använts innefattar flera områden (i) infrastrukturprojekt såsom Förbifart Stockholm, Varberg tunnel och Oslo E18, Norge (ii) mineralprospektering och gruvplanering i Laisvall, Ludvika och Malmberget och Siilinjärvi, Finland (iii) kontaminerad mark i Kristianstad (iv) vattenresurser i Åbo, Finland (v) geologiska utforskningar i Mora, Bollnäs och Åspö.

Resultat

I Varberg mättes 25 profiler i stadsmiljö för att undersöka djup till berggrund och hitta eventuella sprickzoner i berget. Ett flertal borrhål kunde användas för att korrelera djup till berg. I Figur 2 visas resultatet av dessa mätningar i form av tolkat djup till berg baserat

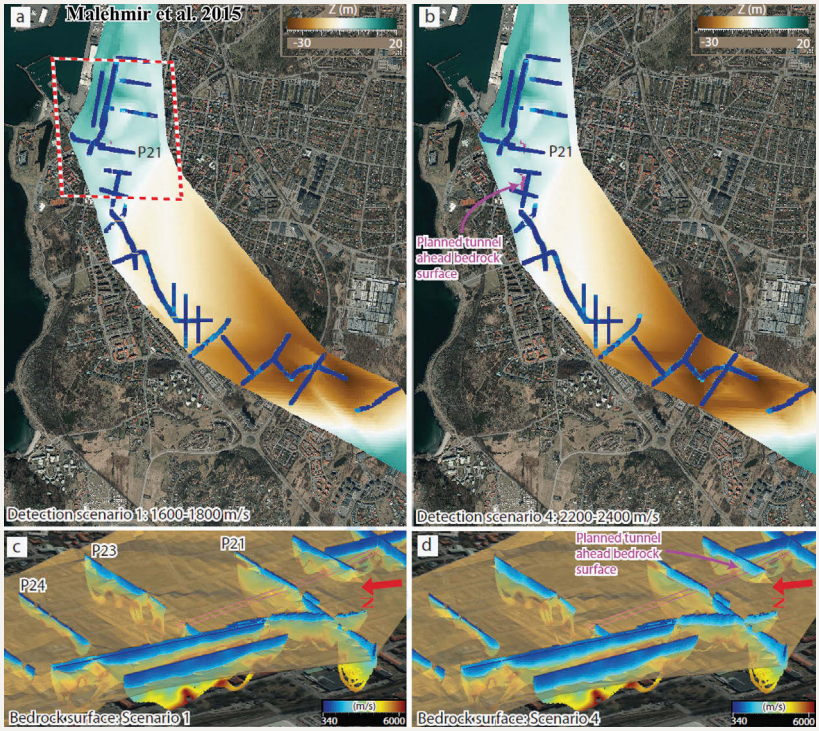

Figur 2. Sesmiska mätningar i Varberg inför ett planerat tunnelbygge. Två scenarion för djup till berggrund redovisas i a) och b). Berggrundsytan har hämtats från de berghastighetsmodeller som visas I c) och d). Det planerade tunnelspåret syns i c) och d) markerat med lila linjer.

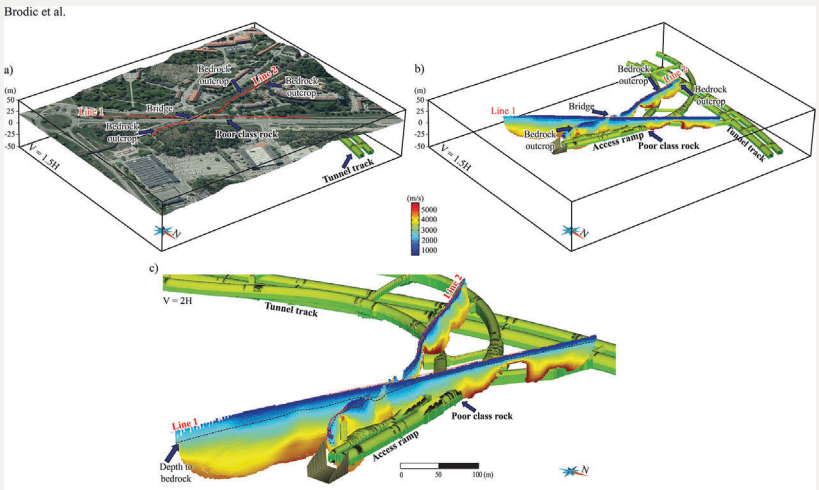

Figur 3. Seismiska mätningar vid en accessramp till Förbifart Stockholm. Berghastighetsmodellen visar lägre hastigheter i berget där planerade tunneln skär profilen. Detta kan indikera en lägre bergkvalitet i detta område.

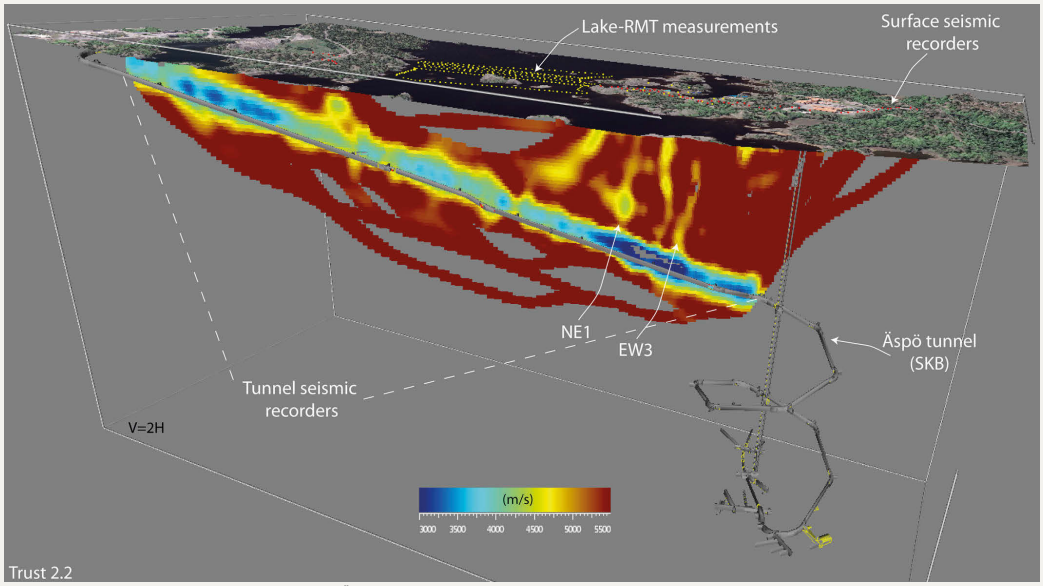

Figur 4. Koordinerade mark och tunnelmätningar i Äspö. Berghastighetsmodellen visar flera zoner (i grönt/gult) med lägre hastighet än omgivande berg (i rött) vilka kan relateras till kända deformationszoner i berget.

på hastighetsmodeller framtagna ur det seismiska mätningarna. Flera potentiella deformationszoner kunde också identifieras från de seismiska mätningarna och dessa jämfördes senare med resultat från andra geofysiska mätningar och från borrningar.

Under seismiska markundersökningar i Förbifart Stockholm mättes två profiler över en planerad accessramp. Resultaten visar på låga hastigheter i berget där tunneln skär profilerna, vilket kan indikera låg bergkvalitet och uppsprucket berg (se Figur 3).

I Äspö testades möjligheten att genomföra koordinerade seismiska mätningar på land och i tunnel. Sensorer placerades i tunneln och på land ovanför tunnelsträckningen och sedan aktiverades den seismiska källan både i tunneln och på landytan. Äspötunneln valdes som testplats eftersom flera kända deformationszoner skär tunneln. Resultaten visar att de seismiska mätningarna effektivt identifierar flera låghastighetszoner som kan relateras till de kända deformationszonerna. I figur 4 syns dessa zoner som gulgröna områden med lägre berghastighet än omgivande berg (i rött).

Slutsatser

En trekomponents MEMs-baserad landstreamer har utvecklats för att förbättra möjligheterna att genomföra högkvalitativa seismiska mätningar i urbana miljöer. Landstreamerns konfiguration tillsammans med trådlösa enheter har visat sig ge stor flexibilitet i urbana miljöer. Dessutom ger de MEMs baserade sensorerna en bättre signal än konventionella geofoner i miljöer med omfattande elektriska störningar. Detta gör landstreamern till ett effektivt verktyg för seismiska markundersökningar i framförallt stadsmiljöer, tunnlar och gruvor, men också för andra ändamål.

Ytterligare information

Kontaktpersoner:

Alireza Malehmir, Uppsala Universitet, tel 018-4712335, e-post: Alireza.Malehmir@geo.uu.se.

Litteratur:

- Multicomponent Broadband Digital-Based Seismic Landstreamer for near-Surface Applications. - Brodic, Bojan, Alireza Malehmir, Christopher Juhlin, Lars Dynesius, Mehrdad Bastani, and Hans Palm. 2015. *Journal of Applied Geophysics* 123 (December): 227–41. doi:10.1016/j.jappgeo.2015.10.009.
- Delineating Structures Controlling Sandstone-Hosted Base-Metal Deposits Using High-Resolution Multicomponent Seismic and Radio-Magnetotelluric Methods: A Case Study from Northern Sweden. - Malehmir, Alireza, Shunguo Wang, Jarkko Lamminen, Bojan Brodic, Mehrdad Bastani, Katri Vaittinen, Christopher Juhlin, and Joachim Place. 2015. *Geophysical Prospecting* 63 (4): 774–97. doi:10.1111/1365-2478.12238.
- Planning of Urban Underground Infrastructure Using a Broadband Seismic Landstreamer — Tomography Results and Uncertainty Quantifications from a Case Study in Southwestern Sweden. - Malehmir, Alireza, Fengjiao Zhang, Mahdieh Dehghannejad, Emil Lundberg, Christin Döse, Olof Friberg, Bojan Brodic, Joachim Place, Mats Svensson, and Henrik Möller. 2015. *GEOPHYSICS* 80 (6): B177–92. doi:10.1190/geo2015-0052.1.
- Multicomponent digital-based seismic land-streamer for urban underground infrastructure planning.- Brodic, Bojan. 2015. Licentiate thesis. Uppsala: Uppsala University, Department of Earth Sciences, 2015, 39 p.

Internet:

http://trust-geoinfra.se/delprojekt/2-2/index.html

Journal of Applied Geophysics 123 (2015) 227–241

Contents lists available at ScienceDirect

Journal of Applied Geophysics

journal homepage: www.elsevier.com/locate/jappgeo

Multicomponent broadband digital-based seismic landstreamer for near-surface applications

Bojan Brodic [a,*], Alireza Malehmir [a], Christopher Juhlin [a], Lars Dynesius [a], Mehrdad Bastani [b], Hans Palm [a]

[a] Department of Earth Sciences, Uppsala University, Villavägen 16, SE 75236, Uppsala, Sweden
[b] Geological Survey of Sweden, Villavägen 18, Box 670, SE 75128, Uppsala, Sweden

ARTICLE INFO

Article history:
Received 3 March 2015
Received in revised form 15 September 2015
Accepted 12 October 2015
Available online 19 October 2015

Keywords:
Landstreamer
MEMS
Tomography
Near-surface
Urban environment

ABSTRACT

During the last few decades there has been an increased demand for infrastructure, along with a greater awareness of environmental issues in the construction industry. These factors have contributed to an increased interest in using seismic methods for near surface characterization, particularly in urban environments. Seismic sensors not affected by anthropogenic electromagnetic noise are therefore important, as well as an acquisition system that is easy to deploy, move and non-invasive. To address some of these challenges, a multicomponent broadband MEMS (micro-electro mechanical system) based landstreamer system was developed. The landstreamer system is fully digital, therefore it is less sensitive to electrical or electromagnetic noise. Crosstalk, leakage and tilting tests show that the system is superior to its predecessors. The broadband nature of the sensors (theoretically 0–800 Hz), 3C (three-component) recording and the close spacing of the sensors enable high-resolution imaging. The current streamer configuration consists of 20 sensors 4 m apart and 80 sensors 2 m apart. The streamer can easily be combined with wireless recorders for simultaneous data acquisition. In this study, we present results from testing of the streamer with various sources, such as a shear wave vibrator and different types of impact sources. MEMS-sensors and their high sensitivity allowed recording clear reflections that were not observed with coil-based sensors. A complementary test was also carried out at a planned access ramp for an urban tunnel where potential poor quality rocks had been identified by drilling. First-break traveltime tomography showed that these poor quality rocks correlate with low velocity zones. The presented landstreamer system has great potential for characterizing the subsurface in noisy environments.

1. Introduction

Population growth with an increased demand for infrastructures, along with environmental considerations, motivate the need for better understanding of near surface geological conditions. In the last two decades, seismic method has became a common tool for shallow subsurface characterization, where new techniques and processing approaches have been developed (Bachrach and Nur, 1998; Bansal and Gaiser, 2012; Bretaudeau et al., 2008; Fabien-Ouellet and Fortier, 2014; Guy, 2004; Keho and Kelamis, 2009; Krawczyk et al., 2013; Malehmir et al., 2013a,b; Miller et al., 1986; Paasche et al., 2013; Polom et al., 2013; Pugin et al., 2004a,b, 2009, 2013a,b; Steeples and Miller, 1998; Steeples, 2004). Characterizing the shallow subsurface is particularly challenging in urban areas where anthropogenic noise, such as from power lines or traffic, among others, are present (Baker, 1999; Keho and Kelamis, 2009; Krawczyk et al., 2012; Polom et al., 2013; Pugin et al., 2004b; Steeples and Miller, 1998). In these environments, conventional planting of geophones is rarely possible and if several kilometers of seismic lines are to be acquired, with a limited number of channels, the whole spread has to be moved many times. Therefore, it is advantageous if the acquisition system is portable and geared for such conditions. To cope with all these issues, Uppsala University has developed a prototype 3C MEMS-based seismic landstreamer.

We can define a landstreamer as an array of sensors that can be pulled along the surface without the need for planting (Inazaki, 1999; Kruppenbach and Bedenbender, 1975; Suarez and Stewart, 2007). Eiken et al. (1989) applied the concept of towing a receiver array over land in the form of a snowstreamer and their work summarizes the preceding studies. The idea itself originates from the marine seismic industry and following the snowstreamer design, many authors have reported the usage of a towed land cable in various places and environments (Almholt et al., 2013; Determann et al., 1988; Huggins, 2004; Inazaki, 1999, 2004, 2006; Krawczyk et al., 2012; Link et al., 2006; Polom et al., 2013; Pugin et al., 2004a,b, 2009, 2013a,b; Pullan et al., 2008; Suarez and Stewart, 2007, 2008a; van der Veen et al., 2000, 2001; van der Veen and Green, 1998). Most of the reported studies

* Corresponding author at: Uppsala University, Villavägen 16, office EK221, SE 75236, Uppsala, Sweden.
E-mail addresses: bojan.brodic@geo.uu.se (B. Brodic), alireza.malehmir@geo.uu.se (A. Malehmir), christopher.juhlin@geo.uu.se (C. Juhlin), lars.dynesius@geo.uu.se (L. Dynesius), mehrdad.bastani@sgu.se (M. Bastani), hans.palm@geo.uu.se (H. Palm).

http://dx.doi.org/10.1016/j.jappgeo.2015.10.009

have been conducted with data acquisition systems that use different types of geophones, typically coil-based (Huggins, 2004). Although coil-based sensors dominate the market nowadays, numerous disadvantages have been noted during the half a century of their usage, among which one can mention electromagnetic (EM) noise pickup, limited bandwidth and sensitivity to tilting, especially for high-resolution and multicomponent imaging (Bansal and Gaiser, 2012; Deidda and Ranieri, 2001; Inazaki, 2004; Malehmir et al., 2013b; Pugin et al., 2004b). The bandwidth limitation is also becoming a more prominent issue in the field of full waveform inversion, where low frequencies are of interest (Adamczyk et al., 2014; Sirgue et al., 2010; Zhang et al., 2013). The same applies to surface-wave analysis of active seismic data (Fabien-Ouellet and Fortier, 2014; Lai et al., 2002; Park et al., 2002, 1999; Socco et al., 2009, 2010; Socco and Garofalo, 2012; Socco and Strobbia, 2004; Xia et al., 2003). In general, using geophone-type sensors, one either sacrifices low frequencies for obtaining high-resolution images of the subsurface or employs low-frequency geophones for surface-wave and/or full-waveform inversions. Aforesaid limitations, along with others (see Kendall, 2006; Mougenot and Thorburn, 2004), motivated the MEMS-based seismic landstreamer developed in this study. This is, to best of our knowledge, the first time that such a state-of-the-art landstreamer is presented and its reliability and potentials are illustrated.

We have assembled our landstreamer and tested it in various environments. Here we report results from two tests in our department's backyard in Uppsala and one from Stockholm where a large underground bypass tunnel is planned to be constructed within the next few years. Other studies with the system have also been carried out (and several others currently on-going; e.g. Malehmir et al., 2015). The recording abilities of the system have been tested using explosives as a seismic source, different size impact sources and a shear wave vibrator. In this paper, our main goal is to present separate studies conducted to validate the capability and reliability of the system for near surface applications. These include:

- comparison of the signals recorded with the landstreamer mounted MEMS-based sensors versus two planted lines with geophones of different resonance frequencies to check for potential unwanted issues of the streamer assembly and its signal quality;
- combination of wireless recorders with the streamer system to obtain information in areas where towing the streamer, or even planting geophones, was impossible;
- analysis of the frequency characteristics and shot gathers of the streamer recorded signal using a mini S-wave vibrator with different sweep ranges for near surface applications.

2. Fully digital multicomponent landstreamer

As a part of an academia-industry partnership project, a 3C MEMS-based seismic landstreamer was developed. The essential difference between the existing landstreamers (e.g., Huggins, 2004) and the one we present here is the digital nature of the sensors, implying fully digital data transmission. It is also much lighter and does not require several cables to power the line and transmit the data to an acquisition system. MEMS sensors measure ground motion as acceleration using a silicon chip with an approximate length of 1 cm, where the residual displacement between the inertial mass and the frame within the chip is on the order of a few nanometers (Gibson et al., 2005; Hons, 2008; Laine and Mougenot, 2014). One of the key benefits of the MEMS sensors is in their broadband linear amplitude and phase response, which allows recording frequencies from 0 to 800 Hz without attenuation (Hauer et al., 2008; Hons et al., 2007; Lawton et al., 2006a; Mougenot et al., 2011; Mougenot and Thorburn, 2004; Stotter and Angerer, 2011). Their resonant frequency (1 kHz) enables recording direct current related to gravity acceleration by which the gravity vector can be used for sensitivity calibration and tilt measurements (Gibson et al., 2005; Kendall, 2006; Mougenot and Thorburn, 2004). A fundamental difference between MEMS sensors and geophones is in their performances. MEMS are designed to work below their resonance frequencies (e.g., below 1000 Hz) while geophones are designed to work above their resonance frequencies (e.g., generally above 4.5–40 Hz). Detailed studies have been conducted in the last decade comparing MEMS with different types of geophones and summarizing their pros and cons (e.g., Alcudia et al., 2008; Hauer et al., 2008; Hons et al., 2007; Hons, 2008; Laine and Mougenot, 2014; Lawton et al., 2006a; Mougenot et al., 2011; Stotter and Angerer, 2011; Suarez and Stewart, 2007, 2008a,b).

We aimed for a relatively light and portable data acquisition system that can be easily deployed, towed by any 2WD or 4WD (2 or 4 wheel drive) vehicle, combined with wireless units that are GPS time stamped (nanosecond accuracy), and used for a variety of applications and field situations. A great amount of time was spent to engineer the base plates "sleds" and materials holding the sensors (Fig. 1a, b). The sensors have been mounted on a non-stretchable belt used in the aircraft industry as cargo straps (Fig. 1b). The sleds weigh approximately 5 kg and with the sensors mounted on them provide excellent gravity based ground coupling (Fig. 1b). To avoid purchasing several telemetric data acquisition units (typically supporting 24 channels or nowadays 48), a decision was made to make the landstreamer based on the Sercel Lite technology and Sercel DSU3 sensors (MEMS-based mounted on the landstreamer). It is important to note that Sercel DSU3 sensors have a noise floor of 40 ng/Hz$^{1/2}$, which is approximately four times higher compared to conventional geophones (Gibson and Burnett, 2005; Hons, 2008; Laine and Mougenot, 2014; Merchant, 2009). The system architecture and the possibility to use up to 1000 active channels along with the Sercel Lite software represent an up-to-date standard in the seismic recording industry. In addition, the system provides sophisticated recording capabilities, such as supporting both geophone-type and MEMS-based sensors (but also hydrophones). Even though DSU3 sensors and the selected recording system are fairly expensive, obtaining the same amount of active channels with commonly used geophone-type telemetric data acquisition systems would require quite a number of them (e.g., 12–15 to come up with the same configuration as the streamer developed in this study). This fact, along with the 3C digital nature of the sensors, and the variety of possible field applications, make our landstreamer relatively comparable in terms of cost with existing telemetric data acquisition systems. With GPS being used for time stamping and data sampling, the system enables both passive and active data acquisition and their combination as well.

The current configuration of the landstreamer (September 2015) consists of five segments of 20 sensors each. Every segment connects to the next by a small trolley carrying a line-powering unit as shown by the red arrow in Fig. 1c. Four segments are of 20 units with 2 m spacing each, and the fifth consists of 20 units 4 m apart. The spacing of the units can be easily reduced in necessity of ultra-high resolution imaging. If longer offsets (than the overall streamer length of 240 m) are required, to obtain deeper penetration depth or imaging steeply dipping structures, wireless recorders (connected to geophones or MEMS-based sensors) can be used in combination. Wireless recorders can also be used to cover areas difficult to access with the streamer (an example of this set up is shown later in the paper). Table 1 summarizes the main characteristics of the streamer and compares it with the most commonly available ones.

In normal field conditions, data acquisition starts after approximately 1 h upon arrival to the site, with a team of 3 to 4 persons for the setup. Data acquisition rates have so far been varying from 600 m to 1200 m/day seismic line, using source and receiver spacings of 2 to 4 m. The shooting usually begins at the end of the spread and advances towards the beginning (where the observer sits in the towing vehicle). After recording all shot locations, the whole spread is moved forward to the next position. The last segment (20 units,

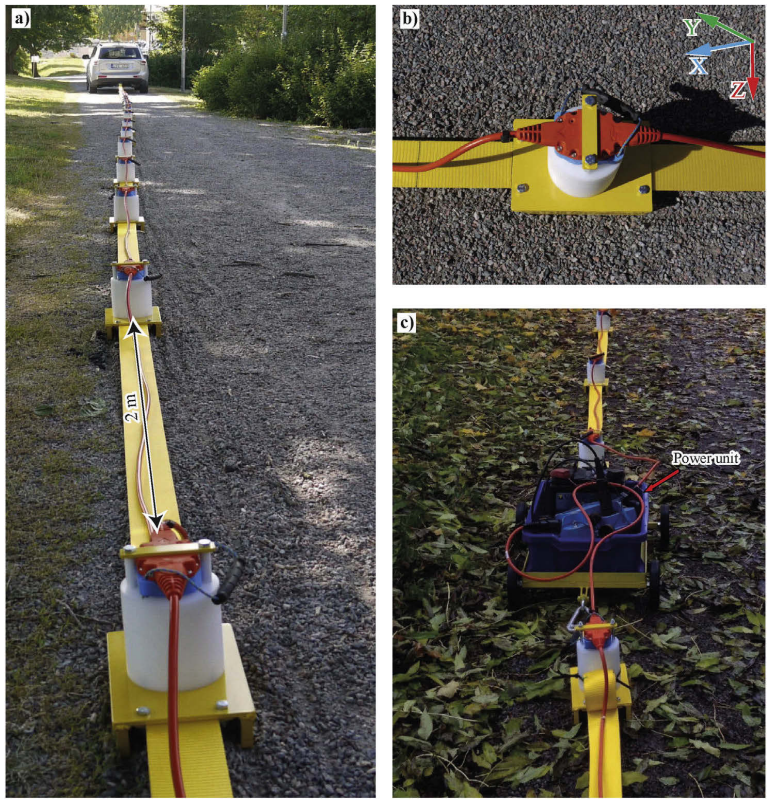

Fig. 1. (a) MEMS-based seismic landstreamer developed in this study towed by a relatively light vehicle. (b) A close-up showing the installation of the 3C sensor on the sled. (c) Small carriage connecting different segments (typically 20 sensors 2–4 m apart per segment) of the landstreamer carrying also a power unit. Photos were taken as a part of Backyard tests in Uppsala, Sweden at the early stage of the development of the streamer.

4 m spaced) often overlaps a portion of the previous landstreamer position allowing improved data coverage at the edge of each spread location and more favorable offsets if dipping structures are present.

3. Case studies

We have conducted several tests and contracted surveys since the streamer was actually assembled in June 2013, using different sources and in different weather conditions. This paper deals with three specific test studies that will be introduced and discussed. Tests I and II (referred here as Backyard tests) were carried out in an open field in the early development stages of the streamer in the department's backyard at Uppsala University. The aim was to check the general reliability of the system. Test III was carried out in the northern outskirts of the city of Stockholm as a part of a major planned underground infrastructure project referred as the Stockholm Bypass (www.trafikverket.se/forbifartstockholm).

Table 1
Summary of the properties of the landstreamer system developed in this study.

Parameters	Developed in this study	Existing landstreamers
Sensor type	3C MEMS-based	Geophones (1C or 3C)
Frequency bandwidth	0–800 Hz	4.5–400 Hz
Tilt measurement	Recorded in the header	Not possible
Acquisition system	Sercel Lite (MEMS + geophones)	Most commonly Geometrics Geode (geophones only)
Max number of channels	1000	24 (per unit)
Sensor spacing	Adjustable 0.2–4 m	Adjustable
Cabling	Single	Several
Data transmission	Digital	Analog
Data format	SEGD	SEG2
GPS time	Recorded in the header	Often not possible

3.1. Backyard tests

The developed landstreamer benefits from constant improvements made by experiences from previous tests and surveys. Ease of access, well-known geology and almost no survey logistics in our department's backyard were ideal for checking different characteristics of the system at different development stages (Figs. 1, 2a). Geologically, this test site is located on an esker structure that consist of approximately 10–25 m of post-glacial sediments, typically fine-grained clays mixed with glacial tills, comprising the top most part of the esker. Deeper down there are coarse-grained materials overlaying granitic bedrock (Heijkenskjöld, 2001; Lundin, 1988).

3.1.1. Test I — Reliability and advantages of the MEMS-based landstreamer

After assembling the first segment of the streamer of 20 DSU3 sensors spaced 2 m apart in July 2013, it was tested against two lines of 20 planted coil-based geophones (10 Hz and 28 Hz resonance

Fig. 2. Photos showing details of the landstreamer versus planted geophones test. (a) Landstreamer was located in the middle of two planted geophone-type (10 Hz on the right-hand and 28 Hz on the left-hand side) lines. Note the difference in cabling involved for the planted lines and the streamer-mounted units. A sledgehammer was used as the seismic source in this study. (b) Side-by-side comparison between planted and streamer mounted 3C (DSU3, MEMS-based) sensors. This test was done to study different characteristics of the seismic wavefield registered on the streamer mounted sensors and if the sleds have some noticeable effects on the wavefield especially the horizontal components. A Bob-cat drop hammer was used as the seismic source in this study.

frequencies) with the same spacing. The aim was to compare the data quality recorded using DSU3s mounted on the landstreamer with the data recorded using the two planted geophone lines (Fig. 2a) and check for potential unwanted issues caused by the overall streamer assembly. The three lines were placed along a gravel bicycle-road; the same acquisition system was used enabling simultaneous recording of all the sensors for the three different line setups. First the assembled streamer segment was towed by a 4WD vehicle to a desired position; then aligned with the streamer sensors, vertical component geophones were planted on each side of the streamer (Fig. 2a; left side 28 Hz, 7 cm spike geophones, right side 10 Hz 7 cm spike geophones). We used a 5-kg sledgehammer as the seismic source. Shots were positioned at every streamer station and at each shot position we recorded 4 hits. These shot records were then vertically stacked to improve the signal to noise ratio. Shot gather quality of all three seismic lines was visually inspected, along with their amplitude spectra, especially for the vertical components. Due to unavailability, no planted horizontal component geophones were used, however, data recorded with the horizontal components of the DSU3s will be shown.

To enable a physically and mathematically correct data comparison, the geophone data need to be differentiated (or the DSU3 data integrated), implying that the comparison should be done in the same domain, either velocity or acceleration (Hons et al., 2007; Hons, 2008; Laine and Mougenot, 2014; Lawton et al., 2006a; Mougenot, 2014, personal communication). Since commercially available landstreamers are geophone based we choose to show the integrated DSU3 data, hence do the comparison in the velocity domain.

To complement the test, a separate study was conducted using 12-planted DSU3 sensors next to 12-streamer mounted DSU3 sensors on a site in south-west Finland (Fig. 2b). This was done to check for possible phase and time differences introduced by the sleds, especially for the horizontal components. Shots were fired along the whole landstreamer length at a 4 m interval, while this set-up was in place. For these data a Bobcat-mounted drop hammer was used as seismic source (Place et al., 2015; Sopher et al., 2014). We present the data for trace-to-trace comparison between the planted and streamer sensors, after removing all the landstreamer sensors that had no accompanying planted pair. The approximately 50 m thick glacial and post-glacial sediments (confirmed by drilling; Jöni Mäkinen, 2014, personal communication) make this site favorable for this comparison since it is unlikely that any significant near surface geological effects will be present in the particle motions of the different phases.

3.1.1.1. Results. An example shot gather (after vertical stacking of the repeated shot records) presenting a comparison of the data from the two planted lines, with 10 and 28 Hz vertical geophones, and all three components (vertical and horizontal inline and crossline) of the landstreamer, with their corresponding amplitude spectra is shown in Fig. 3a, b, c, d, e. Fig. 3f, g shows an overlay of all the vertical component amplitude spectra with both DSU3 non-integrated and integrated data, scaled (Fig. 3f) and unscaled (Fig. 3g). All the amplitude spectra were calculated without using the three nearest-offset traces to minimize source noise contamination and the minor offset between the sensors on all three lines (the sensor pairs were located within 0.5 m radius). Some coherent features may be noted on almost all these data (shown by the red arrows), including the horizontal inline component of the DSU3 sensors. Horizontal component data have a time scale that is half that of the vertical component data to better compare the events marked by the red arrows. Based on the clearly observed reflection in the DSU3 vertical components (shown by the red arrow in Fig. 3c), it appears that the sensors mounted on the landstreamer recorded higher quality data compared with the geophones used here. Note that the reflection shown by the red arrow on Fig. 3a, c is not even observed on the 28 Hz geophones (Fig. 3b), which appears to be strongly contaminated

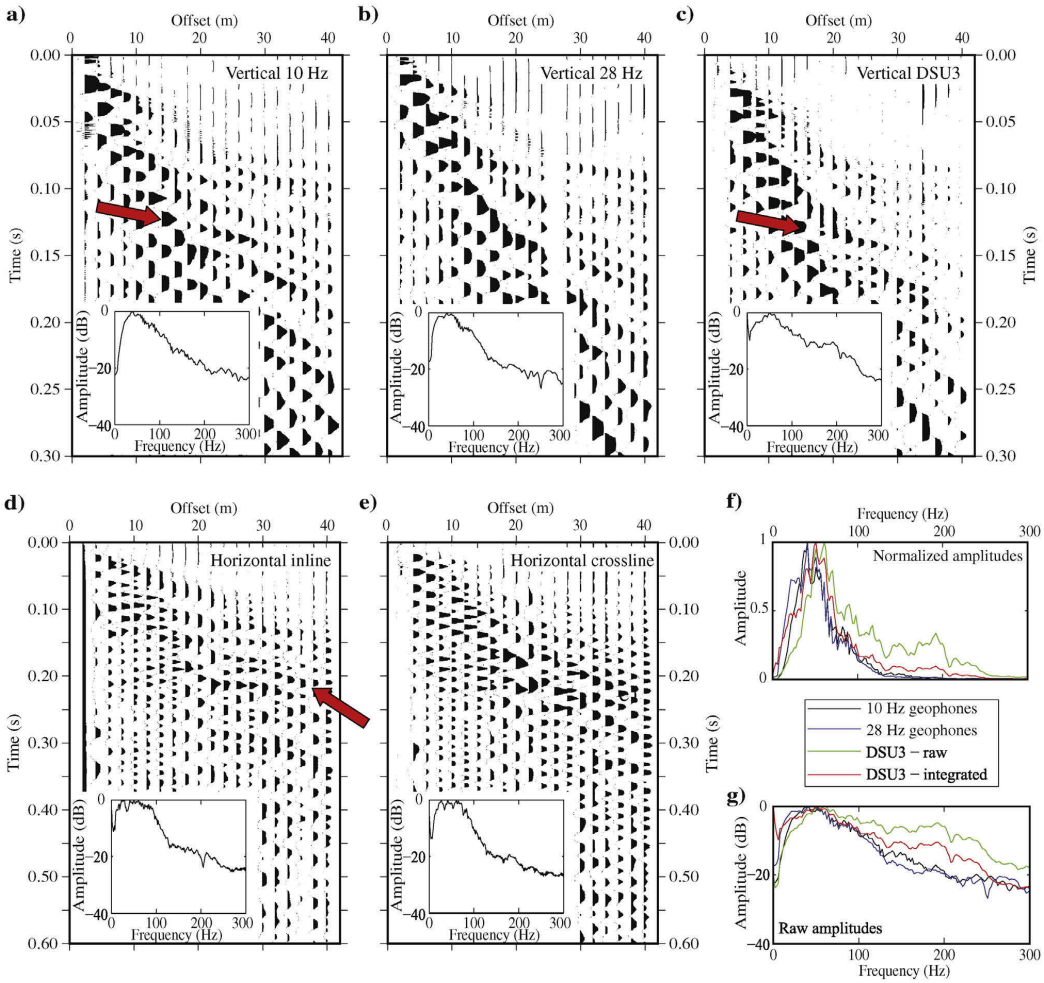

Fig. 3. An example shot gather (after vertical staking of three repeated shots) with the corresponding amplitude spectra from the first backyard test shown for (a) 10 Hz planted geophones, (b) 28 Hz planted geophones, (c) vertical component of the DSU3 sensors from the streamer, (d) horizontal inline component of the DSU3 sensors from the streamer and (e) horizontal crossline component of the DSU3 sensors from the streamer. (f) and (g) show amplitude spectra of all vertical components overlaid, normalized and raw, respectively, along with DSU3 vertical before and after integration. Note that MEMS data (acceleration) have been integrated to provide comparable data to the geophones (velocity) and the amplitude spectra calculated without three traces closest to the shot. AGC has been applied (100 ms window) for display purposes.

by surface waves. After integration, an amplitude increase of surface waves on the vertical component of the DSU3 sensors is generally observed (Hons et al., 2007; Hons, 2008, also notable from Fig. 3f, g), but in our case not as significant as to mask the reflection signal.

Fig. 4 shows an example shot gather from the side-by-side comparison of the planted and streamer mounted MEMS-based sensors (Fig. 2b). Here we also present particle motion plots (hodograms) of various wave types to judge if the sleds introduced suspicious particle motion. Particle motion plots from the noise part of the data (time window above the first arrivals) show slightly higher directionally dependent energy polarization on the horizontal crossline component while the other components have a more random character. This is likely due to wind and the wider nature of the frame holding the streamer sensor (acting as a barrier against wind; Fig. 1b) in this orientation. Otherwise, visual inspection of the particle motion plots does not suggest any significant distortion introduced by the sled. Examination of the trace pairs of all components show identical phases with similar shape and arrival time, with a minor distortion on near offset traces of the horizontal crossline component that will be discussed later.

3.1.2. Test II — Micro shear wave vibrator test

To further explore the capabilities of the landstreamer, we also carried out a test using the micro shear wave vibrator — ELViS (Electro-dynamic Vibrator System; Krawczyk et al., 2012, 2013; Polom et al., 2011, 2013). The small size of the source, its easy handling, high signal reproducibility, no ground damage and low noise level make it attractive to be used with the streamer developed in this study, especially for urban applications. Example field photos from this test are shown in Fig. 5. ELViS version 3 (with a mounted horizontal shaker unit) enables generation of horizontally polarized (SH) seismic energy (see the green arrows in Fig. 5b),

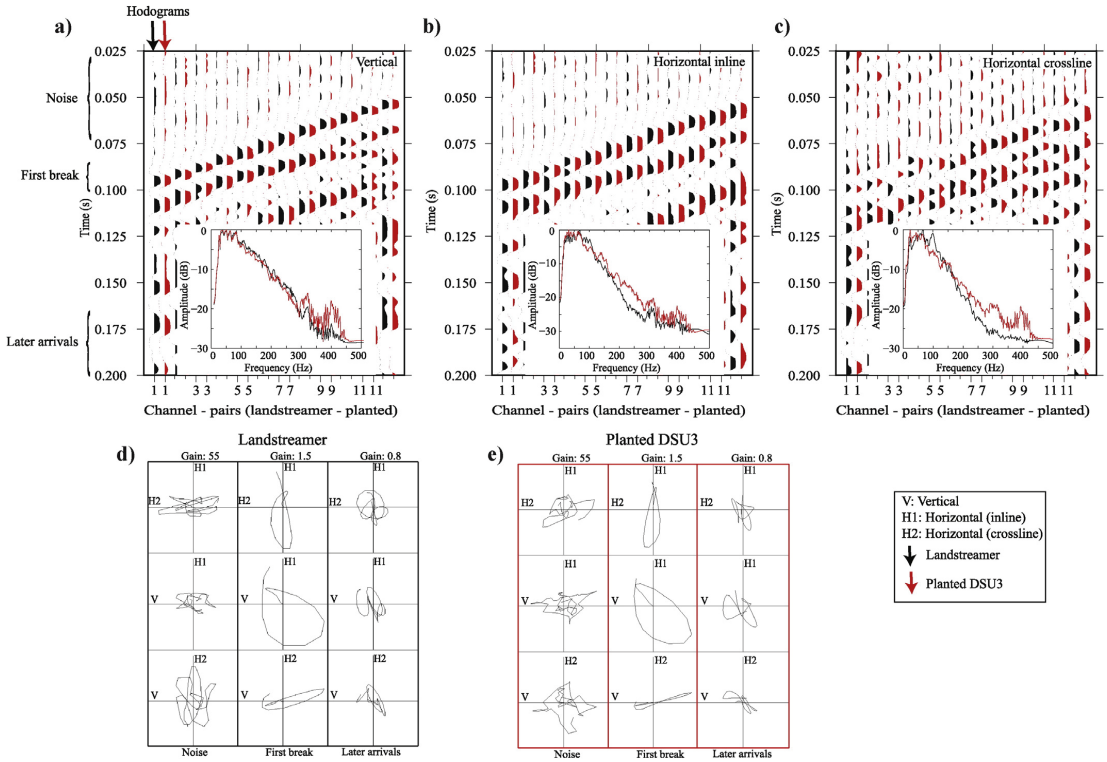

Fig. 4. An example shot gather (after vertical stacking of three repeated shots) from the side-by-side planted (black color wiggles) and streamer mounted (red color wiggles) DSU3 sensors test showing (a) vertical component data, (b) horizontal inline component data, (c) horizontal crossline component data. (d) Hodograms of noise, first break and later arrivals window from a far-offset trace from the streamer mounted sensor. (e) Hodograms of noise, first break and later arrivals time window of the same position trace but from the planted sensor. AGC has been applied (100 ms window) for display purposes. Data are shown in the acceleration (not integrated) domain given the identical nature of the sensors used in the test. Different gains were applied for the particle motion plots for display purposes.

implying that most of the energy should be recorded by the horizontal crossline component of our sensors. Signal control is carried out by a digital-to-analog sweep generator, which is fed by an EPROM (erasable programmable read-only memory) module, containing the desired sweep waveform (ELViS version 3 shaker is restricted to max 360 Hz). Car batteries, 12 V or 24 V, are used to power the source but also to increase the source-to-ground coupling because of their weight (Fig. 5b). In addition, often the source operator sits on it to further improve coupling as shown in Fig. 5a.

Typical shear wave surveys use an SH source and SH geophones (e.g., Bansal and Gaiser, 2012; Deidda and Ranieri, 2001; Garotta, 1999; Polom et al., 2013; Pugin et al., 2013a) to ease the processing (no need for complicated common conversion point binning or non-standard normal moveout corrections) and less contamination with other modes (Hardage et al., 2011). By changing the polarity of the first amplitude onset direction (positive or negative) and stacking two opposite polarity SH signals, minimization of vertical motion leaked into the SH component can be achieved (Garotta, 1999; Krawczyk et al., 2013; Polom et al., 2013).

During the shear wave source test, we acquired one line located perpendicular to the location of the line where the first backyard test was carried out, on a grassy field and with mainly postglacial clay-till sediments (Fig. 5a). We used only 2 segments of the landstreamer totaling 40 DSU3 units, spaced 2 m apart. ELViS with two sets of sweeps varying between 30 and 120 Hz and 30–240 Hz, and a 5-kg sledgehammer were used at every second station along the line. In the middle of the line, shifted approximately 15 m in the perpendicular direction (Fig. 5a), a test using different sweep frequencies was conducted to check for signal attenuation on soft ground and the sensitivity of the streamer for weak shear wave signals coming off the line. The source sweep was 10 s long and recording time was 12 s long; a 1 ms sampling rate was used. At every vibrating point, we acquired 4 records, twice with both "positive" and "negative" polarities. Cross correlation was done using a pilot sensor registering the designed sweep. After cross correlation, source records (reduced to 2 s) were vertically stacked and used for studying signal penetration and amplitude spectra.

3.1.3. Results

The shear wave vibrator test (Fig. 5) was conducted without adjustment of the source frequencies to the ground conditions. Source sweeps were chosen randomly, which might have resulted in the lack of any clear reflections in the shot gathers. Fig. 6a shows an example shot gather with picked first breaks acquired using the 5-kg sledgehammer. Even though both selected sweeps (30–120 Hz and 30–240 Hz) appear not to be suitable and properly adjusted to the ground conditions, we were still able to pick the first breaks of shear waves, with a certain confidence, at least for the 30–120 Hz sweep (Fig. 6b). Fig. 6c shows a collocated shot gather acquired using the 30–240 Hz sweep, where higher noise levels can be seen and that the site attenuated higher source frequencies. First break picking here was extremely difficult and the data needed significant scaling. The collocated data recorded using the 30–120 Hz sweep served as a quality control set and allowed checking of

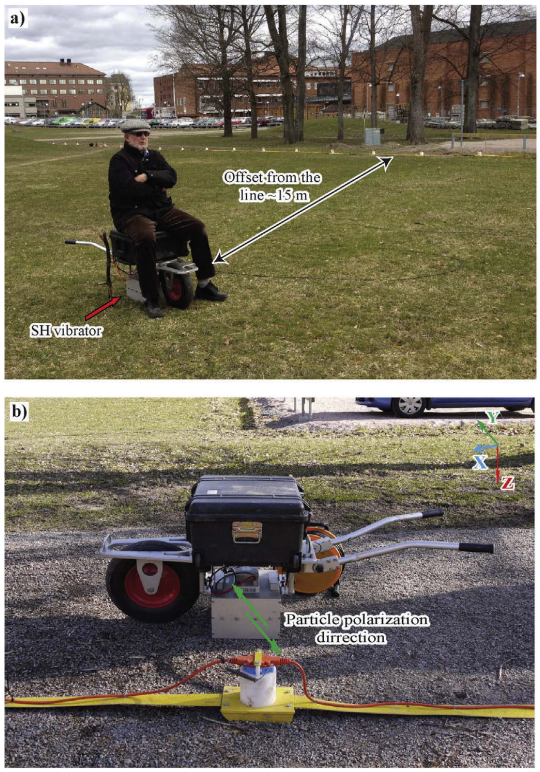

Fig. 5. Photos showing a micro shear wave vibrator (SH source) used in conjunction with the development of the streamer in another backyard test. (a) SH seismic source operating differing sweep frequency ranges but at about 15 m offset from the acquisition line. (b) A close up look at the SH-vibrator with the green arrows representing direction in which the energy is induced (SH–SH data acquisition).

the picked first breaks on the 30–240 Hz gathers. Fig. 6d shows the amplitude spectra of a different frequency range sweep test carried out along the line, with the source positioned with certain offsets from it (see Fig. 5a). Comparison between Fig. 6a and b, c suggests no significant P-wave energy leaked into the horizontal components after the cross-correlation and stacking of the opposite polarity records. It can also be observed from Fig. 6d that, at this site, no significant seismic energy can be seen above 100 Hz, regardless of the source sweep frequency used.

3.2. Test III — Stockholm Bypass

This survey was carried out in the framework of a nation-wide academia-industry joint project (Transparent Underground Structures; TRUST). Stockholm Bypass (also known as Förbifart Stockholm) is a planned underground highway (8 lanes) approximately 21 km long of which more than 17 km is to be tunnel through crystalline bedrock (www.trafikverket.se/forbifartstockholm). It will pass under 3 water bodies, with the deepest point reaching approximately 85 m below sea level. A test site where an access ramp for the tunneling will start, "Vinsta", located in the northern part of Stockholm city was chosen for the streamer test (Figs. 7, 8). Motivation to carry out the test at this site was a priori knowledge about a potential weak zone identified by a number of geotechnical boreholes suggesting poor rock quality (geotechnical Q-value below one) close to where the two seismic lines were designed to intersect each other (Fig. 8). The geophysical objectives of the study were to evaluate the potential of the landstreamer in such a noisy environment, combination of the streamer with wireless units, obtaining information about depth to the bedrock and velocity information that may be linked to the rock quality, especially where the poor quality rocks were inferred to be present.

3.2.1. Data acquisition

During November 2013, we acquired two seismic lines (Lines 1 and 2; Fig. 8) at the site. Due to the urban nature of the site, after a reconnaissance, a decision was made to conduct the whole survey at night to avoid heavy traffic and, most importantly, trams passing next to one of the seismic lines (Line 2). Although we managed to avoid "rush hours", there was still significant traffic during the whole survey time, including trams passing every few minutes up until midnight (Fig. 7b) and heavy trucks passing due to accessibility to the city during the night hours. The trams stopped for four hours during the nights for maintenance between 1 a.m. and 5 a.m., thus allowing a time slot to conduct the survey.

Geologically, both lines cross over areas with variable thickness glacial and post-glacial clays and tills ranging from 1 m to 20 m, overlaying a bedrock consisting of granites, granodiorites and monzonites (Olof Friberg, 2014, personal communication). Bedrock outcrops in several places, especially along Line 2, and their locations were noted during the data acquisition for direct comparison with results obtained in this work. North of Line 1, on the opposite side of the road and our line, rock outcrops were conspicuous, suggesting that the road (Fig. 8) is situated within a depression zone. On the LiDAR (Light Detection And Ranging) data (Fig. 8b), outcropping bedrock is evident where large topographic features are observed.

Line 1 had low topographic relief and was located parallel to the road and almost straight with no bedrock outcrops notable along the whole 560 m length. Data acquisition was done using three segments of the landstreamer (two segments with sensors 2 m apart and one with sensors 4 m apart, in total 160 m long). We used a 5-kg sledgehammer hitting a metallic plate at every 2 m to generate seismic energy. Shots were only activated along the two segments with 2 m station spacing; the remaining segment was used for obtaining data coverage in the zones between the streamer segments and providing far offset data. The spread was moved five times after first deployment. The data acquisition along Line 1 involved a team of five persons and took approximately 8 hours (during the night) to acquire.

Line 2 was logistically challenging due to many factors, such as vicinity to the tram tracks (Fig. 7b), severe topography (Fig. 7c), bedrock outcropping, a major road in the middle (Fig. 8) and concrete stairs for access to the tram station (Fig. 7a) where four sensors of the initial spread deployment had to be placed. It was acquired using a combination of the streamer with 3C wireless recorders of the same type (DSU3) as used in the streamer (Figs. 7, 8). The wireless recorders use a built-in GPS antenna for time stamping and data sampling. Six recorders on each side of the road continuously recorded data during the whole survey time and were kept at their positions while data acquisition continued from one to the other side of the road (see the black points in Fig. 8). After the survey, GPS time stamps of the active data from the landstreamer were used to extract the data from the wireless recorders. These data were later merged with the streamer data and treated similarly for further analysis and use. The information obtained from the wireless units was critical for delineating a zone of poor quality rock close to the road and slightly under it. Without the wireless recorders, it would have been difficult to achieve active signal recordings on both sides of the road using either the landstreamer or any other conventional cabled seismic data acquisition system. The three segments (120 m long) were used on the eastern side, but after moving to the western side of the road we decided to reduce the number of segments to two (in total 80 m long), due to inaccessibility and safety issues for bicycles passing the line overnight. Unfortunately, this reduction

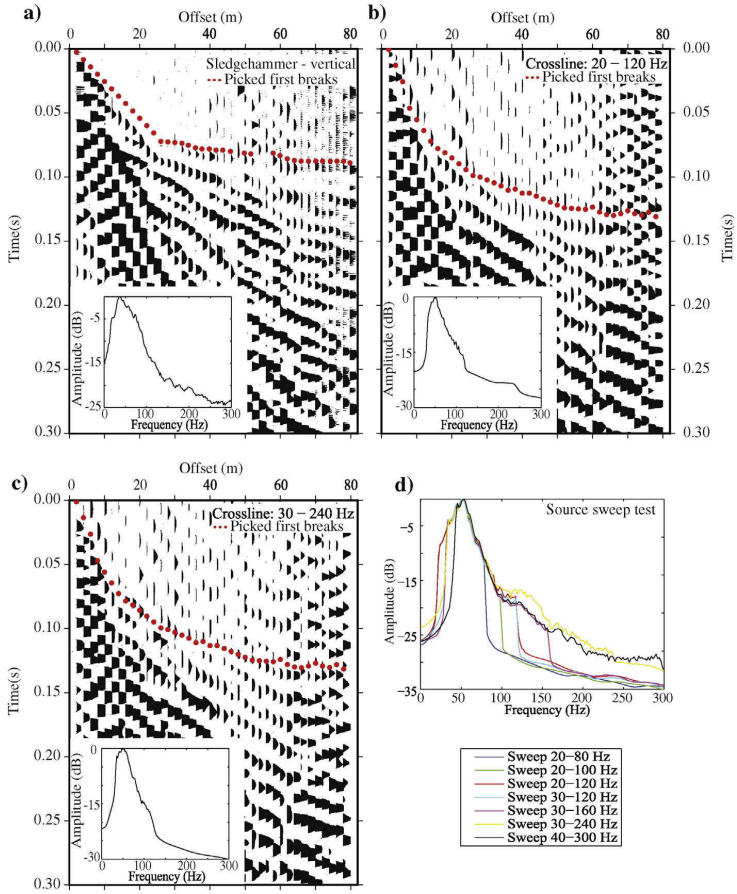

Fig. 6. Shot gathers and amplitude spectra for the data acquired in the second backyard test. (a) Shot gather showing vertical component data obtained using sledgehammer as a source. (b) Horizontal crossline component acquired with the ELViS micro shear vibrator and source sweep frequencies of 30–120 Hz. (c) Shot gather acquired with ELViS and source sweep frequencies 30–240 Hz. (d) Amplitude spectra showing different source sweep ranges test. Note that all the sweeps have almost the same dominant frequency and the signal rapidly attenuates after 100 Hz frequency. For all the shot gathers we used a fixed AGC (100 ms) for plotting purposes and no trace balancing or normalization was applied.

resulted in a lack of data coverage in some zones. The streamer was moved three times on the western side and was fixed on the eastern side, forming a line totally 420 m long (Fig. 8). All the sensor locations were accurately surveyed using a DGPS (differential GPS) system, with an elevation accuracy of a few centimeters, on both lines. Our standard procedure is to survey the coordinates of every streamer unit after deploying them. Each time the streamer is moved, the process is repeated. The wireless units record their coordinates from the GPS automatically, but for high-resolution seismic surveys with dense sensor spacing, the accuracy of this automatic positioning is judged to be inadequate. Hence, the wireless units get surveyed with the DGPS system as well.

3.2.2. Shallow reflections and their imaging potentials

Even in such a noisy environment, reasonably good quality first breaks were observed, especially after vertical staking of the repeated shot records. Example shot gathers from the two lines are shown in Fig. 9. Note the different quality data from these two lines. It is important to note that none of these shots acquired along the two lines show any evidence of spike frequencies (e.g., 50 Hz) from the tram and high-voltage power-lines although they are just a few meters away. This is encouraging given one of the main aims of the streamer was to avoid recording this type of noise.

We spent a significant amount of time for reflection data imaging through various processing approaches. Some shots showed indications of reflections, but not enough convincing. Several stacked sections were generated, but at the end reflections in them believed to be highly contaminated by the remaining parts of source-generated noise, mainly direct and refracted P- and S-wave arrivals. Major problem here were both elevation and field statics. To further evaluate the reflection potential in the data, we carried out seismic elastic finite-difference modeling using a 1D model based on the direct and refracted arrival times for an estimate of the overburden thickness from the crossover distances (Fig. 9b, f). Two scenarios, $V_P/V_S = 5$ and $V_P/V_S = 2.5$, using a three layered earth model (5.5 m thick down to the water-table, $V_P = 500$ m/s, $V_S = 100$ m/s, $\rho = 1600$ kg/m^3; 7.5 m down to bedrock, $V_P = 2500$ m/s, $V_S = 500$ m/s, $\rho = 1900$ kg/m^3; and bedrock $V_P = 5800$ m/s, $V_S = 3400$ m/s and $\rho = 2750$ kg/m^3) were used for the modeling. The first scenario with $V_P/V_S = 5$ corresponds to our actual field situation, while the second one served as a test of the detection ability for more

Fig. 7. Photos showing field condition along Line 2 at the access ramp of Stockholm Bypass at the Vinsta site. (a) Landstreamer units placed at the staircase as a part of the first spread deployment along this line, spacing of 4 m streamer segment reduced to 2 m. (b) Combination of the landstreamer sensors with 12 MEMS-based wireless recorders to cover the inaccessible zone; at the major road cutting the line into two segments. (c) Tram passing during the data acquisition, location of the wireless units on both sides of the road and a view showing the severe topographic variations from one side of the line to another.

common field conditions. Synthetic shot gathers were generated using both elastic and acoustic media with a code available in Seismic Unix (Juhlin, 1995; Juhlin et al., 2012). A Ricker wavelet using a central frequency of 75 Hz, estimated by studying the amplitude spectra of the real data (Fig. 9a, b), was used to generate the synthetic seismograms. After detailed examination and comparison of the synthetic (Fig. 9c, d) and real field shot gathers (Fig. 9a, b), we concluded that the characteristics of the site, along with the source and acquisition set-up used, impairs the detection of the reflected energy from the bedrock in this survey. Reflected energy from the bedrock (see the theoretical traveltimes shown in Fig. 9c, d) is interpreted to occur within the shear wave arrivals and unlikely to be observed after processing. The direct and refracted arrivals are quite consistent both in time and offset when comparing the synthetic and real shot gathers. This is an indication that the model used to generate the synthetic data is a reliable representation of the subsurface. During inspection of the shot gathers on Line 2, no prominent reflection was observed; most likely due to exposed bedrock and thin overburden, hence there was no need for generating synthetic data for this line.

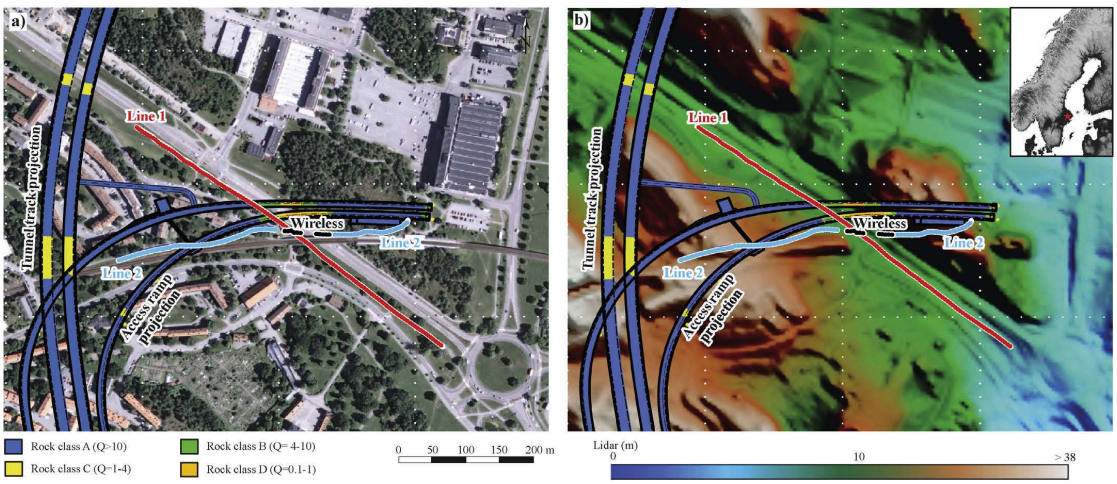

Fig. 8. Location of seismic lines (Lines 1 and 2) with respect to the planned access ramp and the main tunnel projected to the surface (a) aerial photo and (b) LiDAR (elevation) map. Colors on the tunnel track and access ramps show different rock classes identified from geotechnical boreholes. Twelve MEMS-based wireless recorders, six on each side of the road, are marked with the black points. Geotechnical data were kindly provided by the Swedish Transport Administration (Trafikverket).

3.2.3. Tomography, borehole data and 3D visualization

Since our targets were depth to the bedrock and the poor quality rocks inferred from the drilling at the site (Fig. 8a), we performed P-wave first break tomography using the PS_tomo 3D diving-wave tomography code (Tryggvason et al., 2002; Tryggvason and Bergman, 2006). The tomography was done in 3D to fully account for the

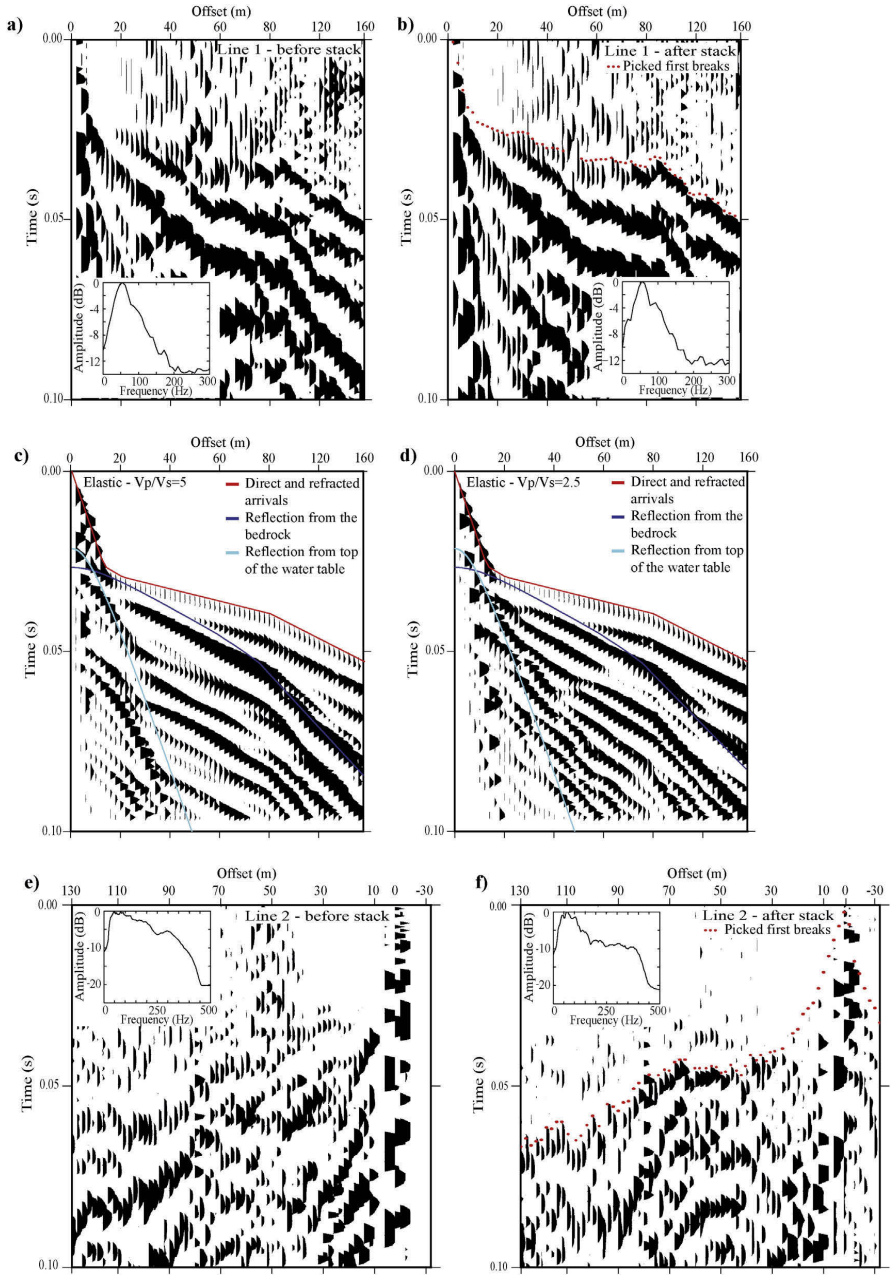

Fig. 9. Example shot gathers from the two seismic lines and their amplitude spectra from the Stockholm Bypass site. (a) Raw data (one hit) and (b) after vertical stacking of three repeated hits from Line 1 showing the quality of the data and first arrivals used for first arrival tomography. (c) Synthetic shot gather generated using an elastic finite-difference algorithm and a three layered earth model constrained from the actual seismic data using $V_P/V_S = 5$. Different color lines showing theoretical direct and refracted arrivals (red line), reflection from the top of water table (cyan, 5.5 m deep) and the bedrock (blue, ~12 m deep). (d) Synthetic shot gather with $V_P/V_S = 2.5$ and overlaid direct and refracted arrivals (red line), reflection from the top of water table (cyan, 5.5 m deep) and the bedrock (blue, ~12 m deep). (e) Raw data and (f) after vertical stacking of three repeated hits with first breaks overlaid from Line 2.

crookedness of the lines and topography variations. A good starting model was the key for obtaining a good velocity model from these lines. To generate the starting model, near offset traveltimes were used. To avoid rays channeling above the topography, the starting model had to be carefully constructed so that regions above it used velocities on the order of 340 m/s (air velocity) and slightly higher than that in the shallow subsurface. This was particularly important for the data along Line 2 given the rapid topography changes. Details of the tomography algorithm can be found in Tryggvason et al. (2002). The final tomographic models (Fig. 10) had an RMS of about 3 ms (after 7 iterations), which was assumed to be sufficient and geologically reasonable, given the noisy nature of some traces and the quality of the first breaks (Fig. 9). The tomography was done using a cell size of 2 m in both the horizontal and vertical directions. Clear shear wave arrivals on the horizontal component data were not present so no shear wave tomography or joint P- and S-wave tomography using the same code, was performed. Information from existing boreholes close to the seismic lines, drilled for a preliminary phase of site investigations, is plotted on the tomography models (Fig. 10). A good match can be seen between the boreholes, our field observations on the locations of the outcrops and the tomography results, with the deviations from the aforesaid corresponding to offsets between the seismic lines and borehole positions. Zones with poor quality rock are reasonably well delineated by low velocity zones, especially as marked in Fig. 8. A slight mismatch between the velocities where the lines cross can be explained as a 3D effect with the rays coming from the side of the line, given its wiggly character and large topographic variations.

To give an estimation of the quality of our picked first breaks, they are shown in Fig. 11a as a function of offset (Line 1 only). Fig. 11b shows traveltime residuals (picked times minus forward calculated times) as a function of offset for the iteration used to present the velocity model in this study. A good match between picked and calculated values with most of the data falling in the error range of 2 ms can be seen. It is interesting to observe clustering of the first breaks into two distinct domains (Fig. 11a). These two domains correspond to two different overburden thicknesses in different parts of the line. This is consistent with the tomography results suggesting a sudden rise of bedrock (high-velocity materials) about 300 m distance along Line 1 (Fig. 10a).

To further illustrate the value of the landstreamer for urban applications we obtained parts of the tunnel model (Stockholm Bypass), including the access ramp, and visualized it with the tomography results obtained in this test and the LiDAR data (Fig. 12). The 3D visualization clearly illustrates how the poor quality rock correlate with a relatively low velocity zone (3000–4000 m/s) and a change in the bedrock geometry (interpreted from the tomography models; Fig. 10a) suggesting the possibility of a fracture system and a small depression zone in the middle of Line 2.

4. Discussion

The MEMS-based 3C landstreamer developed in this study was tested in various places and the results illustrate its capability for imaging and site characterizations, especially in noisy environments. The first backyard test (Fig. 3) indicates the importance of obtaining broadband data. Both MEMS-based 3C sensors mounted on the streamer and the 10 Hz planted geophones image a clear reflection that is notably missing in the 28 Hz planted geophones. The horizontal components of the MEMS-based sensors from the streamer also show evidences of a mode-converted reflection. This mode-converted reflection indicates that there is an imaging potential of the 3C landstreamer using mode converted waves (Eaton and Stewart, 1989; Guy, 2004; Stewart et al., 2002; Stotter and Angerer, 2011). The amplitude spectra of the landstreamer sensors show more energy in the higher frequency part of the signal compared with the geophones tested, making them more suitable for near surface applications (Fig. 3f, g).

The sleds carrying the sensors on the landstreamer do not induce any significant energy decrease, phase difference or additional mode conversions (Fig. 4). We can also observe that the sleds used to mount the units on the landstreamer do not introduce additional phase change or time delays in the data. Judging from the amplitude spectra shown on Fig. 4, it appears that the landstreamer mounted DSU3s are slightly less sensitive to higher frequencies compared with planted ones. This difference is most likely due to site conditions and difference in ground coupling and will be investigated in detail in the near future. The nearest offset traces on the horizontal crossline component occasionally show a tuning effect on some phases (merging two phases into one). This phase behavior could be due to local ground conditions or introduced by the sleds due to bad coupling between them and the surface and is an effect that will be studied more in the future. Amplitude spectra and particle motion plots further support the similar nature of the data for the planted and the streamer mounted MEMS-based sensors. A similar comparison, but using a shear wave source, might be better suited for these types of tests and will be conducted in the near future.

The test with the shear wave vibrator was instructive in the sense that it showed the effect of ground conditions for collecting shear wave data. In soft sediments or over some grassy fields it is unlikely

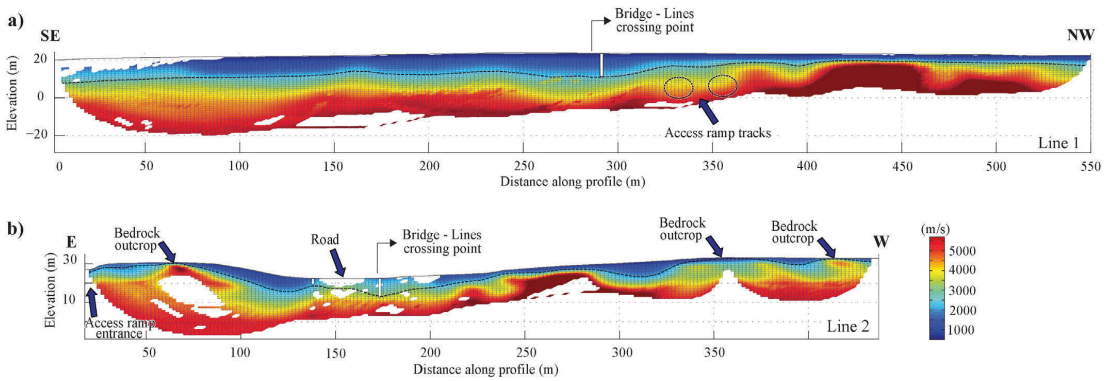

Fig. 10. 3D traveltime tomography results shown with the location of existing boreholes (white bars) identifying the bedrock level at (a) Line 1 and (b) Line 2. Results are shown along the receiver lines where the high-density ray coverage is present (note that the inversion was done in 3D). Arrows show major anthropogenic features, existing bedrock outcrops and approximate location of the access ramps and the black dashed line interpreted depth to the bedrock.

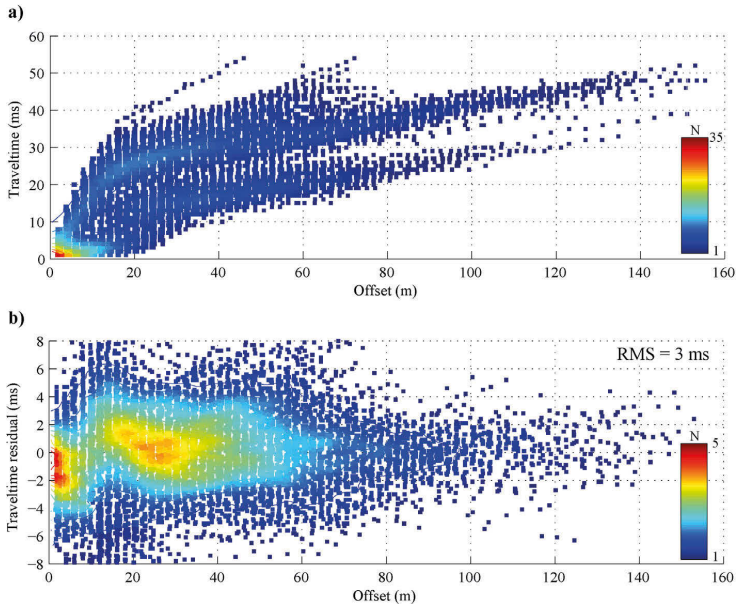

Fig. 11. Quality of the picked first arrivals and the inverted models. (a) Example of picked first breaks as a function of offset for Line 1. (b) Traveltime residuals versus offset for the same line after last iteration of the tomography inversion, with RMS value of 3 ms obtained. Colors correspond to number of points (N) within that range.

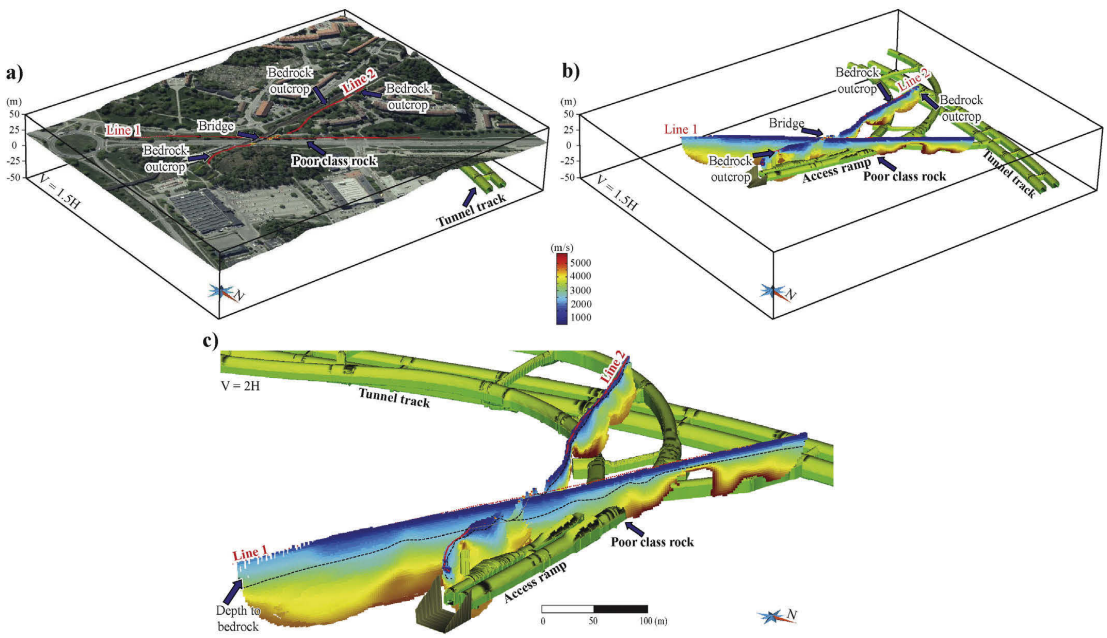

Fig. 12. 3D views showing visualization of the refraction tomography results with the model of the planned tunnel and the access ramp. (a) Aerial photo projected onto the elevation data obtained from LiDAR measurements showing the location of the seismic profiles and main anthropogenic features. (b) Tomography results (3D model) visualized with the tunnel indicating a low velocity zone where the bedrock deepens and where rocks have poor quality. (c) Closer view on the tomography results along with the interpreted depth to the bedrock (black dashed line) and the planned tunnel model. The tunnel model was kindly provided by the Swedish Transport Administration (Trafikverket).

that the use of high-frequency sweeps would be useful since the higher frequencies tend to attenuate quickly (Fig. 6). Even though the source frequencies were not adapted to the site requirements, judging from the shot gathers shown on Fig. 6b, c the high sensitivity of the landstreamer sensors might be the reason we were still able to identify the first arrivals. Comparing the gathers on Fig. 6a to b, c, we note that no contamination with mode leaked P waves is observed and how increasing the source sweep frequencies influences the data. We note from Fig. 6d that not much of the signal can be seen above 100 Hz, therefore better data might have been obtained using source sweeps with lower frequencies. A test conducted by Krawczyk et al. (2013); see also Malehmir et al., 2013a,b) on both a gravel road and farm field (mainly saturated clay) showed that imaging structures at that site using a seismic streamer is possible, but that the quality of the image is significantly different from the farm side than the gravel side. In fact, an issue to consider that favors the use of a multicomponent streamer, especially horizontal crossline data, is the possible absence of Love-waves from the experiments conducted over gravel roads, particularly if the materials below the compacted gravels have lower velocities than the surface. In this case, less Love-waves will be recorded or generated (Krawczyk et al., 2012, 2013; Polom et al., 2013). A thin layer of frozen ground (winter surveys) can also be suitable for such experiments using the streamer (e.g., Malehmir et al., 2015).

Given the urban characteristics of Stockholm Bypass, along with a significant amount of noise observed on the shot gathers, the streamer was still able to record fairly good quality data (Fig. 9). First breaks were picked relatively easily using an automatic picking algorithm. They were later inspected and manually modified (wherever needed), at least for Line 1. Picking first arrivals along Line 2 was more difficult due to bedrock outcrops and the fact that some of the sensors were actually situated on them (or occasionally on the stairs). This produced a level of uncertainty in the first breaks and required investing more time in the picking, compared to Line 1. Nevertheless, a matching result with the drilled boreholes and bedrock outcrops was obtained. Judging from the synthetic shot gathers (Fig. 9c, d), we argue that reflection seismic imaging of the bedrock is unlikely at this site and requires much denser station spacing between the sensors and sources with much higher frequency (Inazaki, 2006; Pugin et al., 2013a; Sloan et al., 2007). The streamer is built so that shorter spacing between the sensors can be achieved and this configuration will be tested in the future studies.

Tomography results along Line 1 (Fig. 10a) suggest that the bedrock deepens towards the southeastern side of the line, but with sharp changes in elevation where the poor quality rocks are observed. The sudden change in the bedrock topography may be an indication of fracturing or faulting, hence the poor quality of rocks at this location. Bedrock in the northwestern side of the line is as shallow as a couple of meters. This is also supported by the two clusters of the first breaks as shown in Fig. 11a. The tomography results along Line 2 (Fig. 10b) suggest an undulating bedrock surface with its deepest point where the road is located (Fig. 8). At almost every location where velocities more than 5000 m/s are observed near the surface there is bedrock outcropping (our observations), supporting the tomography results and further showing the potential of the streamer for this type of application.

At the Stockholm Bypass site we can also note the importance of the GPS time stamped wireless units merged with the streamer system that allowed the delineation of a depression zone that might pose a problem during tunnel construction. Judging from Fig. 12c, the access ramp will be located beneath this zone, where potentially lateral water flow might be expected. Recent information provided by the Swedish Transport Administration (Trafikverket) suggest that the materials above the planned access ramp tunnels (at least one of the two; Fig. 12c) at this location are so weak that a jet grouting program is planned to be conducted prior to their excavation/construction (Ulf B. Eriksson, personal communication, August 2015). This study thus further illustrates the potential of the streamer and its combination with wireless sensors for complex field situations.

While the streamer and the data from it should be further analyzed and tested, we suggest it as a tool for urban applications. There are, however, limitations with the streamer and the data acquisition system used in conjunction with it. In its present configuration, a GPS signal is required. This is mainly for time stamping and data sampling since there is no internal clock in the acquisition system with the required accuracy. If a tunnel experiment is planned, the data recording system must be changed (not the streamer) or a GPS signal needs to be fed into the system, for example using an external clock generating a GPS protocol signal. We are currently working on developing an accurate (and synchronized with GPS) external clock that can locally transmit a GPS protocol signal to the acquisition system and wireless sensors. This is not needed if a surface experiment with the streamer is the goal.

Future studies should also aim at exploiting the potentials of the MEMS sensors for full waveform inversion in near surface environments, given their wider bandwidth, particularly at low frequencies. Towing the streamer segments in parallel might also be an option, and will be conducted in the future in the necessity of a high resolution shallow 3D reflection imaging surveys (e.g. Bachrach and Mukerji, 2001). Three component data and their ability to differentiate between Love- and Rayleigh-waves is another advantage to study (Boiero and Socco, 2014; Socco and Garofalo, 2012; Socco and Strobbia, 2004). These data are complementary and useful for near surface studies since most of these applications deal with the top few meters of the subsurface where there may not be any reflective structures or reflection imaging is difficult (Baker, 1999; Baker et al., 2000; Garotta, 1999; Steeples and Miller, 1998). In combination with the streamer, higher frequency sources should also be developed to take advantage of the broadband nature of the sensors. Future surveys will further explore the usefulness of the multi-component data acquisition. Until then, the current paper provides basic information about the streamer, its reliability and potential for near surface applications.

5. Conclusions

A three-component MEMS-based seismic landstreamer has been developed and tested against planted geophones and similar type sensors as used on the streamer. The broadband nature of the sensors, combined with insensitivity to electrical and electromagnetic noise, makes the system superior to its geophone-type predecessors, especially in urban environments. Tests conducted with the shear wave vibrator showed that a compacted (and saturated) ground is likely required to take the full advantages of the broadband nature of the sensors. Otherwise in dry and highly porous medium, it is unlikely that shear wave frequencies higher than 100 Hz are recorded at the medium to far offsets (50–200 m). As a complementary study, part of the planned Stockholm Bypass tunnel was chosen where depth to the bedrock and a potential weak zone were our main targets. A combination of the streamer with wireless recorders was used to perform 3D first arrival tomography. These results in combination with borehole information, and our own field observations, further demonstrated the capability of the system for urban site characterization. The potential reflection seismic imaging of the bedrock at the Stockholm Bypass site was evaluated through elastic finite-difference seismic modeling. The modeling showed the difficulty in imaging reflections from the bedrock at this site with the given acquisition parameters, but at the same time supported the initial model used to generate synthetic shot gathers when compared with real shot gathers. Although these initial studies of the system do not fully exploit the benefits of 3C MEMS-based sensors, no negative effect such as phase or time difference, polarity change or other effects induced by the overall landstreamer assembly have been noted. The results obtained with the streamer indicate a better signal quality compared to the geophones tested, while the sensitivity and

broadband nature of the 3C sensors open great potential to use it for various near surface applications.

Acknowledgments

All the seismic studies discussed in this work were carried out within the frame of Trust2.2-GeoInfra (http://trust-geoinfra.se) project sponsored by Formas (project number 252-2012-1907), BeFo, SBUF, Boliden, Skanska, SGU, FQM, and NGI. B. Brodic thanks Formas, BeFo, SBUF and Skanska for funding his PhD studies. We thank J. Place, M. Andersson, S. Mehta, N. Juhojuntti, L. Persson, S. Wang, G. Maries and several others from Geophysics Program of Uppsala University for taking part in the data acquisition and helpful discussion during the development of the streamer. The authors wish to thank Andre Pugin, Kevin Brewer and Timothy Cartwright from Geological Survey of Canada and Ulrich Polom from LIAG for their contribution in conceptualizing the present form of the landstreamer and improving the manuscript quality. gOcad Consortium and Paradigm are thanked for providing an academic license of gOcad for 3D visualization of the data. GLOBE Claritas™ under license from the Institute of Geological and Nuclear Sciences Limited (GNS), Lower Hutt, New Zealand was used to process the seismic data. GMT from P. Wessel and W.H.F. Smith and gOcad was used to prepare some of the figures. We thank A. Tryggvason for providing *ps-tomo* tomography code available to use. Swedish Transport Administration (Trafikverket) provided the tunnel 3D model at the Vinsta (Stockholm Bypass) test site for which we are grateful. We are grateful for the valuable comments and suggestions provided by Dr. Ed Kragh, an anonymous reviewer as well as the editor.

References

Adamczyk, A.A., Malinowski, M., Malehmir, A., 2014. high-resolution near-surface velocity model building using full-waveform inversion — a case study from southwest Sweden. Geophys. J. Int. 197, 1693–1704. http://dx.doi.org/10.1093/gji/ggu070.

Alcudia, A.A., Stewart, R., Hall, K., Gallant, E., 2008. Field comparison of 3-C geophones and microphones to high-precision blasting sensors. CREWES Res. Rep. 20, 1–20.

Almholt, A.A., Wisén, R., Jorgensen, R., Ringgaard, J., Nielsen, U., 2013. High resolution 2D reflection seismic land streamer survey for groundwater mapping: Case study from southeast Denmark. SEG Technical Program Expanded Abstracts 2013. Society of Exploration Geophysicists, pp. 1894–1898.

Bachrach, R., Mukerji, T., 2001. Fast 3D ultra shallow seismic reflection imaging using portable geophone mount. Geophys. Res. Lett. 28, 45–48. http://dx.doi.org/10.1029/2000GL012020.

Bachrach, R., Nur, A.A., 1998. Ultra shallow seismic reflection in unconsolidated sediments: Rock physics base for data acquisition. SEG Tech. Program Expand. Abstr. 1998, pp. 866–869.

Baker, G., 1999. Processing near-surface seismic-reflection data. CCourse Notes Series. Society of Exploration Geophysicists.

Baker, G., Steeples, D., Schmeissner, C., Spikes, K., 2000. Collecting seismic-reflection data from depths shallower than three meters. Symposium on the Application of Geophysics to Engineering and Environmental Problems. Environment and Engineering Geophysical Society, pp. 1207–1214.

Bansal, R., Gaiser, J., 2012. An introduction to this special section: applications and challenges in shear-wave exploration. Lead. Edge 32, 12-12. http://dx.doi.org/10.1190/tle32010012.1.

Boiero, D., Socco, L.V., 2014. Joint inversion of Rayleigh-wave dispersion and P-wave refraction data for laterally varying layered models. Geophysics 79, EN49–EN59. http://dx.doi.org/10.1190/geo2013-0212.1.

Bretaudeau, F., Leparoux, D., Abraham, O., 2008. Small scale adaptation of the seismic full waveform inversion method — application to civil engineering applications. Acoust. 08 Paris.

Deidda, G.P., Ranieri, G., 2001. Some SH-wave seismic reflections from depths of less than three metres. Geophys. Prospect. 49, 499–508. http://dx.doi.org/10.1046/j.1365-2478.2001.00280.x.

Determann, J., Thyssen, F., Engelhardt, H., 1988. Ice thickness and sea depth derived from reflection-seismic measurements on the central part of Filchner-Ronne Ice Shelf, Antarctica. Ann. Glaciol. 11.

Eaton, D., Stewart, R., 1989. Aspects of seismic imaging using P-SV converted waves. CREWES Res. Rep. 6, 68–92.

Eiken, O., Degutsch, M., Riste, P., Rød, K., 1989. Snowstreamer: an efficient tool in seismic acquisition. First Break 7. http://dx.doi.org/10.3997/1365-2397.1989021.

Fabien-Ouellet, G., Fortier, R., 2014. Using all seismic arrivals in shallow seismic investigations. J. Appl. Geophys. 103, 31–42. http://dx.doi.org/10.1016/j.jappgeo.2013.12.009.

Garotta, R., 1999. Shear waves from acquisition to interpretation. Distinguished Instructor Series. Society of Exploration Geophysicists.

Gibson, J., Burnett, R., 2005. Another look at MEMS sensors… and dynamic range. CSEG Rec. 20.

Gibson, J., Burnett, R., Ronen, S., Watt, H., 2005. MEMS sensors: some issues for consideration. Lead. Edge 24, 786–790. http://dx.doi.org/10.1190/1.2032249.

Guy, E.D., 2004. Evaluation of near-surface converted-mode seismic reflection imaging potential. Electron. J. Geotech. Eng. 9, 1–35.

Hardage, B., DeAngelo, M., Murray, P., Sava, D., 2011. 3. Multicomponent Data processing. Multicomponent Seismic TechnologyGGeophysical References Series. Society of Exploration Geophysicists, pp. 77–124.

Hauer, G., Hons, M., Kendall, R., Lawton, D., Bertram, M., 2008. Field data comparison: 3C–2D data acquisition with geophones and accelerometers. SEG Technical Program Expanded Abstracts 2008. Society of Exploration Geophysicists, pp. 178–182.

Heijkenskjöld, R., 2001. Landskapsutveckling i Uppsalatrakten. Naturkonsulten, Uppsala.

Hons, M.S., 2008. Seismic sensing: comparison of geophones and accelerometers using laboratory and field data CREWES Theses 2008.

Hons, M., Stewart, R., Lawton, D., Bertram, M., 2007. Ground motion through geophones and MEMS accelerometers: sensor comparison in theory, modeling, and field data. SEG Technical Program Expanded Abstracts 2007. Society of Exploration Geophysicists, pp. 11–15.

Huggins, R., 2004. A report on land streamers: the last geophone you will ever plant? Surf. Views -Surf. Geophys. Sect. Soc. Explor. Geophys. SEG, first quarter vol. 11

Inazaki, T., 1999. Land Streamer; a new system for high-resolution S-wave shallow reflection surveys. Proc. 12th Annu. Symp. Appl. Geophys. Eng. Environ. Probl. SAGEEP1999, pp. 207–216.

Inazaki, T., 2004. High-resolution seismic reflection surveying at paved areas using an S-wave type Land Streamer. Explor. Geophys. 35. http://dx.doi.org/10.1071/EG04001.

Inazaki, T., 2006. High-resolution S-wave reflection survey in urban areas using a woven belt type Land streamer. Surf. 2006 Sept. 4-6 Hels. Finl.

Juhlin, C., 1995. Finite-difference elastic wave propagation in 2D heterogeneous transversely isotropic media. Geophys. Prospect. 43, 843–858. http://dx.doi.org/10.1111/j.1365-2478.1995.tb00284.x.

Juhlin, C., Sturkell, E., Ebbestad, J.O.R., Lehnert, O., Högström, A.E.S., Meinhold, G., 2012. A new interpretation of the sedimentary cover in the western Siljan Ring area, central Sweden, based on seismic data. Tectonophysics 580, 88–99. http://dx.doi.org/10.1016/j.tecto.2012.08.040.

Keho, T., Kelamis, P., 2009. A new era in land seismic: The near surface challenge. SEG Technical Program Expanded Abstracts 2009. Society of Exploration Geophysicists, pp. 3421–3425.

Kendall, R., 2006. Advances in land multicomponent Seismic: acquisition, processing and Interpretation. CSEG Rec. 31, 65–75 (doi: http://csegrecorder.com/editions/issue/2006-03).

Krawczyk, C., Polom, U., Trabs, S., Dahm, T., 2012. Sinkholes in the city of Hamburg — new urban shear-wave reflection seismic system enables high-resolution imaging of subrosion structures. J. Appl. Geophys. 78, 133–143. http://dx.doi.org/10.1016/j.jappgeo.2011.02.003.

Krawczyk, C., Polom, U., Beilecke, T., 2013. Shear-wave reflection seismics as a valuable tool for near-surface urban applications. Lead. Edge 32, 256–263. http://dx.doi.org/10.1190/tle32030256.1.

Kruppenbach, J.A., Bedenbender, J.W., 1975. United States Patent: 3923121 — Towed land cable. 3923121.

Lai, C.G., Rix, G.J., Foti, S., Roma, V., 2002. Simultaneous measurement and inversion of surface wave dispersion and attenuation curves. Soil Dyn. Earthq. Eng. 22, 923–930. http://dx.doi.org/10.1016/S0267-7261(02)00116-1.

Laine, J., Mougenot, D., 2014. A high-sensitivity MEMS-based accelerometer. Lead. Edge 33, 1234–1242. http://dx.doi.org/10.1190/tle33111234.1.

Lawton, D.C., Bertram, M.B., Margrave, G.F., Gallant, E.V., 2006a. Comparisons between data recorded by several 3-component coil geophones and a MEMS sensor at the Violet Grove monitor seismic survey. CREWES Res. Rep. 18, 1–24.

Link, C., Speece, M., Betterly, S., 2006. An Overview of Seismic Land Streamer Projects at Montana Tech. Presented at the Symposium on the Application of Geophysics to Engineering and Environmental Problems 2006. Environment and Engineering Geophysical Society, pp. 1012–1026.

Lundin, S.-E., 1988. Ingenjörsgeologisk Karta Över Uppsala: Engineering Geologoical map of City of Uppsala. Uppsala university, Uppsala 0348-2979 ; 154.

Malehmir, A., Bastani, M., Krawczyk, C., Gurk, M., Ismail, N., Polom, U., Persson, L., 2013a. Geophysical assessment and geotechnical investigation of quick-clay landslides —+ a Swedish case study. Surv. Geophys. 11. http://dx.doi.org/10.3997/1873-0604.2013010.

Malehmir, A., Saleem, M.U., Bastani, M., 2013b. High-resolution reflection seismic investigations of quick-clay and associated formations at a landslide scar in southwest Sweden. J. Appl. Geophys. 92, 84–102. http://dx.doi.org/10.1016/j.jappgeo.2013.02.013.

Malehmir, A., Wang, S., Lamminen, J., Brodic, B., Bastani, M., Vaittinen, K., Juhlin, C., Place, J., 2015. Delineating structures controlling sandstone-hosted base-metal deposits using high-resolution multicomponent seismic and radio-magnetotelluric methods: a case study from Northern Sweden. Geophys. Prospect. 63, 774–797. http://dx.doi.org/10.1111/1365-2478.12238.

Merchant, J., 2009. MEMS Applications in Seismology. Presented at the Seismic Instrumentation Technology Symposium, Palm Springs, CA (http://www.iris.edu/hq/instrumentation_meeting/files/pdfs/MEMS_Seismology.pdf).

Miller, R., Pullan, S., Waldner, J., Haeni, F., 1986. Field comparison of shallow seismic sources. Geophysics 51, 2067–2092. http://dx.doi.org/10.1190/1.1442061.

Mougenot, D., Thorburn, N., 2004. MEMS-based 3D accelerometers for land seismic acquisition: Is it time? Lead. Edge 23, 246–250. http://dx.doi.org/10.1190/1.1690897.

Mougenot, D., Cherepovskiy, A., JunJie, L., 2011. MEMS-based accelerometers: expectations and practical achievements. First Break 29.

Paasche, H., Rumpf, M., Hausmann, J., Fechner, T., Werban, U., Tronicke, J., Dietrich, P., 2013. Advances in acquisition and processing of near-surface seismic tomographic data for geotechnical site assessment. First Break 31.
Park, C., Miller, R., Xia, J., 1999. Multichannel analysis of surface waves. Geophysics 64, 800–808. http://dx.doi.org/10.1190/1.1444590.
Park, C.B., Miller, R.D., Miura, H., 2002. Optimum field parameters of an MASW survey [Exp. Abs.]. SEG-J, Tokyo, pp. 22–23.
Place, J., Malehmir, A., Högdahl, K., Juhlin, C., Persson Nilsson, K., 2015. Seismic characterization of the Grängesberg iron deposit and its mining-induced structures, central Sweden. Interpretation (in print).
Polom, U., Druivenga, G., Grossmann, E., Grüneberg, S., Rode, W., 2011. Transportabler Scherwellenvibrator: Deutsches Patent und Markenamt. Patentschrift DE10327757B4.
Polom, U., Bagge, M., Wadas, S., Winsemann, J., Brandes, C., Binot, F., Krawczyk, C.M., 2013. Surveying near-surface depocentres by means of shear wave seismics. First Break 31.
Pugin, A.J.M., Larson, T., Bergler, S., McBride, J., Bexfield, C., 2004a. Near-surface mapping using SH-wave and P-wave seismic land-streamer data acquisition in Illinois, U.S. Lead. Edge 23, 677–682. http://dx.doi.org/10.1190/1.1776740.
Pugin, A.J.M., Larson, T., Sargent, S., 2004b. 3.5 km/day of high resolution seismic reflection data using a landstreamer. Presented at the Symposium on the Application of Geophysics to Engineering and Environmental Problems 2004. Environment and Engineering Geophysical Society, pp. 1380–1388.
Pugin, A.J.M., Pullan, S., Hunter, J., Oldenborger, G., 2009. Hydrogeological prospecting using P- and S-wave landstreamer seismic reflection methods. Surv. Geophys. 7. http://dx.doi.org/10.3997/1873-0604.2009033.
Pugin, A.J.M., Pullan, S., Duchesne, M., 2013a. Regional hydrostratigraphy and insights into fluid flow through a clay aquitard from shallow seismic reflection data. Lead. Edge 32, 742–748. http://dx.doi.org/10.1190/tle32070742.1.
Pugin, A.J.M., Pullan, S., Hunter, J.A., 2013b. Shear-wave high-resolution seismic reflection in Ottawa and Quebec City, Canada. Lead. Edge 32, 250–255. http://dx.doi.org/10.1190/tle32030250.1.
Pullan, S., Pugin, A., Hunter, J., Cartwright, T., Douma, M., 2008. Application of P-wave seismic reflection methods using the Landstreamer/Minivib system to near-surface investigations. Presented at the Symposium on the Application of Geophysics to Engineering and Environmental Problems 2008. Environment and Engineering Geophysical Society, pp. 614–625.
Sirgue, L., Barkved, O.I., Dellinger, J., Etgen, J., Albertin, U., Kommedal, J.H., 2010. Thematic set: full waveform inversion: the next leap forward in imaging at Valhall. First Break 28. http://dx.doi.org/10.3997/1365-2397.2010012.
Sloan, S.D., Tsoflias, G.P., Steeples, D.W., Vincent, P.D., 2007. High-resolution ultra-shallow subsurface imaging by integrating near-surface seismic reflection and ground-penetrating radar data in the depth domain. J. Appl. Geophys. 62, 281–286. http://dx.doi.org/10.1016/j.jappgeo.2007.01.001.
Socco, L.V., Garofalo, F., 2012. Joint inversion of surface wave and body wave data for the characterisation of a fault system in New Zealand. Presented at the EGU Gen. Assem. 2012, p. 1889.
Socco, L.V., Strobbia, C., 2004. Surface-wave method for near-surface characterization: a tutorial. Surv. Geophys. 2. http://dx.doi.org/10.3997/1873-0604.2004015.
Socco, L.V., Boiero, D., Foti, S., Wisén, R., 2009. Laterally constrained inversion of ground roll from seismic reflection records. Geophysics 74, G35–G45. http://dx.doi.org/10.1190/1.3223636.
Socco, L., Foti, S., Boiero, D., 2010. Surface-wave analysis for building near-surface velocity models — established approaches and new perspectives. Geophysics 75. http://dx.doi.org/10.1190/1.3479491 (75A83–75A102).
Sopher, D., Juhlin, C., Huang, F., Ivandic, M., Lueth, S., 2014. Quantitative assessment of seismic source performance: Feasibility of small and affordable seismic sources for long term monitoring at the Ketzin CO_2 storage site, Germany. J. Appl. Geophys. 107, 171–186. http://dx.doi.org/10.1016/j.jappgeo.2014.05.016.
Steeples, D.W., 2004. Near-surface seismic reflection applications. Presented at the 1st International Conference on Environmental and Engineering Geophysics, Wuhan, China.
Steeples, D., Miller, R., 1998. Avoiding pitfalls in shallow seismic reflection surveys. Geophysics 63, 1213–1224. http://dx.doi.org/10.1190/1.1444422.
Stewart, R., Gaiser, J., Brown, R., Lawton, D., 2002. Converted-wave seismic exploration: methods. Geophysics 67, 1348–1363. http://dx.doi.org/10.1190/1.1512781.
Stotter, C., Angerer, E., 2011. Evaluation of 3C microelectromechanical system data on a 2D line: Direct comparison with conventional vertical-component geophone arrays and PS-wave analysis. Geophysics 76, B79–B87. http://dx.doi.org/10.1190/1.3561769.
Suarez, G.M., Stewart, R.R., 2007. Acquisition and analysis of 3C land streamer data. CREWES Res. Rep. 19, 1–12 (doi:http://www.crewes.org/ForOurSponsors/ResearchReports/2007/2007-19.pdf).
Suarez, G.M., Stewart, R.R., 2008a. Side-by-side comparison of 3-C land streamer versus planted geophone data at the Priddis test site. CREWES Res. Rep. 20, 1–16.
Suarez, G.M., Stewart, R.R., 2008b. A field comparison of 3-C land streamer versus planted geophone data. SEG Technical Program Expanded Abstracts 2008. Society of Exploration Geophysicists, pp. 16–20.
Tryggvason, A., Bergman, B., 2006. A traveltime reciprocity discrepancy in the Podvin & Lecomte time 3d finite difference algorithm. Geophys. J. Int. 165, 432–435. http://dx.doi.org/10.1111/j.1365-246X.2006.02925.x.
Tryggvason, A., Rögnvaldsson, S., ður, T., Flóvenz, Ó.G., 2002. Three-dimensional imaging of the P- and S-wave velocity structure and earthquake locations beneath Southwest Iceland. Geophys. J. Int. 151, 848–866. http://dx.doi.org/10.1046/j.1365-246X.2002.01812.x.
van der Veen, M., Green, A.G., 1998. Land streamer for shallow seismic data acquisition; evaluation of gimbaled-mounted geophones. Geophysics 63, 1408–1413. http://dx.doi.org/10.1190/1.1444442.
van der Veen, M., Buness, H.A., Büker, F., Green, A.G., 2000. Field comparison of high-frequency seismic sources for imaging shallow (10–250 m) structures. J. Environ. Eng. Geophys. 5, 39–56.
van der Veen, M., Spitzer, R., Green, A., Wild, P., 2001. Design and application of a towed land-streamer system for cost-effective 2-D and pseudo-3-D shallow seismic data acquisition. Geophysics 66, 482–500. http://dx.doi.org/10.1190/1.1444939.
Xia, J., Miller, R.D., Park, C.B., Tian, G., 2003. Inversion of high frequency surface waves with fundamental and higher modes. J. Appl. Geophys. 52, 45–57. http://dx.doi.org/10.1016/S0926-9851(02)00239-2.
Zhang, F., Juhlin, C., Ivandic, M., Lüth, S., 2013. Application of seismic full waveform inversion to monitor CO_2 injection: modelling and a real data example from the Ketzin site, Germany. Geophys. Prospect. 61, 284–299. http://dx.doi.org/10.1111/1365-2478.12021.

Multi-component digital-based seismic landstreamer and boat-towed radio-magnetotelluric acquisition systems for improved subsurface characterization in the urban environment

Bojan Brodic[1*], Alireza Malehmir[1], Mehrdad Bastani[2], Suman Mehta[1], Christopher Juhlin[1], Emil Lundberg[1] and Shunguo Wang[1] introduce the two systems and present two case studies illustrating their potential.

Introduction

It is estimated that urban life will be the norm for around 60% of the total world's population by 2040, leading to a more centralized distribution of people and making the city as the main place of residence (Whiteley, 2009). This population centralization inherently implies rapidly expanding cities and imposes the need for more infrastructure within, around and between the present city boundaries. However, infrastructure projects nowadays have to follow strict civil engineering standards that require detailed knowledge of subsurface conditions during different stages of the construction processes. Since direct methods conventionally used for site characterization (e.g., drilling and/or core testing) are still relatively expensive the focus in the last two decades has been on non-invasive, geophysical methods. However, geophysical site characterization in urban areas is not an easy task owing to numerous challenges and various types of noise sources. Challenges such as electric/electromagnetic (EM) noise, pipelines and other subsurface objects (sometimes even unknown or undocumented), the inability to properly couple sensors because of pavement, traffic noises and limited space are common in urban environment. Since geophysical surveys need to be done with the least amount of disturbances to the environment, residents and traffic, new geophysical techniques for fast, non-invasive and high-resolution site characterization are needed.

To overcome some of these challenges, a nationwide joint industry-academia project was launched in 2012 (TUST GeoInfra, www.trust-geoinfra.se). As a component in the project, Uppsala University developed two new data acquisition systems. These are a fully digital MEMS-based (Micro-machined Electro-Mechanical Sensor) three component (3C) seismic landstreamer and a boat-towed radio-magnetotelluric (RMT) acquisition system. Both systems were specifically designed to address urban environments with the RMT system particularly aiming at efficient and cost-effective geophysical surveying on shallow-water bodies, which constitute 7% of Scandinavia. In this article, we will describe the two systems and present two case studies illustrating their potential. A number of published accounts are now available from the two systems showing what type of problems they can address (e.g., Bastani et al., 2015; Brodic et al., 2015; Malehmir et al., 2015a, 2015b, 2016a, 2016b, 2017; Dehghannejad et al., 2017; Maries et al., 2017; Mehta et al., 2017; Brodic et al., 2017).

Seismic landstreamer

Similar to marine seismic surveys, the idea of having a portable receiver array that can be towed along the surface has been intriguing researchers working on shallow subsurface characterization using seismic methods on land as well. In the 1970s, this led to the development of the concept of a seismic landstreamer. Landstreamer is defined as an array of seismic receivers that can be dragged along the surface without the need for 'planting'. The concept was first applied in the form of a snow-streamer (Eiken et al., 1989) and since this pioneering work, seismic landstreamers of various kinds have proven their value and potential. This is particularly true for near-surface mapping and characterization in urban areas, especially on asphalt and/or paved surfaces (see Brodic et al., 2015 and references therein). Published studies involving landstreamers for acquiring seismic data have used various types of geophones, mostly single geophones on a sled (vertical or horizontal), two geophones per sled (one vertical and one horizontal), or in a recent case even single 3C accelerometers (see Brodic et al., 2015 and references therein). In contrast to the mentioned studies, the Uppsala University landstreamer is built with digital 3C, MEMS-based sensors, making this landstreamer a unique system to date.

Compared to geophones that are widespread and conventionally used, the MEMS-based sensors are digital accelerometers designed to work below their resonance frequency (e.g., 1 kHz). Advantages of MEMS over geophones include their broadband linear amplitude and phase response (0-800 Hz), tilt angle measurements up to high angles and insensitivity to contamination from electric or EM noise sources (Brodic et al., 2017). The landstreamer is based on Sercel Lite technology and Sercel DSU3 (MEMS-based) sensors. The sensors are mounted on sleds (receiver holders), and the sleds fixed firmly to a non-stretchable

[1] Department of Earth Sciences, Uppsala University, Sweden | [2] Geological Survey of Sweden
[*] Corresponding author, E-mail: bojan.brodic@geo.uu.se

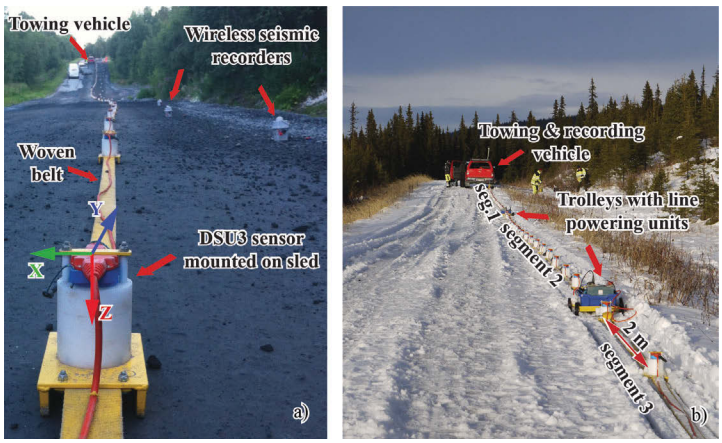

Figure 1 Sensor-sled assembly mounted on a non-stretchable woven belt with internal co-ordinate system of the sensor (a). Note here the wireless seismic recorders working in autonomous mode providing long offset data and a towing vehicle far in the back. (b) Different segments of the seismic landstreamer connected by trolleys carrying line powering units towed by a vehicle. In the test shown, the towing vehicle was also used as the recording vehicle.

Parameters	UU Landstreamer
Sensors	3C MEMS
Frequency bandwidth	0 - 800 Hz
Tilt angle	Recorded in the header
Acquisition system	Sercel Lite (MEMS + geophones)
Max number of channels	2000
Present configuration: 4 segments 1 segment	100 sensors on 5 segments each 20 units and spaced 2 m 20 units and spaced 4 m
Cable connection	Sensors on a single cable
Data transmission	Digital
Data format	SEGD
GPS time of the record	Recorded in the header

Table 1 Technical details of the system developed in this study

1.	Less sensitivity to tilting or can be easily estimated and corrected for it using built in tilt test
2.	Full digital data transmission avoids any pick-up noise, crosstalk and sensitivity to leakage
3.	It is lighter and requires less number of batteries compared to the existing and comparable technology available on the market
4.	No need for sensor planting, an issue in big cities, mines, etc.
5.	High-resolution imaging using densely spaced sensors
6.	Covering large areas relatively fast
7.	Easily combined with wireless units to extend the line or cover inaccessible areas
8.	Can be towed in series (2D surveys) or parallel (3D surveys)
9.	Can be used for both passive (ReMi, MASW) and active data acquisition

Table 2 Summary of the important characteristics of the developed landstreamer

woven belt used in the aircraft industry (Figure 1a). The system was designed to support both DSU3 sensors and geophones and can be combined with wireless units for complementary acquisition if longer offsets are necessary (Figure 1a). Technical details of the developed system can be found in Table 1.

The present-day configuration of the streamer consists of five segments with each of the segments having 20 sensors mounted. The segments are interconnected by small carriages carrying line-powering units (Figure 1b). Four of the segments contain 20 units spaced 2 m, while the fifth one has 20 units spaced at 4 m. The spacing can be reduced to 25 cm, if required. The entire five segments long spread connected by small trolleys was designed to be as light as possible and easily pulled by a 2WD or 4WD vehicle. With a team of 3 to 4 persons for the set-up, data acquisition rates vary from 600 m to 1200 m of seismic line in a day using a source spacing of 2 m to 4 m. A summary of the key landstreamer properties can be found in Table 2.

Boat-towed RMT

The boat-towed RMT system is developed for shallow fresh water surveys to support the planning phase of underground infrastructure developments in the city of Stockholm (Bastani et al., 2015) and evolved from the EnviroMT acquisition system (Bastani, 2001) that has been traditionally used for land surveying. The RMT method uses distant radio-transmitters in the very low frequency range (VLF, 15-30 kHz) and low-frequency range (30-300 kHz) as the EM source. Compared with traditional VLF measurements, RMT covers a wider frequency range and the data are used to model the variations of the electrical resistivity in the subsurface. The boat-towed RMT system remains the same as for the land surveys, with the difference of the analog part of the equipment being mounted on a floating platform made of wood and Styrofoam and towed by a boat (Figure 2). The analog parts include a 3C magnetic field sensor (MFS), steel electrodes, analog filter (AF) box and other electronics. Three components of the Earth's magnetic field are measured by the MFS on the platform. Measurement of the two components of the electric field is enabled by two pairs of steel electrodes (with buffer amplifiers used to minimize capacitive

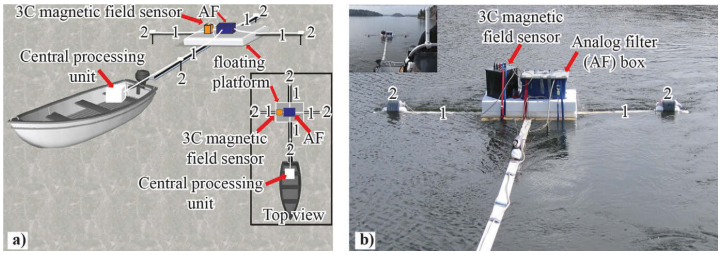

Figure 2 Boat-towed RMT acquisition system schematic (a) and a photo of the actual look of the system with inset showing it dragged behind the boat (b). Arms and cables for electric field measurements are marked with '1', while '2' marks 4 steel electrodes with buffer amplifiers. Modified after Bastani et al. (2015).

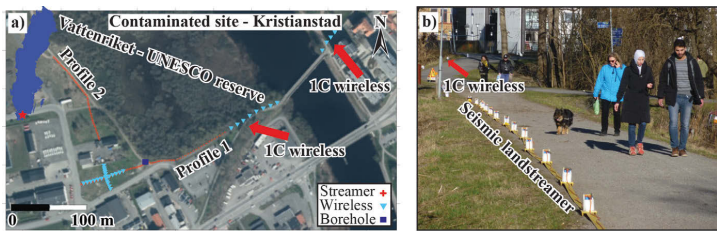

Figure 3 Location of the site and seismic lines acquired in Kristianstad (a) and a photo showing the streamer at one of the lines during data acquisition (b).

leakage in the cables) fixed on a pair of 2.5-metre-long arms (Figure 2, marked by '1' and '2'). The floating platform is towed at a distance of 10 m behind the boat and connected to an additional arm carrying the cable used to transfer the analog signal to the digital part of the system that is positioned inside the boat (Figure 2a, central processing unit). The measurements with the boat-towed RMT system are carried out while the boat is moving, making the data acquisition much more efficient and faster compared to the land surveys.

Landstreamer seismic survey at a contaminated site

During the early stage of the development of the streamer (in 2014) its potential was tested at a site contaminated by chlorinated hydrocarbons in Kristianstad, southern Sweden (Figure 3). The main goals of the survey were to characterize the depth to bedrock and possible fracture zones within, that could provide potential migration pathways of pollutants to the river and groundwater. The seismic data were acquired in an urban part of the city (Figure 3a) at a site where an old chemical-cleaning facility was located in the past. Soil analysis at the site shows high concentrations of chlorinated hydrocarbons, known as tetrachloroethylenes (PCE), that were used for the chemical-cleaning process and have leaked into the subsurface. The tetrachloroethylenes are highly harmful and carcinogenic (Guha et al., 2012) and could possibly have spread from the site through groundwater. Geologically, the site consists of 5-20 m thick glacial tills and clays overlaying an 80 m average thick limestone layer sitting on top of a regional glauconite aquifer. A great concern exists that the PCEs might infiltrate into the deep glauconite aquifer, used for the regional water supply, or migrate towards a nearby Unesco biosphere reserve called Vattenriket (Johansson et al., 2017).

At the Kristianstad site, two seismic profiles were acquired using a combination of the seismic landstreamer and single component (1C) wireless seismic recorders connected to 10 Hz vertical-component geophones (Figure 3). To generate a seismic signal, a source with the same principle as the 'Betsy seismic gun' charged with 12 mm blank cartridges was used (Miller et al., 1986). Shots were fired every 4 m and coincident with the nearest receiver. Along both profiles, ground conditions varied from asphalt bicycle roads to grass fields. The wireless recorders were used as an extension of the landstreamer and to overcome the problems associated with existing infrastructure and the river crossing the site. At the time of acquisition the landstreamer consisted of four segments with 20 3C-MEMS-based units in each segment. Three segments had sensor spacings of 2 m, while the 4th one had sensors spaced at 4 m. In addition, a short segment consisting of five units spaced at 2 m was also used, making the total length of the spread 210 m. Profile 1 is approximately 400 m long, extending from the western part of the site and east over the river. The eastern part of the profile (from 210-400 m) was covered with eight 1C wireless seismic recorders deployed at a distance of 10 m, while 4 wireless units with 10 m spacing were deployed west of the river. Profile 2 was acquired with the landstreamer on the northern part and 12 1C wireless recorders spaced at 4 m located further away. The sample rate used along both profiles was 1 ms and for every shot 5 s of data were recorded. The acquisition system used to acquire the data, Sercel Lite, operates using GPS time and stores the GPS timestamp of every shot in the trace headers. This provided a common reference time for every shot to download the data from the wireless units operating in autonomous mode and allowing the two data sets to be merged.

Here we focus on the vertical component of the 3C seismic landstreamer using both refraction tomography and reflection seismic imaging. P-wave first arrival tomography was done using the ps_tomo code (Tryggvason et al., 2002) with 2 m cell size in inline and depth, while a wide cell in the crossline direction was used to obtain a 2D velocity distribution. After 8 iterations no more changes in the models were observed and RMS errors of 3.2 ms (Profile 1) and 3.1 ms (Profile 2) were obtained. Both tomography models suggest bedrock dipping towards the river.

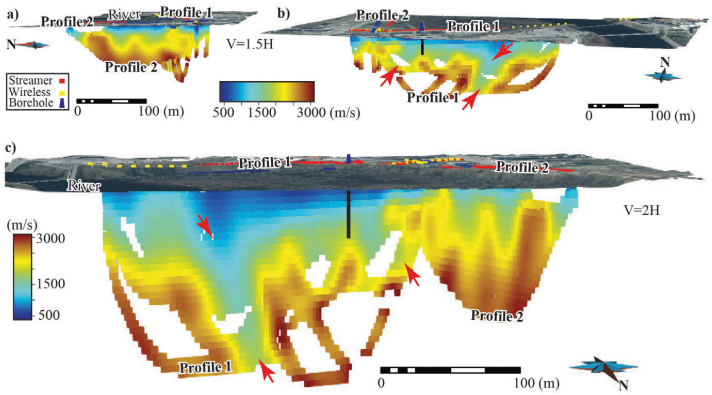

Figure 4 (a) Tomography model along Profile 2 with aerial photo projected on elevation surface. (b) Tomography model along Profile 1 with aerial photo projected on elevation surface, red arrows pointing at possible fractures in the bedrock and black line showing drilled depth to bedrock. (c) Both tomography models of Profile 1 and Profile 2 with elevation surface shown together.

Bedrock depth is well delineated on all results shown in Figure 4 and correlate well with borehole information. Along Profile 2, no major low-velocity zone in the tomography model can be noted that could indicate possible fracture zones. Significant velocity decreases can be seen in at least two zones in the tomography model of Profile 1 (red arrows in Figure 4b), indicating weak zones or fractured bedrock.

In addition to the refraction tomography, reflection seismic processing was performed with the processing steps shown in Table 3 and the results shown in Figure 5. The reflection seismic section along Profile 2 indicates that the bedrock is well delineated and dips towards the river, supporting the tomography result. Certain discontinuities of the reflections along Profile 2 can be seen, but with no clear evidence in the tomography models to support their interpretation as weak zones or fractures. An interruption of the reflection continuity, coinciding with a major low velocity zone seen on the tomography model of Profile 1, can be seen in Figure 5b,c (shown by the red arrows), which may additionally indicate fractured bedrock.

Boat-towed RMT survey in the city of Stockholm

To illustrate the potential of the boat-towed RMT system, an RMT survey was conducted close to the city of Stockholm where one of the largest underground infrastructures in Sweden is being built, a 21 km long multi-lane bypass-tunnel (Förbifart Stockholm). Several RMT profiles were acquired in the lake Mälaren to determine the depth to bedrock and investigate possible fracture zones that were inferred by geotechnical investigations. The tunnel will pass beneath three water passages and the deepest point will reach about -80 m (or 65 m below sea level). Here, we will focus on one of the three water passages, Kungshatt-Löven (Figure 6a,b). The tunneling is planned with two separate tunnels, each with three lanes. The longest part of the tunnel is 16.5 km between the Kungens kurva and Lunda access ramps. Construction began in early 2015 and is expected to take ten years to complete. When up and running, 140,000 vehicles per day are expected to use the bypass. Approximately 15 km of RMT profiles, with 15 m average spacing, were surveyed during three days, 3-5 hours each day (Figure 6a). Compared

Parameter	Profile 1	Profile 2
Remove all but vertical component Merge streamer and wireless Add geometry	Yes Yes Yes	Yes Yes Yes
Trace edit	Yes	Yes
Pick first arrivals	Yes	Yes
Spectral balancing FK mute – remove wind noise Refraction static correction	15-25-90-120 Hz Yes Yes	15-25-90-120 Hz Yes Yes
Datum correction	0 m, 1200 m/s	0 m, 1200 m/s
Automatic gain control Velocity analysis NMO correction Stack	100 ms Yes 70 % stretch mute Yes	100 ms Yes 70 % stretch mute Yes
Bandpass filtering f-x deconvolution Trace balance	20-30-80-90 Hz Yes Entire trace	20-30-110-120 Hz Yes Entire trace
Phase-shift migration	Yes	Yes

Table 3 Processing parameters applied for both lines

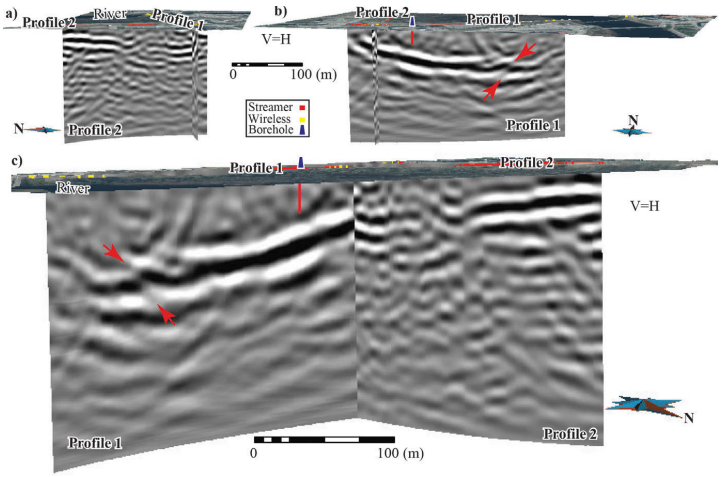

Figure 5 (a) Migrated reflection section of Profile 2 and Profile 1 (b) with aerial photo projected on elevation surface and red line showing drilled depth to bedrock. Note the discontinuity in the reflection shown by the red arrows indicating possibility of a fracture zone in the bedrock. (e) Both migrated reflection sections of Profile 1 and Profile 2 are shown together.

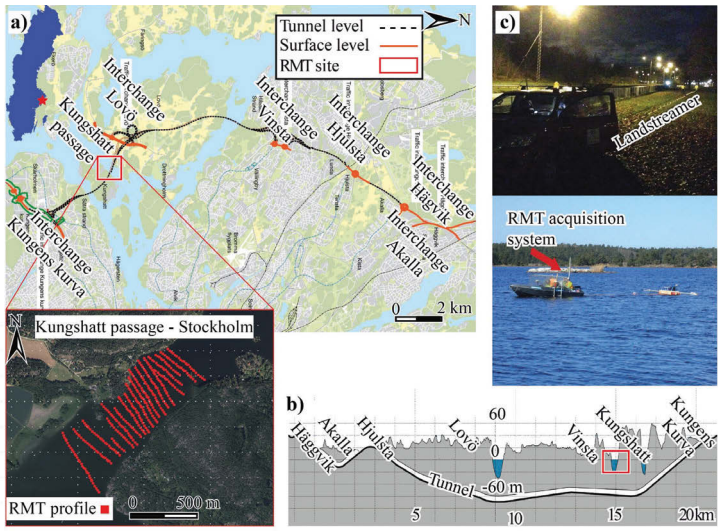

Figure 6 Location of the Stockholm Bypass (a) and an overview of the planned excavation depth along different segments of the tunnel (b). (c) Photos showing the two developed systems (seismic landstreamer and boat-towed RMT) side by side, (up) landstreamer towed by a vehicle, (down) boat-towed RMT system. (a) and (b) modified from the Swedish Transport Administration (Trfikverket; http://www.trafikverket.se/).

to traditional RMT land surveys, under normal field conditions (0.5 km long profile per day with 10 m station spacing), the new system is around 10 times faster. Details of the data acquisition and processing can be found in Bastani et al. (2015) and Mehta et al. (2017). Certain issues associated with the urban environment, such as cultural noise, can be seen on the raw data. Furthermore, the power cable underlying the water column also had adverse effects on data quality at some stations. These noises had to be identified and filtered before the inversion.

The data inversion was carried out with the code EMILIA based on damped Occam algorithm (Kalscheuer et al., 2008). Figure 7a,b shows 3D views from the 2D modelling of the RMT data together with information from an inclined well, B4, along with the model of the planned tunnel track. Fracture systems found during the core analyses are marked as K1-K5. Some cores analysed showed clays, graphite, salt and sulphide minerals within them likely contributing to the low-resistivity features seen in the models. The top of the bedrock is well resolved near the shorelines, but not as clearly in the middle of the water passages owing to the diffusive behavior of EM signals, making the direct interpretation of the fractured bedrock ambiguous. A small island visible on the aerial photo is clearly resolved by the RMT models. The top resistive layer is interpreted to be the fresh water in Figure 7b, particularly note the resistive fresh water, with conductive sediments and a resistive bedrock near the small island on the Löven side of the profiles. These models show the reliability and potential of this prototype boat-towed RMT system in shallow water conditions with it being both cost effective and efficient. Thus, it has encouraged us to build a more robust and sophisticated acquisition system for future use. One of the drawbacks of RMT is the limited depth of penetration. Acquisition of lower frequencies using a controlled source are planned in the future. Details concerning resolution and a sensitivity analysis can be found in Mehta et al., (2017).

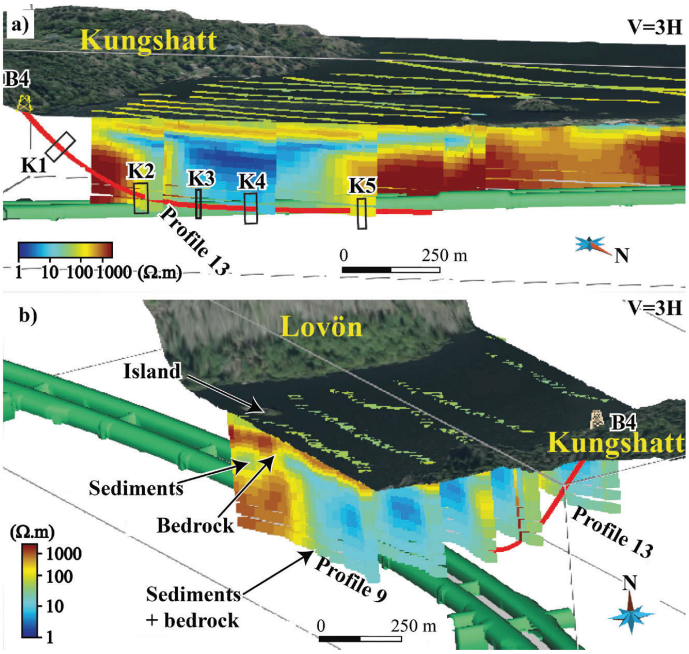

Figure 7 3D views showing (a) the directional borehole, B4, along with the RMT resistivity models and tunnel model shown in green. Five major fracture systems and their widths were mapped in the cores from B4, four (K2–K5) are likely to be contributing to the conductivity zone in the middle of the water passage. (b) A small island at the site and its response observed in the RMT model. Note that the RMT data resolve the water column, lake sediments and the underlying bedrock clearly in this part of the model.

Discussion and conclusions

Two modern geophysical systems have been developed with a particular focus on urban underground infrastructure planning projects and that can also be used for various near-surface applications. Data acquired by the two systems show excellent quality, allowing high-resolution imaging of the subsurface structures in urban environments. The two systems are currently being used in several infrastructure planning projects and there is still room for improvements based on the feedback from their applications. Future developments will include exploiting the broadband frequency nature of the streamer data and development of a 3C source that can generate broad frequency range signals that the streamer sensors are capable of recording. The boat-towed RMT system will require new hardware and software developments. A DGPS system was recently linked to the system to provide high-precision geodetic surveying of the acquisition points, which is essential for this type of survey. The boat-towed RMT works quite efficiently, e.g., 5 km line-data per day, and shows high reliability for bedrock mapping and fracture zone delineation, particularly over shallow water bodies. The signal penetration depth of the boat-towed system can also be enhanced using additional lower frequency controlled source (control source RMT).

Here, we presented a case study of the seismic landstreamer at a site contaminated with chlorinated hydrocarbons to image the bedrock and possible fracture zones that can be used as pathways for contaminant migration. Tomographic results along both profiles show that the bedrock depth is well determined and indicate the existence of at least two fracture zones in the bedrock. The reflection seismic section along Profile 1 shows a clear interruption of the interpreted bedrock reflection, indicating a potential fracture zone and supporting the tomography results. The boat-towed RMT case study from the Förbifart Stockholm also shows the potential of this method for mapping purposes in a time- and cost-effective manner on fresh or brackish water bodies. This is particularly important and can provide important information for where detailed drilling and geotechnical investigations should be carried out. The two systems have so far been used in several related studies in Sweden, Finland, Norway and Denmark, which encourages us to improve them further.

Acknowledgments

This study was conducted within the framework of Trust 2.2 (Trust-GeoInfra; http://www.trust-geoinfra.se,) sponsored by Formas (project number: 252-2012-1907), SGU (363-26512013), BeFo (BeFo 340), SBUF, Skanska, FQM and NGI. B. Brodic, S. Mehta and S. Wang PhD studies are supported by Trust 2.2 project. We thank Marcus Wennermark and Kristofer Hellman from Lund University for their help during the seismic acquisition in Kristianstad. We would like to thank Kristianstad municipality for permitting us to do the survey. Lund University (and their partners) through the Trust 4.2 project provided the seismic source used in the seismic study for which we are thankful. GLOBE Claritas under licence from the Institute of Geological and Nuclear Sciences Limited (GNS), Lower Hutt, New Zealand was used to prepare and process the seismic data. We thank A. Tryggvason for providing the ps_tomo tomography code. gOcad from Paradigm was used for 3D visualization and viewing of the data and results.

References

Bastani, M. [2001]. *EnviroMT: A new controlled source/radio magnetotoelluric system*, Uppsala University, Department of Geophysics.

Bastani, M., L. Persson, S. Mehta, and A. Malehmir [2015]. Boat-towed radio-magnetotellurics — A new technique and case study from the city of Stockholm. *Geophysics*, **80** (6), B193–B10, doi:10.1190/geo2014-0527.1.

Brodic, B., A. Malehmir, C. Juhlin, L. Dynesius, M. Bastani, and H. Palm [2015]. Multicomponent broadband digital-based seismic landstreamer for near-surface applications. *J. Appl. Geophys.*, **123**, 227–241, doi:10.1016/j.jappgeo.2015.10.009.

Brodic, B., A. Malehmir and C. Juhlin [2017]. Delineating fracture zones using surface-tunnel-surface seismic data, P-S and S-P mode conversions. *J. Geophys. Res. Solid Earth*, n/a–n/a, doi:10.1002/2017JB014304.

Dehghannejad, M., A. Malehmir, M. Svensson, M. Lindén, and H. Möller [2017]. High-resolution reflection seismic imaging for the planning of a double-train-track tunnel in the city of Varberg, southwest Sweden. *Surf. Geophys.*, **1** (1), 226–240, doi:10.3997/1873-0604.2017011.

Eiken, O., M. Degutsch, P. Riste, and K. Rød [1989]. Snowstreamer: an efficient tool in seismic acquisition. *First Break*, **7** (1223), doi:10.3997/1365-2397.1989021.

Guha, N., D. Loomis, Y. Grosse, B. Lauby-Secretan, F. E. Ghissassi, V. Bouvard, L. Benbrahim-Tallaa, R. Baan, H. Mattock, and K. Straif [2012]. Carcinogenicity of trichloroethylene, tetrachloroethylene, some other chlorinated solvents, and their metabolites. *Lancet Oncol.*, **13** (12), 1192–1193, doi:10.1016/S1470-2045(12)70485-0.

Johansson, S., C. Sparrenbom, G. Fiandaca, A. Lindskog, P.-I. Olsson, T. Dahlin, and H. Rosqvist [2017]. Investigations of a Cretaceous limestone with spectral induced polarization and scanning electron microscopy. *Geophys. J. Int.*, **208** (2), 954–972, doi:10.1093/gji/ggw432.

Kalscheuer, T., L.B. Pedersen, and W. Siripunvaraporn [2008]. Radiomagnetotelluric two-dimensional forward and inverse modelling accounting for displacement currents. *Geophys. J. Int.*, **175** (2), 486-514, doi: 10.1111/j.1365-246X.2008.03902.x.

Malehmir, A., S. Wang, J. Lamminen, B. Brodic, M. Bastani, K. Vaittinen, C. Juhlin, and J. Place [2015a]. Delineating structures controlling sandstone-hosted base-metal deposits using high-resolution multicomponent seismic and radio-magnetotelluric methods: a case study from Northern Sweden. *Geophys. Prospect.*, **63** (4), 774–797, doi:10.1111/1365-2478.12238.

Malehmir, A., F. Zhang, M. Dehghannejad, E. Lundberg, C. Döse, O. Friberg, B. Brodic, J. Place, M. Svensson, and H. Möller [2015b]. Planning of urban underground infrastructure using a broadband seismic landstreamer — Tomography results and uncertainty quantifications from a case study in southwestern Sweden. *Geophysics*, **80** (6), B177–B192, doi:10.1190/geo2015-0052.1.

Malehmir, A., L. V. Socco, M. Bastani, C. M. Krawczyk, A. A. Pfaffhuber, R. D. Miller, H. Maurer, R. Frauenfelder, K. Suto, S. Bazin, K. Merz, and T. Dahlin [2016a]. Near-Surface Geophysical Characterization of Areas Prone to Natural Hazards: A Review of the Current and Perspective on the Future. *Adv. Geophys.*, **57** (1), 51–146, doi:http://dx.doi.org/10.1016/bs.agph.2016.08.001.

Malehmir, A., M. Andersson, S. Mehta, B. Brodic, R. Munier, J. Place, G. Maries, C. Smith, J. Kamm, M. Bastani, and H. Mikko [2016b]. Post-glacial reactivation of the Bollnäs fault, central Sweden; a multidisciplinary geophysical investigation. *Solid Earth*, **7** (2), 509–527, doi:10.5194/se-7-509-2016.

Malehmir, A., S. Heinonen, M. Dehghannejad, P. Heino, G. Maries, F. Karell, M. Suikkanen, and A. Salo [2017]. Landstreamer seismics and physical property measurements in the Siilinjärvi open-pit apatite (phosphate) mine, central Finland. *Geophysics*, **82** (2), B29–B48, doi:10.1190/geo2016-0443.1.

Maries, G., E. Ahokangas, J. Mäkinen, A. Pasanen, and A. Malehmir [2017]. Interlobate esker architecture and related hydrogeological features derived from a combination of high-resolution reflection seismics and refraction tomography, Virttaankangas, southwest Finland. *Hydrogeol. J.*, **25** (3), 829–845, doi:10.1007/s10040-016-1513-9.

Mehta, S., M. Bastani, A. Malehmir, and L. B. Pedersen [2017]. Resolution and sensitivity of boat-towed RMT data to delineate fracture zones – Example of the Stockholm bypass multi-lane tunnel. *J. Appl. Geophys.*, **139**, 131–143, doi:10.1016/j.jappgeo.2017.02.012.

Miller, R., S. Pullan, J. Waldner, and F. Haeni [1986]. Field comparison of shallow seismic sources. *Geophysics*, **51** (11), 2067–2092, doi:10.1190/1.1442061.

Tryggvason, A., S. ður T. Rögnvaldsson, and Ó. G. Flóvenz [2002]. Three-dimensional imaging of the P- and S-wave velocity structure and earthquake locations beneath Southwest Iceland. *Geophys. J. Int.*, **151** (3), 848–866, doi:10.1046/j.1365-246X.2002.01812.x.

Whiteley, R. [2009]. Application of geophysics to underground space development for improvement of urban environments. *20th Geophysical Conference*, Extended Abstracts.

AGU PUBLICATIONS

JGR

Journal of Geophysical Research: Solid Earth

RESEARCH ARTICLE
10.1002/2017JB014304

Key Points:
- Surface-tunnel-surface seismic experiment was conducted at the Äspö Hard Rock Laboratory in Sweden
- Tomography results image the rock mass between the tunnel and the surface, as well as fracture systems
- Strong *P-S* and *S-P* mode conversions are observed from the fracture zones and their V_p, V_s, Q_p, Q_s, V_p/V_s, and Poisson's ratio estimated

Correspondence to:
B. Brodic,
bojan.brodic@geo.uu.se

Citation:
Brodic, B., A. Malehmir, and C. Juhlin (2017), Delineating fracture zones using surface-tunnel-surface seismic data, *P-S*, and *S-P* mode conversions, *J. Geophys. Res. Solid Earth*, *122*, doi:10.1002/2017JB014304.

Received 9 APR 2017
Accepted 23 JUN 2017
Accepted article online 27 JUN 2017

Delineating fracture zones using surface-tunnel-surface seismic data, *P-S*, and *S-P* mode conversions

B. Brodic[1], **A. Malehmir**[1], **and C. Juhlin**[1]

[1]Department of Earth Sciences, Uppsala University, Uppsala, Sweden

Abstract A surface-tunnel-surface seismic experiment was conducted at the Äspö Hard Rock Laboratory to study the seismic response of major fracture systems intersecting the tunnel. A newly developed three-component microelectromechanical sensor-based seismic landstreamer was deployed inside the noisy tunnel along with conventional seismic receivers. In addition to these, wireless recorders were placed on the surface. This combination enabled simultaneous recording of the seismic wavefield both inside the tunnel and on the surface. The landstreamer was positioned between two geophone-based line segments, along the interval where known fracture systems intersect the tunnel. First arrival tomography produced a velocity model of the rock mass between the tunnel and the surface with anomalous low-velocity zones correlating well with locations of known fracture systems. Prominent wave mode converted direct and reflected signals, *P-S* and *S-P* waves, were observed in numerous source gathers recorded inside the tunnel. Forward travel time and 2-D finite difference elastic modeling, based on the known geometry of the fracture systems, show that the converted waves are generated at these systems. Additionally, the landstreamer data were used to estimate V_p/V_s, Poisson's ratio, and seismic attenuation factors (Q_p and Q_s) over fracture sets that have different hydraulic conductivities. The low-conductivity fracture sets have greater reductions in *P* wave velocities and Poisson's ratio and are more attenuating than the highly hydraulically conductive fracture set. Our investigations contribute to fracture zone characterization on a scale corresponding to seismic exploration wavelengths.

1. Introduction

The seismic response of fractures and cracks has interested the hard rock seismic exploration community since the early works of *O'Connell and Budiansky* [1974], *Hudson* [1981], and *Mair and Green* [1981]. Fractured media have strong effects on seismic wave propagation, such as causing shear wave birefringence, scattering, and attenuation or changes in the elastic parameters [*Crampin*, 1981; *Hudson*, 1981; *Eaton et al*., 2003]. In addition to these, oriented fractures are considered to be a common cause for seismic anisotropy [*Thomsen*, 1986; *Yardley and Crampin*, 1991; *Thomsen*, 2002]. Apart from the influence on seismic properties, fractures in crystalline rock environments act as conduits for gas and fluid migration, hence affecting the local stress field, the hydrogeological regime, underground infrastructures, and drilling and mining activities, among others. When the fractures are saturated with a compressible fluid or gas, the media may be highly attenuating [*Anderson et al*., 1974; *O'Connell and Budiansky*, 1974; *Johnston et al*., 1979; *Mavko and Nur*, 1979; *Mukerji and Mavko*, 1994]. Compared to laboratory studies, sonic logging, or studies conducted using vertical seismic profiling (VSP), there are few reports on seismic field experiments that investigate the relation between the permeability of fractures and their seismic response [*Green and Mair*, 1983; *Paulsson et al*., 1985; *Juhlin*, 1995b; *Lundberg et al*., 2012; *Liu and Martinez*, 2013]. To address some of the above-mentioned issues, we conducted a novel surface-tunnel-surface seismic survey at the Äspö Hard Rock Laboratory (HRL) in southern Sweden during April 2015. Well-documented fracture systems, extending from the surface and intersecting the tunnel at different depths [*Kornfält and Wikman*, 1988; *Kornfält et al*., 1997; *Rhén et al*., 1997; *Berglund et al*., 2003], provided a unique opportunity to evaluate their seismic response using a digital three-component (3C) seismic landstreamer [*Brodic et al*., 2015; *Malehmir et al*., 2015a, 2015b] in the tunnel. Both sources and receivers were located on the surface and inside the tunnel and the seismic wavefield simultaneously recorded on all receivers. Compared to other published experiments addressing the seismic response of fractures [*Maurer and Green*, 1997; *Angioni et al*., 2003; *Gritto et al*., 2003; *Daley et al*., 2004; *Gritto et al*., 2004; *Dietrich and Tronicke*, 2009; *Martínez and Mendoza*, 2011], the use of sources both inside the rock mass and on the surface makes this study rather unique. Our primary objectives were

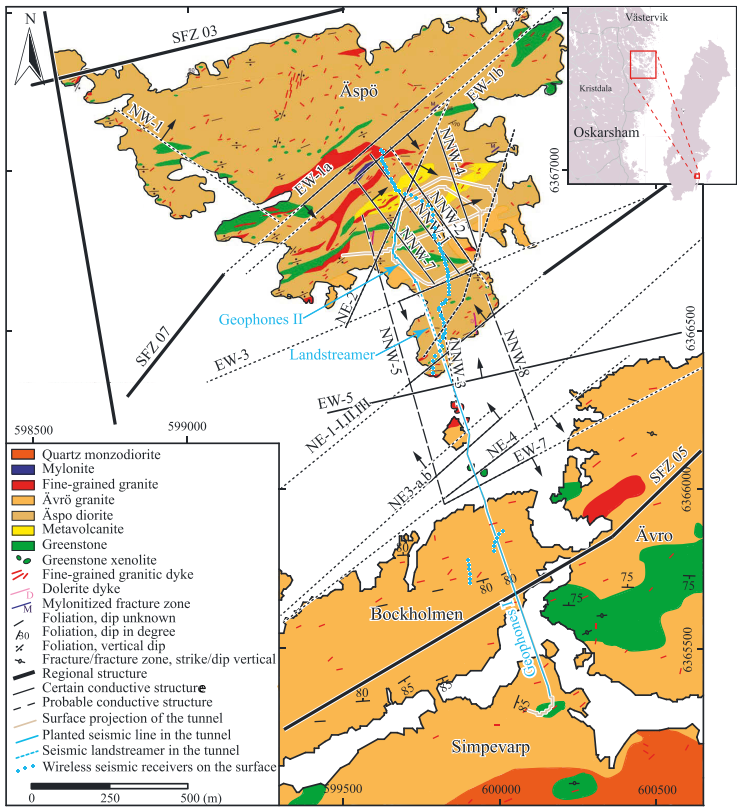

Figure 1. Geographical location, geological and structural map of the Äspö HRL site, with surface projection of the tunnel track and the location of the seismic stations inside the tunnel and wireless receivers on the surface shown. The arrows show the dip direction of the structures while the structure orientation corresponds to true azimuth. The NE-1 and EW-3 fracture systems were the primary targets of the seismic study. Also shown are mapped occurrences of foliations with their dip angles and occurrences of fine-grained granitic dikes. The white regions represent the sea surrounding the island.

1. high-resolution fracture zone delineation in underground facilities using the seismic method and checking the performance of the seismic landstreamer inside the rock mass,
2. estimating elastic properties and seismic attenuation of the fracture zones with different hydraulic properties and host rock at the site,
3. studying and modeling the seismic response and wave mode conversions observed in the vicinity of the fracture systems,
4. characterization of the rock mass between the tunnel and surface by first arrival travel time tomography given the unique acquisition geometry, and
5. verifying the capability of the digital-based seismic sensors in a highly electromagnetically noisy environment in comparison with traditional geophone-type sensors.

2. Äspö Hard Rock Laboratory

The Äspö HRL is an underground research facility located in southeastern Sweden (Figure 1), operated by the Swedish Nuclear Fuel and Waste Management Company (SKB). It was established at the end of the 1980s, with the goal of studying the properties and behavior of rock masses, testing methods for storage of spent nuclear fuel, characterization of prospective repository sites, and development and testing of new

characterization methods in the crystalline environment [*Berglund et al*., 2003]. The laboratory consists of several facilities on the surface and about 3.6 km of tunnels at different levels. From the surface (approximately 15 m above sea level), the main access tunnel goes for approximately 1.6 km downward reaching an elevation of −230 m below sea level. After this, it spirally continues downward until it reaches the final −450 m level. An elevator shaft connects the main facility building on the surface and different tunnel depths within this spiral part.

Geologically, Äspö is located predominantly within the metamorphosed granitoid-volcanic rocks of Småland-Värmland [*Kornfält et al*., 1997; *Stanfors et al*., 1999; *Stephens*, 2009; *Lundberg and Juhlin*, 2011; *Lundberg*, 2014]. The oldest rocks in the area formed during the Svecokarelian orogeny (1.85–1.65 Ga) with periods of alkali-calcic magmatism. They are represented by granitoidic to dioritoidic and gabbroidic rocks and fine-grained granitic or aplitic dikes emplaced at around 1.45 Ga. The Sveconorwegian orogeny (1.1–0.9 Ga) was coeval with the emplacement of dolerite dikes that are up to 10 m in thickness. The youngest rocks in the area are meta-sandstones deposited during the Late Precambrian, Early Cambrian period [*Kornfält and Wikman*, 1988; *Gustafson et al*., 1989; *Kornfält et al*., 1997; *Berglund et al*., 2003]. Metamorphic overprinting resulted in structural, mineralogical, and chemical changes, all contributing to the complex geology of the area. Recently, glacial processes have modified the area, giving the present-day surface consisting of exposed bedrock and occurrences of moraines and glacial sediments of up to 5 m in thickness [*Kornfält and Wikman*, 1988].

On a local scale, two rock types are dominant, along with the occurrences of fine-grained, intermediate rocks and dikes of fine-grained granite and pegmatite [*Kornfält et al*., 1997; *Rhén et al*., 1997; *Berglund et al*., 2003]. These are Ävrö granites (densities 2640–2700 kg/m^3) and Äspö diorites (densities 2700–2800 kg/m^3). Figure 1 shows the geographical location of the site, major geological units, and structural features of the Äspö HRL. The geological information is based on site-scale geological mapping, open trenches, drill cores, information from the tunnel, and geophysical information [*Kornfält and Wikman*, 1988; *Kornfält et al*., 1997; *Rhén et al*., 1997; *Berglund et al*., 2003; *Rønning et al.*, 2003; *Wahlgren et al*., 2006]. Tectonic features shown represent their surface intersections inferred in the same way. Reports on hydraulic conductivity are based on direct observations in the tunnel and drilling [*Rhén et al*., 1997; *Berglund et al*., 2003].

The approximately 1.85 Ga complex structural history of the region has resulted in the formation of several deformation zones at the Äspö HRL site. *Stanfors et al.* [1999] defines seven different tectonic episodes during this period. The deformation zones commonly consist of several parallel fracture sets with different degrees of alteration and hydraulic properties, where dip angles and widths change with depth [*Rhén et al*., 1997; *Berglund et al*., 2003]. Some of the fracture systems are estimated to be more than 10 km long and extend to at least 1.5 km depth [*Rhén et al*., 1997]. Among the structures shown in Figure 1, we focus here on the NE-1 and EW-3 fracture systems crossed by the seismic recorders in the tunnel. According to *Ask* [2006] and *Andersson* [2007], where the two fracture systems of interest are encountered in the tunnel, the major principal stress (σ_1) has a magnitude of 25–35 MPa, trending 310°, and a plunge of 0–30°. Magnitude of the intermediate principal stress (σ_2) ranges from 10 to 17 MPa, with the direction of 90° and a plunge 53–90°. Minor principal stress (σ_3) ranges from 6 to 10 MPa, with the direction 220° and a plunge of 0–20°.

During the preliminary phase of site investigations, the NE-1 fracture system was clearly delineated by surface and borehole geophysical methods [*Rhén et al*., 1997]. In the excavation phase, it caused significant problems due to severe water inflow (once grouted, 1600 liters per minute was flowing through an open valve on a 57 mm diameter borehole drilled into it; Figure 2 [*Rhén et al*., 1997]). Where the fracture system intersects the tunnel, three parallel branches of NE-1 are separated by less fractured host rock composed of Äspö diorite and fine-grained granite, both having been metamorphosed to a certain extent. These are referred to as NE-1-I (20 m wide), NE-1-II (12 m wide), and NE-1-III (30 m). NE-1-I and NE-1-II are separated by about 8 m of fractured host rock while NE-1-II and NE-1-III are separated by about 10 m of less fractured host rock, giving a total width of the system of about 80 m. The widths and distances given are based on our own observations during the seismic experiment using the fracture locations and markers identified by SKB on the tunnel walls. In addition, a study by *Berglund et al.* [2003] provides information on the different hydraulic properties of the individual fracture sets. The first two fracture sets (NE-1-I and NE-1-II) are described as highly fractured, partly clay altered with the latter being more hydraulically conductive then the former. NE-1-III is referred to as fractured and highly hydraulically conductive (Figure 2). Its central part is a 5–8 m wide partly clay altered zone.

Figure 2. Water inflow (1600 L/min, 57 mm diameter hole) from NE-1-III showing the significance of fracture zone delineation and characterization in the preliminary site planning stage. Photo from *Rhén et al.* [1997].

All three sets are described as water bearing with an average fracture frequency of approximately 15 fractures/m [*Wahlgren et al.*, 2006]. The EW-3 zone (Figure 1) is about 12 m wide, with five different fracture sets within it with low to medium degrees of clay alteration, medium to strong tectonization, and an average fracture frequency of approximately 17/m. The central fracture set is 1.5–2 m wide with altered clay fillings [*Berglund et al.*, 2003]. The whole zone represents the contact between Äspö diorite and fine-grained granite. Prior to being sealed, it leaked 90 liters of water per minute. According to *Berglund et al.* [2003], NE-1 and EW-1 (Figure 1) represent major zones of weaknesses, marking the southern and northern boundary of a block.

Aside from the two aforesaid fracture systems, another one striking mainly NE-SW, located between the NE-1 and EW-3 (Figure 1, dashed line between the NE-1 and EW-3), was also crossed by the seismic line. This fracture zone was identified in the earlier studies by *Kornfält and Wikman* [1988] and *Rydström and Gereben* [1989], but no naming or structural information on it was found by our literature studies.

3. Äspö HRL Seismic Experiment

The seismic survey at the Äspö HRL site was conducted using a combination of conventional 10 Hz vertical geophones, a seismic landstreamer [*Brodic et al.*, 2015; *Malehmir et al.*, 2015a], 1C wireless recorders (connected to 10 Hz vertical geophones), and 3C wireless recorders (connected to MEMS-based, DSU3™ sensors). A Sercel Lite™ acquisition system was used for data recording. Based on experience from other crystalline rock environments, a 500 kg weight-drop hammer mounted on a commercially available skid steer loader was used as the seismic source [*Sopher et al.*, 2014; *Place et al.*, 2015; *Malehmir et al.*, 2017]. At every source location, the drop hammer was released 5 times onto a square-shaped hard aluminum plate (60 cm by 60 cm and about 2.5 cm thick) mounted at the bottom of the hammer casing. The hits were recorded within a time window of 25 s and later vertically shifted to zero and stacked together to increase the S/N. The resulting stacked source gathers were reduced to 1 s record length for further processing and analysis. Table 1 shows the main acquisition parameters of the seismic survey.

GPS-time synchronization of the seismic data was obtained by placing the recording vehicle outside the tunnel and connecting it to the tunnel seismic line via a 50 m long extension cable. Starting from about 50 m away from the entrance to the tunnel, to ensure good sensor-ground coupling, we drilled and planted 279 vertical component 10 Hz geophones (7 cm spike) at every 4 m. Geophones were vertically planted in drill holes made on the rock exposed on the side of the tunnel, 5–35 cm from the tunnel floor (labeled as Geophones I in Figures 1 and 3; also see Figure 4a). Four meters away from the last planted geophone, the

Table 1. Main Acquisition Parameters of the Tunnel-Surface Seismic Survey at Äspö HRL

Acquisition System	Sercel Lite
Total number of receivers in the tunnel	413
Planted vertical 10 Hz geophones	333 (4 m apart)
Landstreamer units	80-3C DSU3 (20 × 4 m + 60 × 2 m)
Total number of receivers on the surface	75 (51-1C 10 Hz and 24-3C DSU3)
Nominal surface receiver spacing	12 m
Recording length	25 s (reduced to 1 s after vertical stacking)
Sampling rate	1 ms
Source	Skid steer loader mounted drop hammer (500 kg)
Number of hits per source location	5
Nominal source spacing	8 m
Total number of source points	229 (tunnel and surface)

seismic landstreamer (MEMS-based, 80 DSU3 units, 200 m long) was deployed. The units were placed along the edge of the asphalt on the tunnel floor, in the continuation of the planted geophone line segment (landstreamer in Figure 3; also see Figure 4). Due to the 3C nature of the landstreamer units, it was positioned along the intersection of the NE-1 and EW-3 zones and the tunnel. In addition to these, 54 vertical component 10 Hz geophones, at 4 m intervals, were planted in drill holes at the tail of the landstreamer (Geophones II in Figures 1 and 3). The total length of the seismic spread with all different segments inside the tunnel was about 1500 m. To obtain simultaneous recording of the seismic wavefield both inside the tunnel and on the surface, another seismic line was designed using 75 wireless recorders (labeled as wireless in Figure 3). Twenty-four three-component (same type as the ones used in the streamer, DSU3™) and 51 single-component, connected to 10 Hz vertical geophones, units were deployed on the surface. Spacing between the wireless units varied from 8 to 16 m. Figure 4b shows a 10 Hz geophone planted in a drilled hole in the rock and connected to a wireless seismic recorder.

Data acquisition started in the lower tunnel part before the spiral part and advanced toward the surface with a source spacing of 4–16 m. After recording all the source points in the tunnel, the source was moved to the surface, where sources were made at all the wireless units that were accessible to the source (55 source locations). During the surface recording, data were also recorded on the seismic line inside the tunnel, and similarly, the surface receivers were recording the sources activated in the tunnel. Coordinates of all surface receivers and source positions were surveyed using a DGPS surveying system (centimeter accuracy). Inside the tunnel, known markers and their positions were used to position the receivers into the internal coordinate system used in the tunnel. These coordinates were later transformed to the same system as the surface data.

Parallel to our seismic experiment, an independent seismic survey was conducted on the sea above the tunnel, next to a small island in the central part of the site (Figure 3; marine seismic experiment arrow)

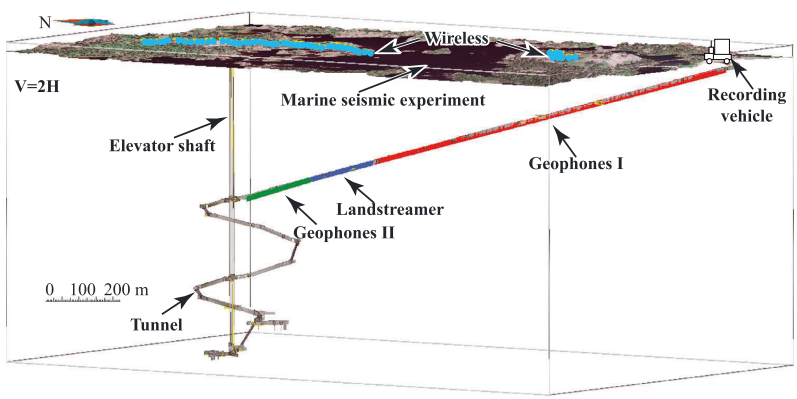

Figure 3. Tunnel model and an aerial photo projected on top of lidar (elevation) data with different parts of the seismic spread labeled and shown in different colors. Twice vertically exaggerated.

Figure 4. Examples of planted geophones in drill holes in the rock (a) in the tunnel and (b) on the surface. (c) The seismic landstreamer used in the tunnel in the downdip direction (known from drilling) of the NE-1-III fracture zone.

[see *Ronczka et al*., 2016]. Data from four of these explosive sources were merged into our data set. Since no shooting could be done in the southern part of the line with the weight drop, these marine explosive sources partly contribute to imaging the rock mass in the southern part of the survey area.

4. Seismic Data of the Äspö HRL Site

Strong electric or electromagnetic noise is present in the tunnel and most apparent on the planted line segments (Geophones I and II in Figure 5). This noise is absent on the landstreamer data. Aside from the dominant 50 Hz electric power grid frequency, both higher- and lower-order power harmonics can also be seen. The spacing of the landstreamer units on three of the segments is 2 m, while all geophones and the units on the fourth landstreamer segment are spaced at 4 m. This irregular unit spacing results in the apparent change of slope of the direct arrivals and should not be mistaken for refracted arrivals.

Applying several notch filters corresponding to the frequencies of the individual current harmonics helped in attenuating the electric noise from the planted geophones. For the main 50 Hz current noise, a band-stop filter between 49 and 51 Hz was used, with a 2 Hz cosine taper on both sides. Aside from the electric current, noise trains coming from the southern side of the tunnel, most probably originating from the nuclear power plant located in the site's vicinity, were problematic. Vertical stacking of the repeated hits partly helped to attenuate them. However, for some records these remained quite strong, but with low frequencies and low apparent velocity. To further attenuate them, a carefully designed F-K filter was applied (Figure 6a). Inspection of Figures 5a and 6a shows observable converted and reflected events in both records, indicating that they are real features and not artifacts of the F-K filter processing.

The F-K filter was not applied to the data from the streamer or to the Geophone II part because of the steep nature of the important events likely generated from the fracture systems. Figure 6b shows an example source gather with the source being located on the landstreamer part of the seismic line, close to the edge of the NE-1 fracture system (source location 300, corresponding to receiver 300 on the seismic line). For this gather, only notch filters and the band-stop filter were applied. Note here the more distinct, more consistent, and narrower wavelets of the same events and higher-frequency content of the landstreamer units compared to the geophone segments. Comparing Figure 6a with 6b shows how the F-K filter suppresses noise coming from the side of the seismic line. This noise is more prominent in Figure 6b, but not sufficient to obscure the different seismic events of interest.

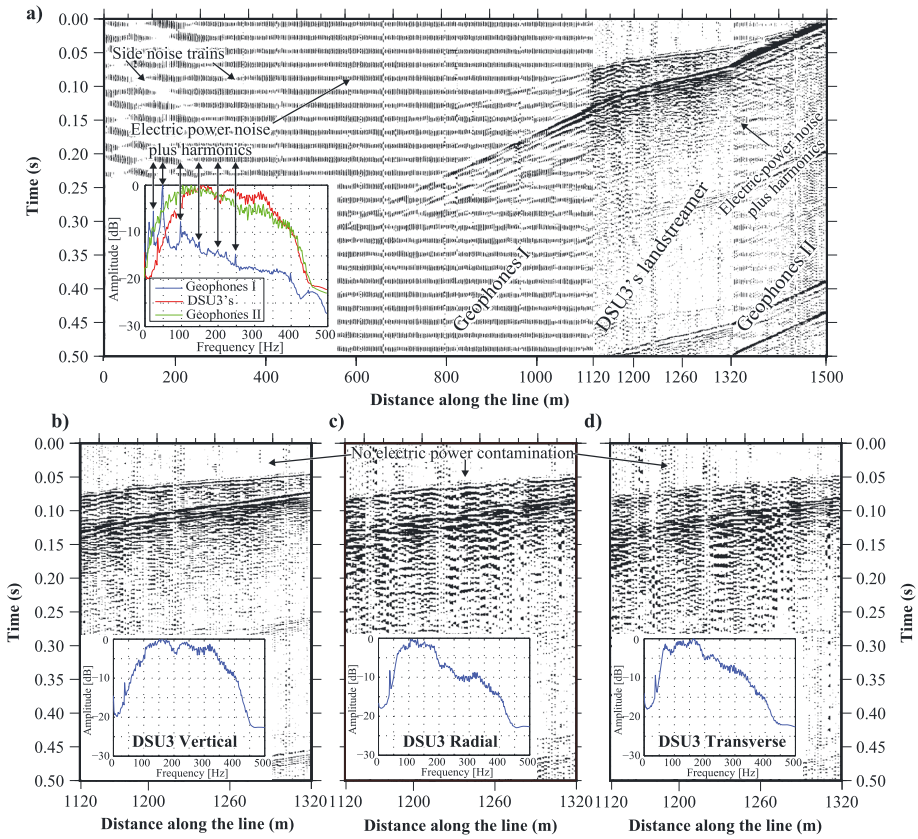

Figure 5. An example raw source gather from the seismic line inside the tunnel with trace normalization applied. (a) First 279 planted 10 Hz geophones (Geophones I), followed by 80 DSU3 unit landstreamer (DSU3's landstreamer) and 54 planted 10 Hz geophones (Geophones II), with their corresponding amplitude spectra. (b–d) An enlarged view of the data from the streamer part showing vertical, radial, and transverse components of the data, respectively, and their corresponding amplitude spectra calculated within the same window as displayed.

In addition to the source gathers shown in Figures 5 and 6, an example source gather from one of the marine explosive sources with the merged wireless and hydrophone data is shown in Figure 7a. Figure 7b shows the same explosive source simultaneously recorded on the receivers in the tunnel with some interpreted events marked. Notable are high-quality *P* and *S* wave arrivals on almost all the receivers of our seismic spread. Additionally, clear *P-S* wave mode conversion at the seafloor and both *P-S* and *S-P* conversions at the fracture system for the downgoing wavefields are observed (Figure 7b). A delay in the *P* wave first arrivals where the NE-1 fracture system is located can also be observed. Particle motion plots for receiver 280 (first unit on the landstreamer inside the tunnel) within different windows show strong vertical polarization, including *P-S* and direct *S* wave arrivals (Figure 8). This is typical for all landstreamer 3C units.

5. Seismic Imaging of the Fracture Systems

To initially characterize the rocks and fracture zones located between the tunnel and the surface we used first arrival tomography. On almost all source gathers from the tunnel the most prominent arrivals in the vertical component data are the direct shear waves (e.g., Figure 8). Strong shear waves are likely due to the large velocity contrast between the rock and the air in the tunnel, converting most of the energy to shear waves right at the tunnel floor [*Bellefleur et al.*, 2004; *Malehmir and Bellefleur*, 2010]. Particle motion plots (hodograms) of the

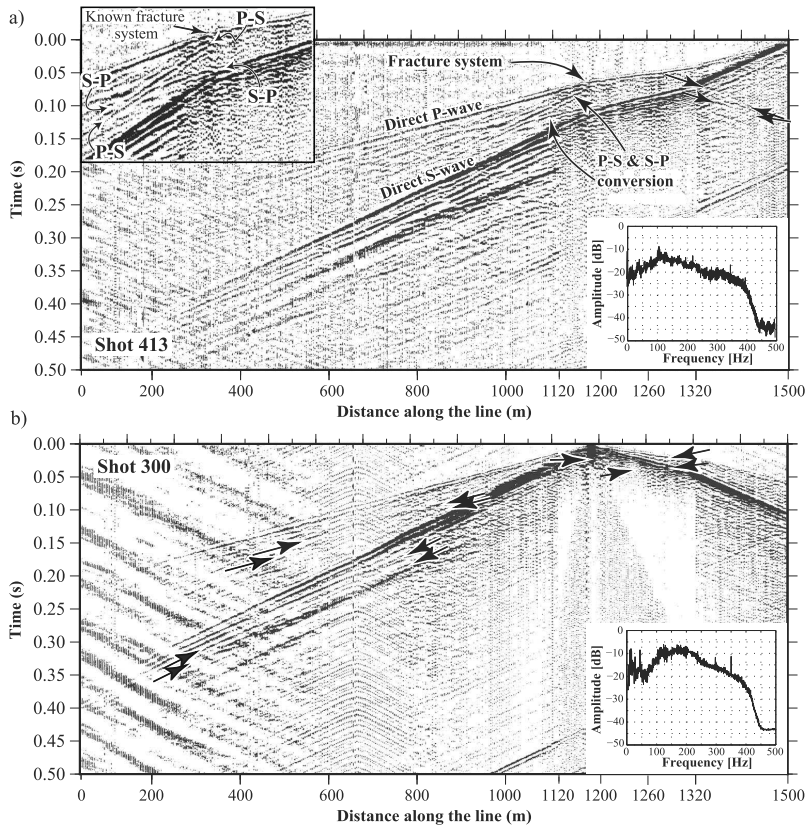

Figure 6. Example source gathers showing the quality of the seismic data after preprocessing applied. (a) Source location 413 corresponding to the last receiver (receiver 413) in the tunnel and (b) source gather for a source located at receiver 300 belonging to the landstreamer portion of the seismic line. Source location 300 is located in the zone of the NE-1 fracture system. Note the strong *P-S* and *S-P* wave modes originating from one of the known fracture zones in the tunnel, low-frequency energy at the beginning of the line, and various events marked by the arrows. The different receiver spacing of the streamer and planted geophones causes the apparent change in slope of the first arrivals.

shear wave window (Figure 8) suggest vertical polarization and no strong evidence of surface waves. Inclination of the tunnel and seismic source at an angle to vertical to the tunnel floor may have also contributed to the generation of shear waves.

Both *P* and *S* wave first arrivals from the active tunnel line and wireless recorders were manually picked. Manual picking was chosen to make sure that the delays noted on the *P* wave first arrival trend across the NE-1 fracture system were preserved (Figures 6a and 8). The picking resulted in 67,690 *P* wave and 64,540 *S* wave first arrivals from 230 sources recorded on 528 receivers, including receivers from the marine seismic experiment (40 receivers on 4 shots). Noisy traces where the arrivals could not be clearly distinguished were excluded from picking. Joint *P* and *S* wave first arrival travel time tomography was performed using the PS_tomo 3-D diving-wave tomography code [*Podvin and Lecomte*, 1991; *Hole*, 1992; *Hole and Zelt*, 1995; *Tryggvason et al.*, 2002; *Tryggvason and Linde*, 2006]. Variance-based weighting of the *P* and *S* wave travel times was used for the inversion. Due to the sparse source-receiver setup on the surface and line crookedness, the tomography was done using large cells in the lateral direction. The cell sizes in the inline and depth directions were 4 m, and to obtain a 2-D model of the velocity distribution (a 2-D slice from the 3-D velocity volume), 200 m wide cells in the lateral (crossline) direction were used. Nine iterations were carried out in the

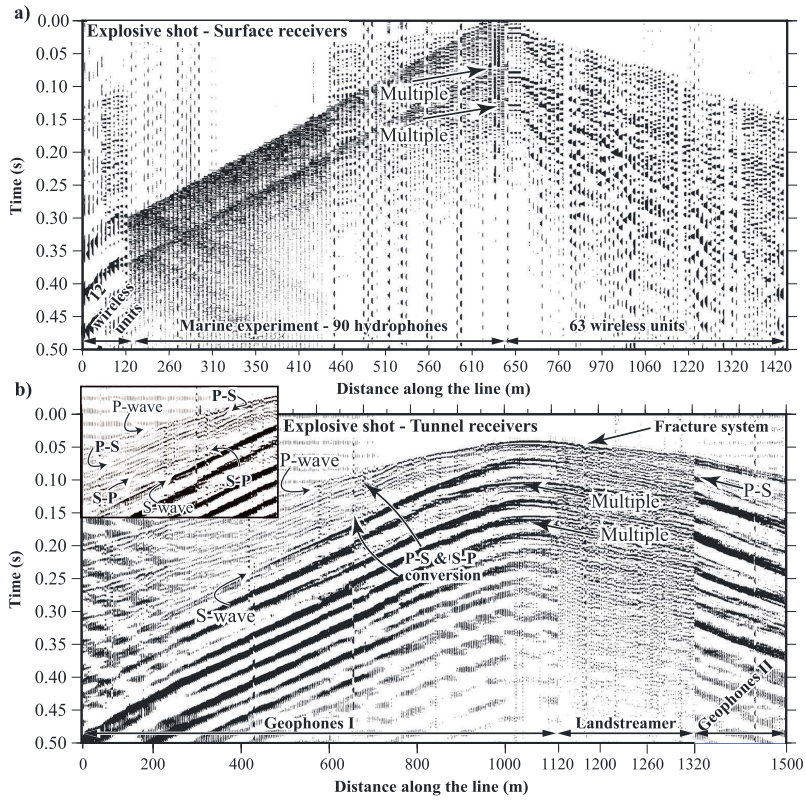

Figure 7. Example source gathers from one of the four explosive sources fired in the sea above the tunnel with (a) merged wireless and hydrophone data and (b) same explosive source simultaneously recorded by the receivers in the tunnel with certain events marked. Note the strong shear wave energy produced at the seafloor and converted back to *P* wave energy at the fracture zone.

inversion process with an RMS error of the final velocity model of 2.1 ms for the *P* and 1.4 ms for the *S* waves. Since the *S* wave tomography shows similar results as the *P* wave, to avoid redundancy, we only show and discuss the *P* wave result. Examples of first arrival picking, an overview of the distribution of all picked first arrivals, and the travel time residuals of *P* waves are shown in Figure 9.

Figure 9a also shows the three subsets of the NE-1 and less fractured and intact host rock around them (NE-1-I to NE-1-III and HR-1 to HR-4). Inspection of the source gather suggests that direct shear arrivals are less sensitive to the fracture system and show no noticeable delays on the arrival times (Figure 9a, *S* wave direct arrivals). Significant delay, however, can be noted on the *P* wave direct arrivals (Figure 9a, *P* wave direct arrivals, arrow pointing at NE-1-II zone). All arrivals align along a linear trend (Figure 9b), implying little or no refracted waves in the data and no noticeable effect of the excavation damage zone (EDZ) on the first arrivals. This is in accordance with the field situation, where even on the surface, drill holes had to be made to plant most of the geophones.

The spatial position of the EW-3 zone and its dip corresponds to a low-velocity zone seen in the *P* wave velocity model (Figures 10a and 10b). The NE-1 and NNW-3 fracture systems appear to be responsible for a complex weak zone bounded by the two and characterized by a decrease of the seismic velocities in the tomogram (Figure 10d). The velocity model shown additionally indicates a low-velocity anomaly between EW-3 and NE-1, which may be related to a minor unnamed fracture system shown in Figure 1. This fracture

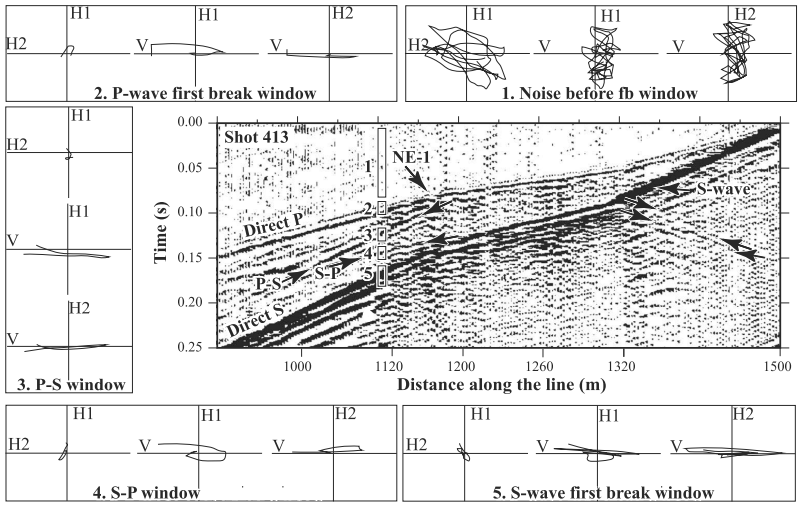

Figure 8. An enlarged view of the source gather shown in Figure 6a showing the *P* and *S* wave direct arrivals as well as features interpreted to be wave mode conversions (direct *P*-to-*S* and *S*-to-*P*) from the fracture system NE-1. Additionally, particle motion plots for different windows for receiver 280 are also shown (V: vertical, H1: radial and H2: transverse component of the landstreamer sensor). Note the delay of the *P* wave first arrivals where the NE-1 fracture system is located and strong vertical polarization for most of the events. Different gains were used for plotting particle motions to allow for better visual inspection.

system appears to change dip from the surface downward, and its intersection with the tunnel is not mapped. The low-velocity halo around the tunnel is rather an effect of the 3-D source-receiver geometry with seismic rays traveling around the tunnel (a mix of longer and shorter paths depending on source locations on the surface) squeezed into the 2-D domain during the inversion, rather than an EDZ effect [*Bohlen et al*., 2007; *Lüth et al*., 2008].

5.1. Fracture Detection and Characterization Using Wave Mode Conversions

Some surface seismic data and, in particular, borehole seismic surveys have shown that zones of high impedance contrast to the host rocks, such as fluid-filled fracture systems, ductile shear zones, and massive sulfide bodies, can increase reflectivity and generate significant amounts of *P-S* and *S-P* converted energy [*Ayarza et al*., 2000; *Bellefleur et al*., 2004; *Malehmir and Bellefleur*, 2010; *Bellefleur et al*., 2012; *Lundberg et al*., 2012; *Melanson et al*., 2015]. To provide a possible explanation of the origin of the events seen in Figures 6 and 8, two modeling approaches were used:

1. 3-D constant-velocity ray tracing travel time modeling [e.g., *Ayarza et al*., 2000] and
2. 2-D finite difference elastic modeling [e.g., *Juhlin*, 1995a].

All available information on the fracture systems in the tunnel was used as input to the modeling, such as dip angles, azimuths, width of the zones, and the average densities of the rocks hosting the fracture systems [*Rhén et al*., 1997; *Berglund et al*., 2003]. From our seismic data, we extracted apparent velocities and locations where the fractures intersect the seismic line. To obtain velocities for the fracture sets of NE-1, we analyzed data recorded on the 80 stations of the landstreamer covering it. Source gathers from the southern part of the tunnel where the arrivals could not be clearly picked were excluded, resulting in about 150 source stations being used. Furthermore, only source gathers with high S/N ratio located 200 m before, along the 200 m long landstreamer, and 200 m after it with clearly distinguishable *P* and *S* wave first arrivals were used. The landstreamer data were first divided into seven zones (NE-1-I to NE-1-III and HR-1 to HR-4) as shown in Figure 9a. Separation was done by assigning to each zone only the receivers and first arrivals belonging to that particular zone. After assigning the receivers to a particular zone, a linear regression analysis was

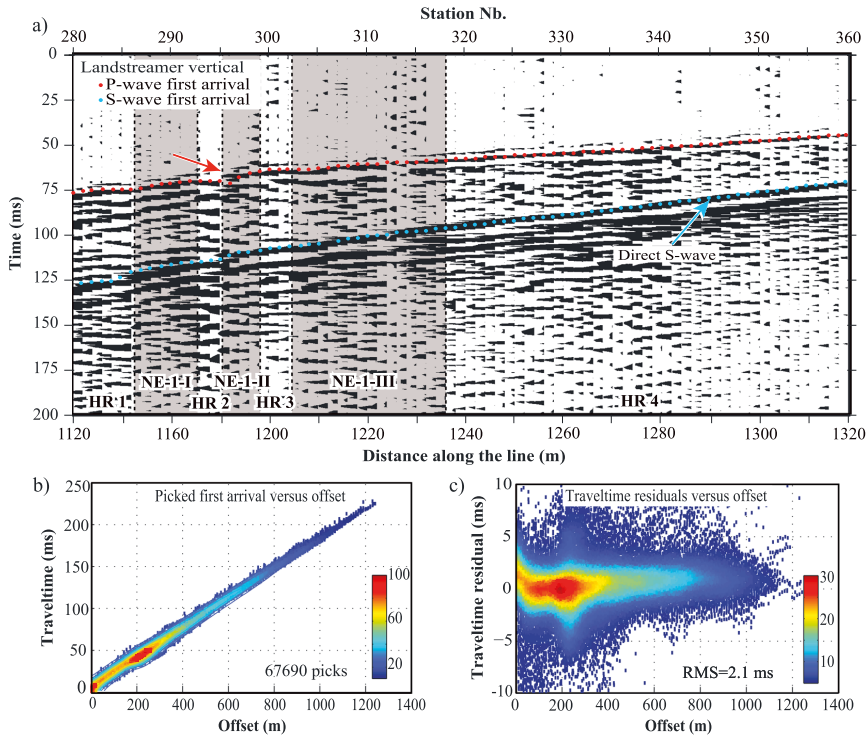

Figure 9. (a) An example of picked first arrivals of both *P* and *S* waves along the NE-1 fracture zone. Same figure shows widths and locations of different sets of NE-1 (NE-1-I to NE-1-III) and less fractured host rock separating them (HR-1 to HR-4). Locations and widths correspond to the field situation as intersected by the landstreamer in the tunnel. (b) Overview of the distribution of all *P* wave picked first arrivals and their trend with the accompanying color scale corresponding to the number of picked arrivals falling within a specific range. (c) Travel time residuals as a function of offset for the final *P* wave velocity models with RMS = 2.1 ms and color scale showing number of picks within a specific range.

performed on picked *P* and *S* wave first arrivals as a function of their offsets to obtain an estimate of the velocity for each zone. Figures 11a and 11b show a boxplot of the obtained velocities for *P* and *S* waves in the vicinity of NE-1, based on the regression analysis. Median velocities of the three NE-1 sets (NE-1-I to NE-1-III) were taken as representative of the sets for ray tracing modeling purposes. For EW-3, a median value of the differentiated travel times for the neighboring receivers located within the EW-3 zone and the same 150 sources were used to obtain an estimate of its *P* and *S* wave velocities. Near and midoffset first breaks were used as an estimate of the *P* and *S* wave velocities for the host rock further away from NE-1. Table 2 contains the geometrical information and aforesaid velocities used as input values for the two modeling approaches.

The seven zones in Figure 11 show a distinct signature on both the *P* and *S* wave velocities. Host rock HR-1 shows high velocities corresponding to the intact rock. Slightly lower velocities are seen in the host rock after NE-1 (HR-4) compared to HR-1, perhaps due to the influence of the EW-3 fracture system located at the end of the landstreamer. All zones show a decrease of velocities compared to HR-1, with *P* waves appearing more affected than the *S* waves, particularly in the HR-3 zone. Since both HR-2 and HR-3 are described as fractured host rock [*Rhén et al.*, 1997; *Berglund et al.*, 2003], the velocity changes within the two may indicate differences in the intensity of fracturing. Compared to fracture sets NE-1-I and III, the two mentioned host rock segments are not hydraulically conductive or mineralized [*Rhén et al.*, 1997; *Berglund et al.*, 2003].

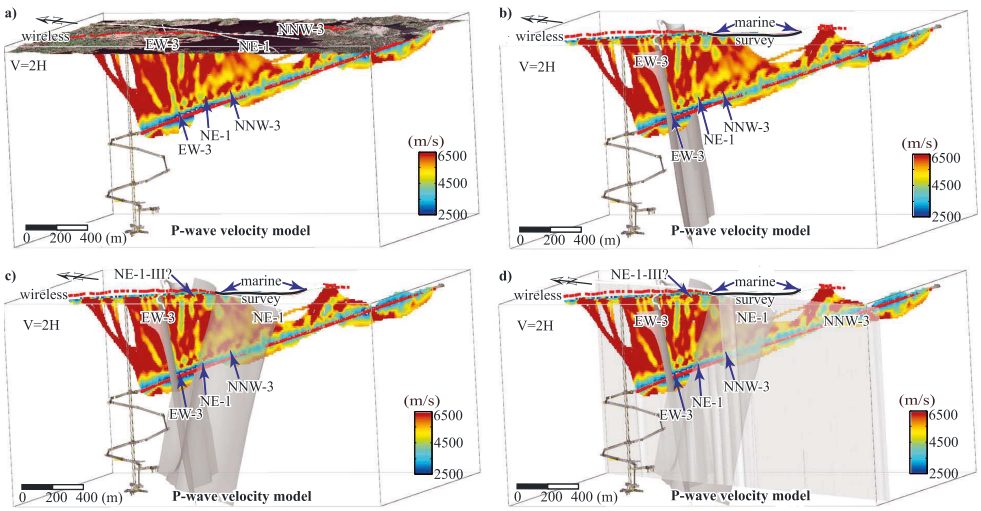

Figure 10. The 3-D view from the west of the final *P* wave velocity models obtained from joint *P* and *S* wave tomography inversion. (a) *P* wave velocity model with aerial photo projected on top of the lidar surface, tunnel model, surface projections of the fracture systems, and their intersection with the tunnel, along with location of seismic receivers both in the tunnel and on the surface shown by red dots. Same *P* wave velocity model with tunnel model, surface projections of the fracture systems, and seismic receivers and (b) EW-3 fracture zone model; (c) EW-3 and NE-1 fracture zone models; and (d) EW-3, NE-1, and NNW-3 fracture zone models shown. The *P* wave velocity model shown has both source and receiver statics applied [*Bergman et al.*, 2004; *Yordkayhun et al.*, 2009].

5.1.1. Modeling the Response of the Fracture Systems Using the 3-D Reflection Travel Time Approach

The 3-D constant-velocity ray tracing travel time modeling is based on the assumption of a homogeneous rock with a predefined constant velocity with a reflecting planar surface of known 3-D geometry within it [*Ayarza et al.*, 2000]. Commonly, a trial and error approach on the 3-D geometry is used to fit a reflection observed on a source gather (or stacked section) to a model. In our case, the geometry of the NE-1 and EW-3 fracture systems are considered known; thus, their travel time response can be calculated based on the medium velocity. Here the NE-1 fracture system consisting of three different fracture sets (NE-1-I to III zones) was modeled as a single planar reflector with velocity equal to the average of the three and dips as shown in Table 2. Host rock velocities were constant for the entire model. All aforesaid parameters were used as the model input, and travel times of all the arrivals (e.g., direct *P* wave, direct *S* wave, *P-P*, *P-S*, *S-S*, and *S-P* reflections) from the two fracture systems (NE-1 and EW-3) were calculated for the same two source locations as shown in Figure 6 (Figure 12). High-amplitude waves coming off the NE-1 fracture system corresponding to *P-S* and *S-P* converted energy show a good match between calculated direct arrivals and the real data

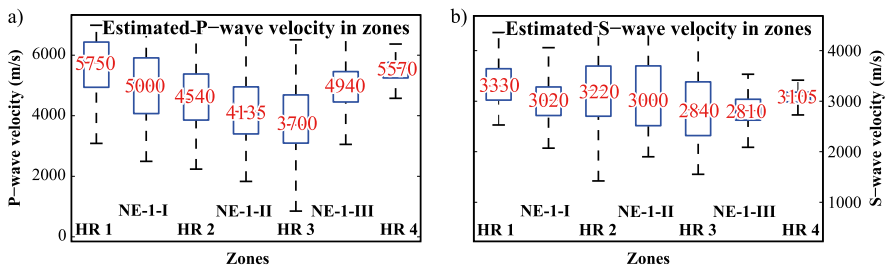

Figure 11. Estimated velocities from linear regression analysis within seven specific zones (NE-1-I to NE-1-III and HR-1 to HR-4) in the vicinity of NE-1 fracture system from (a) *P* wave and (b) *S* wave first arrivals. Only landstreamer recorded data were used and the values shown are based on approximately 150 sources with good S/N ratio. The numbers in red within boxes represent the median velocity of every zone.

Table 2. Parameters Used for Seismic Modeling

Feature	Azimuth (°)	Dip Angle (°)	Width (m)	V_P (m/s)	V_S (m/s)
Host rock	-	-	-	5650	3300
NE-1-I	231	64	20	5000	3020
NE-1-II	231	64	8	4135	3000
NE-1-III	231	64	31	4940	2810
EW-3	89	73	12	5000	3000

(Figure 12a). For EW-3, trapped energy between the two fracture systems appears to dominate near offsets (Figure 12b). Therefore, matching the events originating from the EW-3 system is based on far offsets only. The position of our seismic line makes characterization of EW-3 more complicated, since it is located where the landstreamer part of the seismic line connects to the second part of the planted geophone line (Geophones II; Figures 1 and 3).

5.1.2. Modeling the Wave Propagation Through Fracture Systems

To increase the level of confidence on the interpretation of the events shown in Figure 12a, we modeled the response of the two fracture systems for the same source location using a 2-D elastic finite difference code available in Seismic Un*x [*Juhlin*, 1995a; *Stockwell*, 1997; *Juhlin et al*., 2012]. Finite difference modeling was done assuming an isotropic media and the parameters shown in Table 2. Widths of the fracture systems and distances between individual sets were kept consistent to the field situation. To suppress additional edge

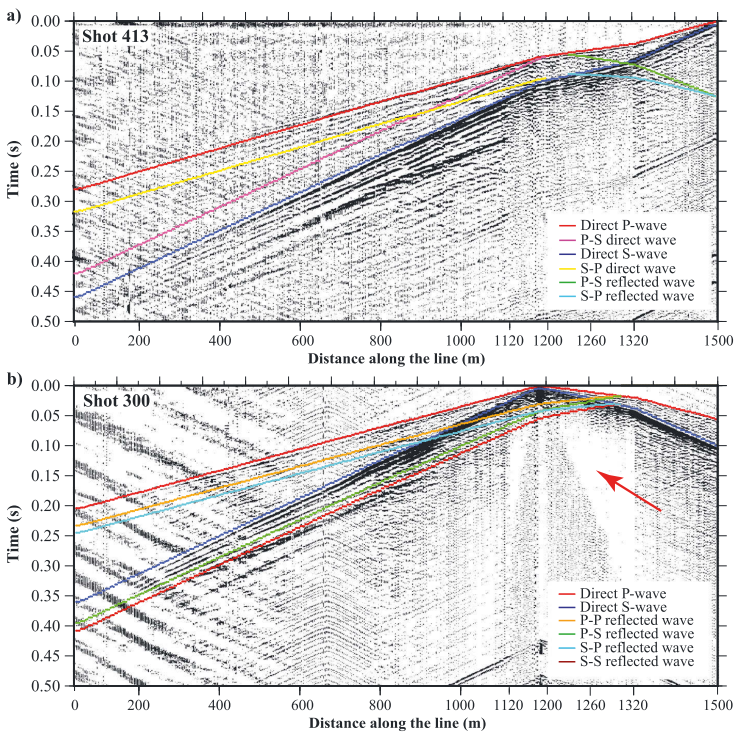

Figure 12. Results of 3-D ray tracing travel time modeling for fracture systems NE-1 and EW-3. (a) Source gather showing modeled travel times for corresponding events as shown in Figure 6a. (b) Result of travel time modeling for the EW-3 fracture system and events shown in Figure 6b. Note the damped amplitude zone (red arrow) due to trapped energy between the two fracture systems. For plotting purposes, trace normalization was applied.

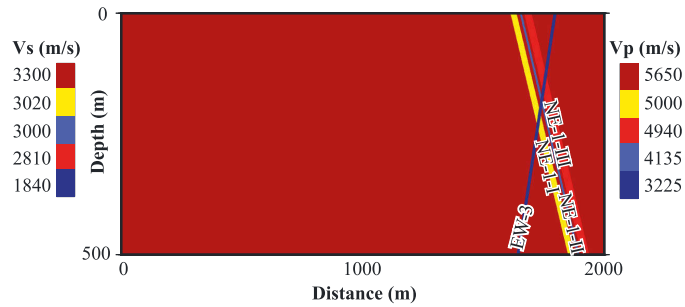

Figure 13. Velocity model used for 2-D elastic finite difference modeling. The velocities shown here are the same ones as used for 3-D travel time modeling. Over the entire model, the density was kept uniform.

effects, apparent velocities of the host rock shown in Table 2 were used as velocities of host rock segments (HR-1 to HR-4) separating the fracture sets of NE-1. A uniform density of 2755 kg/m^3 was used for the entire medium, corresponding to the average of the densities of all the rock types mapped in the northern part of the tunnel [*Rhén et al*., 1997]. For the isotropic case, the code calculates the C_{11} and C_{55} Voigt elastic stiffness. To include the fracture systems (Figure 13), a percentage decrease of each of the elastic stiffness within the zones where the fracture systems are located was calculated to match the parameters shown in Table 2. Conceptually, the model was made assuming that its top represents the tunnel floor where the seismic receivers were placed.

Since the data show quite a broadband frequency character (Figure 6), a Ricker wavelet with a dominant frequency of 180 Hz was used to generate synthetic seismograms. To prevent numerical artifacts, a grid cell size of 1 m in both the vertical and the horizontal directions was used. A free surface boundary condition was applied at the top and absorbing boundary conditions on the model sides to avoid strong reflections off the model boundaries. Intrinsic attenuation was not included ($Q = \infty$). The calculated travel times using the 3-D ray tracing approach correspond well to both the real and synthetic source gathers (Figure 14) with a good match of the modeled responses with those observed on the real source gather as shown in Figure 14c. Strong scattering from the edges of cells as seen in Figures 14a and 14b is a consequence of the way the fracture zones were introduced into the model. Nevertheless, it is not so strong as to obscure the recognition of the events of interest.

5.2. Dynamic Elastic Properties of the Fracture Systems

Subsurface elastic property estimation is essential for engineering purposes, reducing drilling and mining risks, maximizing oil and gas reservoir productivity, or understanding crustal stresses driving tectonic processes. Based on how they are determined, the elastic properties of materials can be classified into static and dynamic ones. By definition, the static moduli are obtained directly in deformational (stress-strain) experiments, while the dynamic ones are calculated from the seismic velocities and density [*Mavko et al*., 2009; *Meléndez-Martínez and Schmitt*, 2016]. Unless conducted on an ideally elastic material, the calculated value of the dynamic moduli and measured static ones will differ, with the dynamic ones generally indicating more competent rocks. The difference between the two can be related to the different strain (deformation) amplitudes involved in static measurements and those caused by a passing seismic wave (about 10^{-3} and 10^{-6}, respectively) [*Barton*, 2007; *Mavko et al*., 2009]. Additionally, the presence of cracks, joints or pores, and their fluids play an important role [*Blake and Faulkner*, 2016]. Regardless of the differences between the two, the dynamic elastic properties for the NE-1 fracture system, namely, V_p/V_s and Poisson's ratios, were estimated to test if the highly permeable fracture sets of NE-1 show distinct signatures. To obtain the ratios, two approaches were used. According to *Geldart and Sheriff* [2004], the V_p/V_s ratio can be approximated as the travel time ratio of *S* and *P* wave direct arrivals, t_S/t_P picked on the same receiver. For this step, we used the same 150 sources and 80 landstreamer stations as used for obtaining the velocities shown in Figure 11. The values obtained using the travel time ratios are influenced by all the rock a seismic wave

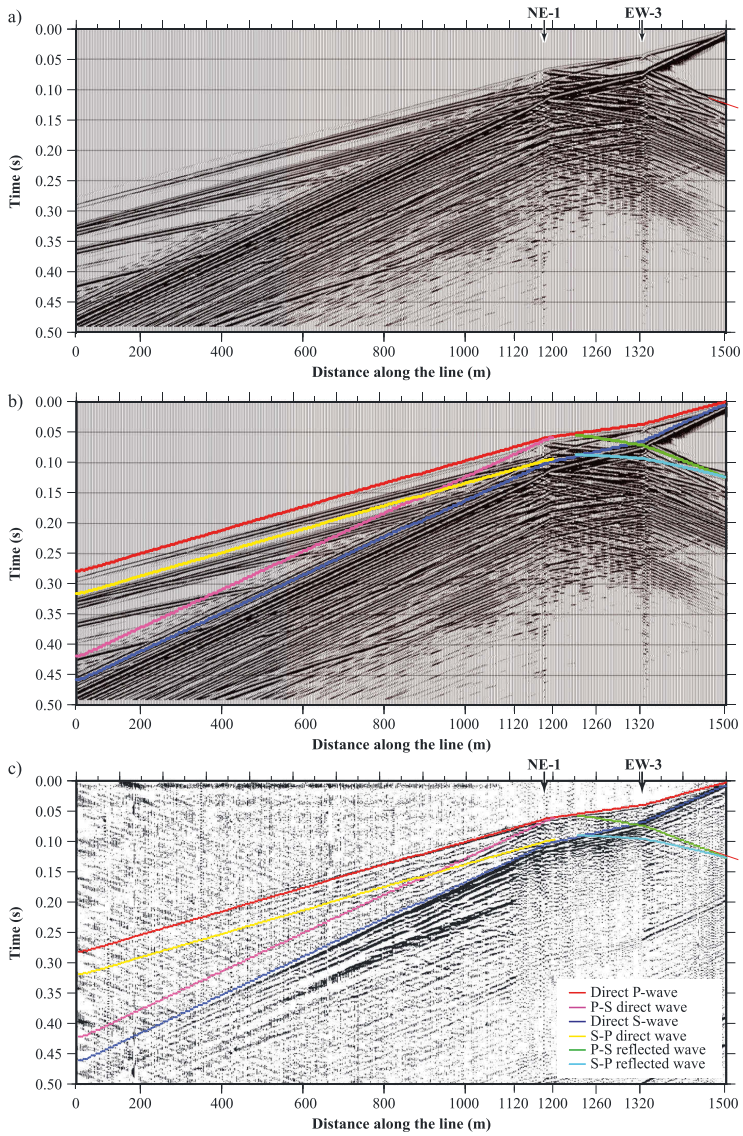

Figure 14. (a) Synthetic seismograms generated using the 2-D elastic finite difference modeling approach with arrows showing the location of the corresponding fracture systems. (b) Same seismograms with superimposed travel times from the NE-1 fracture system modeled using the 3-D ray tracing approach and the direct *P* and *S* wave velocities. (c) Real data source gather with calculated travel times superimposed.

encountered along its propagation, hence corresponding to the path average ratio. In the second approach, to obtain a more focused and local analysis, the velocities shown in Figure 11 were used to calculate V_p/V_s and Poisson's (σ) ratio for the seven zones in the vicinity of NE-1. The Poisson's ratio (σ) was calculated using the isotropic case formula [*Geldart and Sheriff*, 2004]:

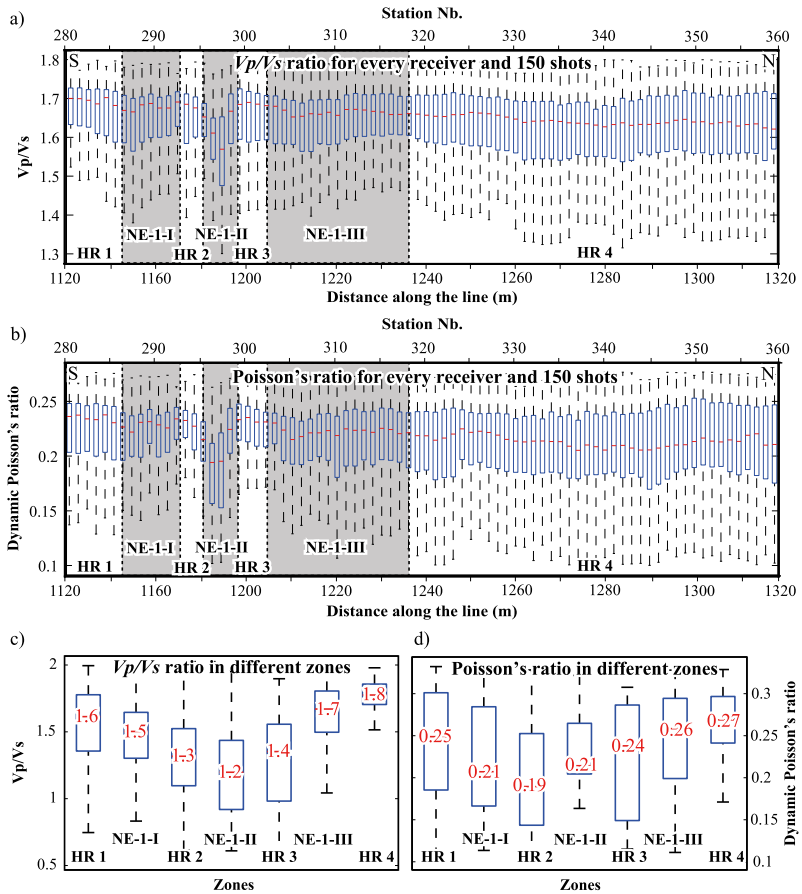

Figure 15. Variations of dynamic elastic properties in the zone of the NE-1 fracture system calculated using two different approaches. (a) V_P/V_S ratio variation and (b) Poisson's ratio variation based on the ratio of picked first arrivals of the *S* and *P* waves from 150 sources along a portion of the seismic line in the tunnel. (c) V_P/V_S ratio variation and (d) Poisson's ratio variation within seven different zones as shown in Figure 9 and velocities obtained from regression analysis. HR represents host rock before and after NE-1 (HR 1 and 4) and between its different sets (HR 2 and 3).

$$\sigma = \frac{(Vp/Vs)^2 - 2}{2\left[(Vp/Vs)^2 - 1\right]} \tag{1}$$

Figures 15a and 15b show boxplots of V_P/V_S and Poisson's ratio calculated using the travel time ratios of the picked *S* and *P* wave direct arrivals (t_S/t_P), while Figures 15c and 15d show the variation within the seven different zones based on using the velocities in Figure 11. Red lines and numbers inside blue boxes bounded by the first and third quartiles depict the median value per zone. Individual fracture sets of NE-1 are marked with NE-1-I to NE-1-III and the host rock separating them with HR-1 to HR-4. Even though seismic wavelengths are estimated to be on the order of 20–25 m, the fracture system still produces a distinct seismic signature as seen on the source gather shown in Figures 8 and 9. The most prominent decrease can be seen in the portion of the NE-1-II fracture set, with a distinct drop of all parameters (Figure 15). According to the hydraulic conductivity description by *Rhén et al.* [1997] and *Berglund et al.* [2003], this may indicate a transition from a high fluid conductivity to a non or low-conductivity environment. The distinct drop of the parameters spatially coincides

with the *P-S* and *S-P* wave mode conversions seen both in the real data and supported by the modeling studies. Considering the seismic wavelengths, size, and position of the NE-1-II, this marked decrease is likely an average over the fracture set and the more competent host rock separating it from the NE-1-III and NE-1-I.

5.3. Seismic Quality Factor *Q* of Fracture Zones

Seismic attenuation, in the most general sense, represents the loss of energy or amplitude of a seismic wave as it propagates through a medium [*Knopoff*, 1964; *Sheriff*, 2002]. It has been a topic of research for almost 40 years now, and different attenuation mechanisms have been proposed [*Johnston et al*., 1979; *Kjartansson*, 1979; *Toksöz et al*., 1979; *Holliger and Bühnemann*, 1996; *Wang*, 2008; *Ekanem et al*., 2013]. Attenuation involves loss of energy due to geometrical spreading, scattering, and anelastic or intrinsic attenuation resulting from grain boundary friction or fluid movements [*Johnston et al*., 1979; *Mavko et al*., 2009]. Knowledge of the attenuation is important since it can provide insight into the intensity of fracturing, lithology, and porosity or indicate hydrocarbons in reservoir characterization [*Kjartansson*, 1979; *Dasgupta and Clark*, 1998; *Xu and Stewart*, 2006; *Wang*, 2008]. To quantify to what extent the different hydraulically conductive sets of the NE-1 fracture system influences the attenuation of passing seismic waves, we calculated *Q* within the same zones as used for the calculation of the velocities (Figure 11) and dynamic mechanical parameters (Figure 15). According to *Tonn* [1991], the *Q* value can be estimated as the amplitude ratio of the same seismic event recorded by two receivers located at distances x_1 and x_2 using

$$Q = \frac{\omega \Delta x}{2c}\left[\ln\left(\frac{A(x_1)}{A(x_2)}\right)\right]^{-1}, \tag{2}$$

with $A(x_1)$ and $A(x_2)$ being the amplitudes at two receiver locations, c the velocity, and $\omega = 2\pi f$ the dominant angular frequency. For the purpose of our study, we assume that Q is frequency independent in the frequency range of our data. To calculate Q based on the amplitude decay method, the same 150 source gathers and 80 receivers were used after a geometric spreading correction had been applied using the source-receiver offsets as the scalar. Noisy traces and traces with offsets less than 80 m (to suppress source-induced noise) were excluded from the analysis. For every source gather, we extracted data within a 10 ms window around the *P* and *S* wave direct arrivals (3 ms cosine taper on both ends). Extracted data were then subdivided by receivers located inside each of the seven zones as used for calculation of velocities shown in Figure 11. Within the zones, natural logarithms of the peak amplitude of every receiver were calculated, and as function of offset, used as the base for linear regression analysis (Figure 16). A minimum of four stations per zone was used for the analysis (Figure 16). Offsets from the source positions were used as distance (Δx in the formula) within each of the seven individual zones and the slope of the line from the previous step used to calculate average *Q* [*Juhlin*, 1990; *Tonn*, 1991; *Juhlin*, 1995b]. This was done for both *P* and *S* wave direct arrivals with dominant frequencies of 180 Hz and 160 Hz, respectively. For every zone, the median velocities shown in Figure 11 for zones HR-1 to HR-4 and NE-1-I to NE-1-III were used to calculate *Q* (Figure 17).

Q values within and around NE-1-II are quite low, suggesting the zone and neighboring rocks to be highly attenuating. Other regions of the host rock show a higher *Q* value, implying more competent rocks. The hydraulically conductive set of NE-1 (NE-1-III) shows high *Q* values compared to the other sets and the HR-1 segment. The *S* wave attenuation shows a similar pattern, with NE-1-III being less attenuating compared to other sets or the fractured host rock segments separating them. Since the final results of the *Q* estimates are shown as a boxplot (Figure 17), no norm of residuals or standard errors are shown to avoid redundancy.

6. Discussion

6.1. Surface-Tunnel-Surface Velocity Tomography

Studies involving tunnel-to-surface experiments have previously been reported by *Gritto et al.* [2003, 2004]. Compared to them, the study presented here was done with simultaneous data recording on the surface and inside the tunnel, allowing better spatial coverage for the travel time tomography. The velocity model shown in Figure 10 was forced to be 2-D (wide crossline cell of 200 m), although a 3-D inversion was performed and a 3-D source-receiver setup was used for travel time calculations; hence, its interpretation should be viewed with certain caution. An attempt to do a 3-D inversion of the first arrivals was made using a grid size of 12 m in the crossline direction, which resulted in numerous gaps in the inverted velocity model, making the interpretation of the results difficult. To ensure that features in the velocity models are not inversion

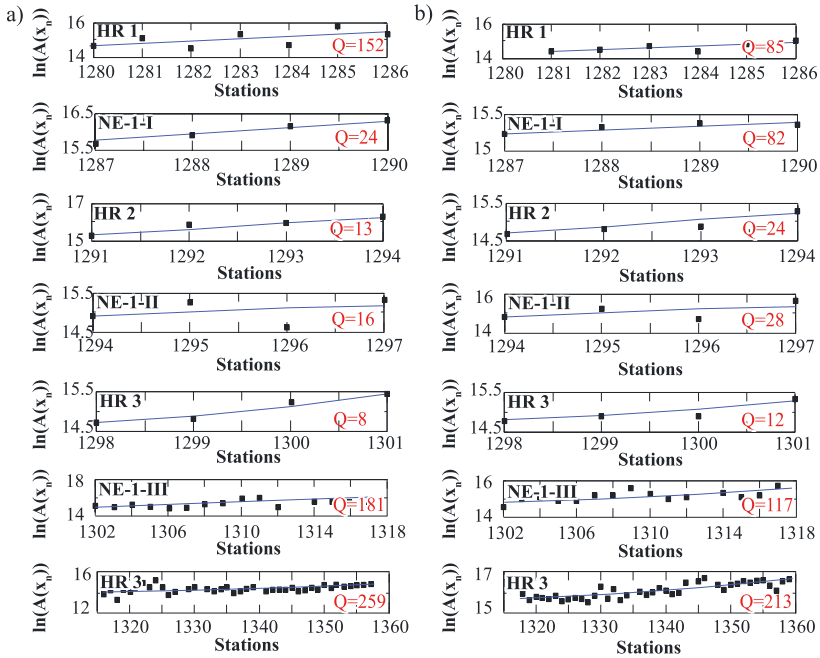

Figure 16. An example of linear regression fitting to the peak amplitudes of the receivers within the seven zones and a 10 ms tapered window around picked first arrivals. (a) *P* and (b) *S* wave example. $ln(A(x_n))$ represents the logarithmic value of the amplitude of the corresponding station.

artifacts, we tried to perturb the picked first arrival travel times by adding a series of randomly generated travel times with a mean value of ±3 ms [*Malehmir et al.*, 2015b]. This did not significantly influence the result, with the anomalous zones still being preserved. Additional tests of the initial model perturbation, and a test of possible errors introduced by the coordinate transformation from internal coordinate system in the tunnel to the one used [*Maurer and Green*, 1997; *Malehmir et al.*, 2015b], was based on adding a randomly generated series of ±0.5 m (mean value) to the receiver coordinates and reinverting this new data set. Again, no major change was seen in the final velocity model.

The northern part of the line has good data coverage, so the velocity anomalies related with the NE-1 and EW-3 systems could still be reasonably well resolved. Significant improvement and more spatially constrained

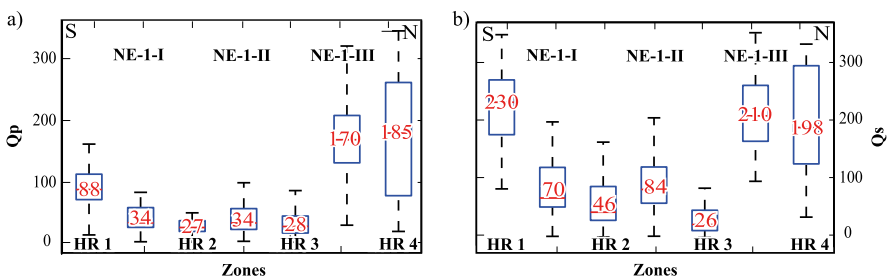

Figure 17. Seismic quality factor *Q* across the NE-1 fracture system obtained using the amplitude decay method on (a) *P* wave direct arrivals and (b) *S* wave direct arrivals. To calculate the *Q*, median velocities of all zones shown in Figure 11 were used. The red numbers inside the box represent the median value of *Q* per zone.

low-velocity anomalies related to the fracture systems were obtained with the joint inversion than with inverting only for *P* wave arrivals. In the case of EW-3, the number of source and receiver pairs, and their spatial positions favor the imaging of the fracture system itself (Figure 10b, EW-3 arrow). The fracture models extracted from the SKB database confirm that this velocity decrease spatially corresponds to the EW-3 system. Low-velocity anomalies that follow the dip of NE-1 can be seen in the velocity model, but constraining their lateral extent based only on the tomography result remains uncertain. Additional complexities in interpreting the velocity anomalies related to NE-1 are introduced by the presence of the NNW-3 fracture zone. A low-velocity zone having its root where the NE-1 crosses the tunnel and continuing upward with opposite dip is also present on the *P* wave velocity model (Figure 10c, arrow NE-1-III). This low-velocity zone may be connected with the NE-1-III fracture set of the NE-1 zone that appears to change its dip angle above the tunnel intersection. Surface projection of this low-velocity region corresponds to a lineament seen on the aerial photo, supporting the claim that this zone is rather a geological feature than an inversion artifact (Figure 10a, NE-1-III arrow). The modeling studies of *Berglund et al.* [2003] also conclude that the NE-1 zone appears to change its dip angle from the surface downward. Another consistent zone where the velocities decrease in the velocity model can be seen following the EW-3 (Figure 10, velocity decrease after EW-3 in the downdip direction).

6.2. Seismic Signature of the Fracture Systems

Lack of a significant decrease in the *S* wave velocity over the NE-1 zone (Figures 8 and 11) may be an effect of the preferred fracture orientation within the zone. Open fractures may be controlled by the original development of the fracture system and aligned parallel to the dip or they may be controlled by the stress field, giving rise to extensive-dilatancy anisotropy [*Crampin*, 1981, 1987; *Yardley and Crampin*, 1991]. Cracks aligned parallel to the dip of the fracture system, either original or due to the current stress field, would favor the delay of *P* waves over *S* waves propagating across the system. For an *S* wave as shown in Figure 8, with cracks aligned parallel to the dip angle of the fracture system and assuming that it is radially polarized (particles polarized parallel to the plane of cracks), no significant effect on its propagation would be observed [*Anderson et al*., 1974].

Studies have reported that fully fluid saturated fracture zones will tend to have lower seismic velocities and possibly higher hydraulic conductivity [*Juhlin*, 1995b]. High hydraulic conductivity may increase the pore pressure, hence reducing the effective stresses further decreasing the velocities, increasing attenuation, and making the fracture effect more pronounced [*Dvorkin et al*., 1999; *Siggins and Dewhurst*, 2003; *Wang et al*., 2012]. However, only a small decrease of velocities in the highly hydraulically conductive NE-1-III zone indicates the opposite to be the case. Whether this effect is due to mineralization of the fractures, fracture intensity, apertures of the cracks and fractures, presence of clays and clay alteration, or due to grout in the fractures remains uncertain. Changes to the nature of the zone due to the grouting cannot be ruled out. The seismic waves may not be sampling the unaffected portion of the zone.

A significant amount of *S-P* mode converted energy is associated with the NE-1 fracture system. We can note that the *P-P* and *S-S* reflected waves are difficult to identify in the real data, while the *P-S* and *S-P* mode converted direct and reflected waves are clearly present (Figure 12a). Considering the spatial location of the mode conversions of the direct *P* and *S* waves, we argue that the mode conversions are related to the transition between the highly hydraulically conductive portion of the NE-1 fracture system (NE-1-III) and its low hydraulically conductive neighbor NE-1-II and fractured host rock segments HR-2 and HR-3. Accounting for the wavelengths of our data set (20–25 m), it is likely that the mode conversions are a cumulative effect of the mentioned zones. To obtain a more constrained interpretation, other information would be required, such as, e.g., full-waveform sonic borehole logging. The nature of the direct *S-P* mode conversions observed in the data and the delays in the *P* wave first arrivals (Figure 8) still remain uncertain. *Hardage et al.* [2011], for example, argue that, in the case of aligned fractures, increased fracture density could noticeably decrease velocity of a *P* wave propagating normal to the fracture plane, while the radially polarized shear wave velocity remains the same. Even though this argument supports our observation, it does not explain why strong *P-S* conversion occurs at the zone. The mode conversions and delays are likely a joint effect of the different density, spacing, apertures of the cracks and fractures, and their alignment, which in return influences the hydraulic conductivity of the fracture sets [*Anderson et al*., 1974; *Hardage et al*., 2011]. The EW-3 fracture system is less hydraulically conductive (90 L/min prior to grouting) and relatively narrow

(12 m), and no noticeable *P-S* and *S-P* direct wave conversions from it are seen in the data. The energy trapped between the two fracture systems (red arrow on Figure 12b) makes the interpretation of the EW-3 exact location in the source gathers a difficult task due to noise masking all the reflected arrivals at near offsets. Nevertheless, far offset events on the real data appear to match relatively well with the calculated travel times (Figure 12b).

The finite difference elastic modeling result shown in Figure 14 was done in 2-D assuming the tunnel bottom as the top of the model. Taking into account the tunnel shape and seismic sources and receivers along it, the 2-D assumption may be valid for modeling of the shallow events originating from the boundaries of the fracture systems. If deeper structures are to be imaged, or the contact of NE-1 and EW-3, 3-D modeling should provide more accurate results, where the dip of the two, along with their widths, should be used as the model input. One drawback of the modeling strategy of introducing the fracture systems in the code was more "edge effects" due to sharp changes of the neighboring cell properties. Even with the severe scattering seen in the results, important information was obtained that allowed us to partly reconstruct the delay of the *P* wave first arrivals seen in the real data and fully reconstruct the *P-S* and *S-P* mode conversions. A good match with the real data can be noted, indicating proper selection of the modeling parameters shown in Table 2.

6.3. Dynamic Elastic Properties and Seismic Attenuation Estimation

The most distinct variation in the dynamic elastic properties is over the NE-1-II fracture set (Figure 15), particularly indicated by a marked decrease in V_p/V_s. The NE-1-I fracture zone also shows a decrease in V_p/V_s and Poisson's ratio, but not as clearly as NE-1-II. The highly hydraulically conductive NE-1-III set shows an increase in the Poisson's ratio, compared to those subsets that are not highly water bearing. These variations may be due to changes in the fracture intensity and hydraulic conductivity, which in turn influence the fluid pressure and effective stresses within the fracture sets [*Dvorkin et al*., 1999; *Carcione and Cavallini*, 2002; *Siggins and Dewhurst*, 2003; *Wang et al.*, 2012]. Considering the estimated accuracy of the first break picks (±1–2 ms), the calculated velocities in the fracture sets are somewhat uncertain. However, given the width of the individual fracture sets, the more intact host rock separating them, and the seismic wavelengths, we suggest that the values shown in Figure 15 are slightly underestimated and represent average values of the fracture sets and the host rock separating them. Nevertheless, the three fracture zones appear to give a clear signal in the seismic data and estimated dynamic elastic properties. The lower *S* wave velocity in NE-1-III compared to the other two (Figure 11) suggests that this zone is more fractured, and therefore more water bearing.

Compared to single-fold VSP studies [e.g., see reviews by *Tonn*, 1991; *Toverud and Ursin*, 2005], the data in this study involved the analysis of 150 source gathers around the fracture systems. Although *Q* values in certain zones shown in Figure 17 are calculated based on only four receivers, the amount of data used for the calculations provides a rough estimate of *Q* within each zone. The higher *Q* values within the zones are in the range of those observed for granites and diorites [*Knopoff*, 1964; *Badri and Mooney*, 1987; *Barton*, 2007]. The low hydraulically conductive sets of NE-1 (NE-1-I and NE-1-II) show low *Q* values for *P* and *S* waves. Compared to the intact rock, the lower *Q* values within these two fracture sets are expected and show similar characteristics to faults investigated by *Harris et al.* [1997] and *Worthington and Hudson* [2000]. The NE-1-III set, on the other hand, shows a high *Q* value for both *P* and *S* waves (Figure 17). *Pyrak-Nolte et al.* [1990], based on lab analysis of fractured rock samples, concluded that at 30 MPa confining pressures (pressures of the in situ seismic studies), the *Q* factor of high water-bearing rocks is higher than those that are less water-bearing. Hydraulic conductivity, along with clays or other minerals in the cracks of NE-1-III, may have additional effects on *Q* [*Boadu and Long*, 1996; *Rubino and Holliger*, 2012; *Kong et al*., 2013]. Both segments of the host rock before and after the NE-1 system show high *Q* values (HR 1 and HR 4 in Figure 17), indicating a less attenuating environment and more competent rocks. *P* wave attenuation within the HR 1 zone is higher than HR 4, possibly due to the number of stations used for linear regression purposes (HR 1 is calculated using 7 receivers, while HR 4 included about 40 receivers; Figure 16). Both *P* and *S* wave results in Figure 17 show low values in the two host rock segments (HR 2 and HR 3) separating NE-1-II from its neighboring sets. These results indicate less intact and fractured rocks, also consistent with previous studies [*Rhén et al*., 1997; *Berglund et al*., 2003]. Generally, the *P* wave appears more attenuated than the *S* wave, supporting the idea that preferred fracture orientations are highly influencing the wave speeds.

In summary, the two less hydraulically conductive zones have lower V_p/V_s and Poisson's ratio than the more conductive NE-1-III zone. These zones also have lower *Q* values (Figure 17). Combined, these observations

suggest that NE-1-I and NE-1-II are of a different nature than NE-1-III and their seismic signature can be used to characterize them.

7. Conclusions

A surface-tunnel-surface seismic experiment was conducted at the Äspö Hard Rock Laboratory in southern Sweden with sources and receivers both in the tunnel and on the surface. First arrivals from all sources and receivers were manually picked and used for joint *P* and *S* wave travel time tomography. The obtained *P* wave velocity model shows low-velocity zones that correlate relatively well with the locations and dip angles of the NE-1 and EW-3 fracture systems investigated in this study. Additionally, minor fracture systems appear as low-velocity anomalies. Some of these minor fracture systems observed in the velocity model were mapped in previous studies and others are new in this study.

Inspection of source gathers shows that the NE-1 fracture system generated significant mode-converted direct and reflected *P* and *S* wave energy. The 3-D ray tracing reflection travel time modeling was performed to verify these observations. It was illustrated that the fracture system was responsible for generation of *P-S* and *S-P* reflections. The EW-3 zone has a smaller spatial extent and is less hydraulically conductive than parts of the NE-1 system, and for this fracture system, all reflected and mode-converted waves were modeled using the same approach. The modeled travel times for EW-3 show a reasonable match between the events seen in the source gathers and the ones modeled, at least at far offsets. The velocities extracted from the seismic data were used to further model the response of the two fracture systems using a finite difference elastic modeling method. This modeling suggests that *P-S* and *S-P* energy conversion from the two is possible, and synthetic seismograms show a good correspondence to real source gathers, and the travel times calculated using the ray tracing approach.

The NE-1 fracture system causes noticeable delays in the *P* wave first arrivals for the seismic receivers located across it in the tunnel. These delays were used as a basis for the estimation of dynamic mechanical parameters of the fracture sets, namely, V_p/V_s and Poisson's ratio, and the variation of these parameters across the fracture sets. The variation was correlated to different degrees of fluid conductivity of the different fracture sets of the NE-1 system. Estimation of the seismic *Q* factor shows that the fractures with different degrees of hydraulic conductivity show different attenuation characteristics. The low or nonhydraulically conductive fracture sets of NE-1 are highly attenuating for both *P* and *S* waves compared to the rocks further away from it. The highly hydraulically conductive part of the NE-1 fracture system (NE-1-III) appears less attenuating compared with the low permeable and low water-bearing neighboring sets.

This study illustrates the potential of active-source surface-tunnel-surface seismic data to resolve structures between the tunnel and the surface. Additionally, it shows the potential of this approach to characterize fracture zones using various parameters such as *P* and *S* wave velocities, V_p/V_s, Poisson's ratio, and the quality factors Q_p and Q_s. At the Äspö site, the more hydraulically conductive fracture zone investigated by the seismic experiment is characterized by its higher velocities and higher *Q* value compared to the less conductive ones.

Acknowledgments

The seismic study presented here was carried out within the framework of the Trust2.2-GeoInfra (http://trust-geoinfra.se) project sponsored by Formas (project 252-2012-1907), BeFo, SBUF, Skanska, SGU, FQM, and NGI. B. Brodic thanks Formas, BeFo, SBUF, and Skanska for funding his PhD studies. We thank M. Bastani, J. Place, G. Maries, E. Lundberg, S. Wang, and M. Dehghannejad from the Geophysics Program of Uppsala University for their data acquisition contributions and helpful discussion before and during the fieldwork. SKB and Nova FoU partly sponsored this work for which we are grateful. We particularly thank M. Ask for initiating the project, Tyréns, and SKB personnel for providing support data and access to the underground facility. Lund University (and their partners) through the Trust 4.2 project provided the four sea source records used in this study for which we are thankful. GLOBE Claritas™ under license from the Institute of Geological and Nuclear Sciences Limited (GNS), Lower Hutt, New Zealand, was used to prepare and process the seismic data. GMT from P. Wessel and W.H.F. Smith and Seismic Un*x were used in this study. We thank A. Tryggvason for providing the *ps_tomo* tomography code. gOcad™ from Paradigm was used for 3-D visualization and viewing of the data and results. We thank the Associate Editor and two anonymous reviewers for their comments and suggestions that helped through a number of revisions to significantly improve the study presented in this paper. Regarding the data availability and sharing, contact Alireza Malehmir (alireza.malehmir@geo.uu.se).

References

Anderson, D. L., B. Minster, and D. Cole (1974), The effect of oriented cracks on seismic velocities, *J. Geophys. Res.*, *79*, 4011–4015, doi:10.1029/JB079i026p04011.

Andersson, C. J. (2007), *Äspö Hard Rock Laboratory, Äspö Pillar Stability Experiment, Final Report, Rock Mass Response to Coupled Mechanical Thermal Loading*, TR, 310 pp., Swedish Nuclear Waste Management Co. - SKB, Stockholm.

Angioni, T., R. D. Rechtien, S. J. Cardimona, and R. Luna (2003), Crosshole seismic tomography and borehole logging for engineering site characterization in Sikeston, MO, USA, *Tectonophysics*, *368*(1–4), 119–137, doi:10.1016/S0040-1951(03)00154-9.

Ask, D. (2006), Measurement-related uncertainties in overcoring data at the Äspö HRL, Sweden. Part 2: Biaxial tests of CSIRO HI overcore samples, *Int. J. Rock Mech. Min. Sci.*, *43*(1), 127–138, doi:10.1016/j.ijrmms.2005.05.012.

Ayarza, P., et al. (2000), Integrated geological and geophysical studies in the SG4 borehole area, Tagil volcanic arc, middle Urals: Location of seismic reflectors and source of the reflectivity, *J. Geophys. Res.*, *105*, 21,333–21,352, doi:10.1029/2000JB900137.

Badri, M., and H. Mooney (1987), *Q* measurements from compressional seismic waves in unconsolidated sediments, *Geophysics*, *52*(6), 772–784, doi:10.1190/1.1442344.

Barton, N. (2007), *Rock Quality, Seismic Velocity, Attenuation and Anisotropy*, 729 pp., Taylor & Francis Group, London, U. K.

Bellefleur, G., C. Müller, D. Snyder, and L. Matthews (2004), Downhole seismic imaging of a massive sulfide orebody with mode-converted waves, Halfmile Lake, New Brunswick, Canada, *Geophysics*, *69*(2), 318–329, doi:10.1190/1.1707051.

Bellefleur, G., A. Malehmir, and C. Müller (2012), Elastic finite-difference modeling of volcanic-hosted massive sulfide deposits: A case study from Half Mile Lake, New Brunswick, Canada, *Geophysics*, *77*(5), WC25–WC36, doi:10.1190/geo2011-0445.1.

Berglund, J., P. Curtis, T. Eliasson, T. Olsson, P. Starzec, and E.-L. Tullborg (2003), *Äspö Hard Rock Laboratory Update of the Geological Model 2002*, IPR, 130 pp., Swedish Nuclear Waste Management Co. - SKB, Stockholm.
Bergman, B., A. Tryggvason, and C. Juhlin (2004), High-resolution seismic traveltime tomography incorporating static corrections applied to a till-covered bedrock environment, *Geophysics*, *69*(4), 1082–1090.
Blake, O. O., and D. R. Faulkner (2016), The effect of fracture density and stress state on the static and dynamic bulk moduli of westerly granite, *J. Geophys. Res. Solid Earth*, *121*, 2382–2399, doi:10.1002/2015JB012310.
Boadu, F. K., and L. T. Long (1996), Effects of fractures on seismic-wave velocity and attenuation, *Geophys. J. Int.*, *127*(1), 86–110, doi:10.1111/j.1365-246X.1996.tb01537.x.
Bohlen, T., U. Lorang, W. Rabbel, C. Müller, R. Giese, S. Lüth, and S. Jetschny (2007), Rayleigh-to-shear wave conversion at the tunnel face—From 3D-FD modeling to ahead-of-drill exploration, *Geophysics*, *72*(6), T67–T79, doi:10.1190/1.2785978.
Brodic, B., A. Malehmir, C. Juhlin, L. Dynesius, M. Bastani, and H. Palm (2015), Multicomponent broadband digital-based seismic landstreamer for near-surface applications, *J. Appl. Geophys.*, *123*, 227–241, doi:10.1016/j.jappgeo.2015.10.009.
Carcione, J. M., and F. Cavallini (2002), Article details—Poisson's ratio at high pore pressure, *Geophys. Prospect.*, *50*(1), 97–106, doi:10.1046/j.1365-2478.2002.00299.x.
Crampin, S. (1981), A review of wave motion in anisotropic and cracked elastic-media, *Wave Motion*, *3*(4), 343–391.
Crampin, S. (1987), Geological and industrial implications of extensive-dilatancy anisotropy, *Nature*, *328*(6130), 491–496, doi:10.1038/328491a0.
Daley, T. M., E. L. Majer, and J. E. Peterson (2004), Crosswell seismic imaging in a contaminated basalt aquifer, *Geophysics*, *69*(1), 16–24, doi:10.1190/1.1649371.
Dasgupta, R., and R. Clark (1998), Estimation of *Q* from surface seismic reflection data, *Geophysics*, *63*(6), 2120–2128, doi:10.1190/1.1444505.
Dietrich, P., and J. Tronicke (2009), Integrated analysis and interpretation of cross-hole *P*- and *S*-wave tomograms: A case study, *Surf. Geophys.*, *7*(2), 101–109.
Dvorkin, J., G. Mavko, and A. Nur (1999), Overpressure detection from compressional- and shear-wave data, *Geophys. Res. Lett.*, *26*, 3417–3420, doi:10.1029/1999GL008382.
Eaton, D. W., B. Milkereit, and M. H. Salisbury (2003), *Hardrock Seismic Exploration*, *Geophys. Dev. Ser.*, No. 10, 270 pp., Soc. of Explor. Geophys., Tulsa, Okla.
Ekanem, A. M., J. Wei, X.-Y. Li, M. Chapman, and I. G. Main (2013), *P*-wave attenuation anisotropy in fractured media: A seismic physical modelling study, *Geophys. Prospect.*, *61*, 420–433, doi:10.1111/j.1365-2478.2012.01127.x.
Geldart, L. P., and R. E. Sheriff (2004), *Problems in Exploration Seismology and Their Solutions*, *Geophys. Ref. Ser.*, No. 14, 514 pp., Soc. of Explor. Geophys., Tulsa, Okla.
Green, A. G., and J. A. Mair (1983), Subhorizontal fractures in a granitic pluton; their detection and implications for radioactive waste disposal, *Geophysics*, *48*(11), 1428–1449, doi:10.1190/1.1441428.
Gritto, R., T. M. Daley, and E. L. Majer (2003), Estimating subsurface topography from surface-to-borehole seismic studies at the Rye Patch geothermal reservoir, Nevada, USA, *Geothermics*, *32*(3), 275–295, doi:10.1016/S0375-6505(03)00022-1.
Gritto, R., V. A. Korneev, T. M. Daley, M. A. Feighner, E. L. Majer, and J. E. Peterson (2004), Surface-to-tunnel seismic tomography studies at Yucca Mountain, Nevada, *J. Geophys. Res.*, *109*, B03310, doi:10.1029/2002JB002036.
Gustafson, G., R. Stanfors, and P. Wikberg (1989), *Swedish Hard Rock Laboratory Evaluation of 1988 Year Reinvestigations and Description of the Target Area, the Island of Äspö*, 152 pp., TR, Swedish Nuclear Waste Management Co. - SKB, Stockholm.
Hardage, B., M. DeAngelo, P. Murray, and D. Sava (2011), *Multicomponent Seismic Technology*, *Geophys. Ref. Ser.*, No. 18, 318 pp., Soc. of Explor. Geophys., Tulsa, Okla.
Harris, P. E., C. Kerner, and R. E. White (1997), Multichannel estimation of frequency-department *Q* from VSP data1, *Geophys. Prospect.*, *45*(1), 87–109, doi:10.1111/j.1365-2478.1997.tb02272.x.
Hole, J. A. (1992), Nonlinear high-resolution three-dimensional seismic travel time tomography, *J. Geophys. Res.*, *97*, 6553–6562, doi:10.1029/92JB00235.
Hole, J. A., and B. C. Zelt (1995), 3-D finite-difference reflection travel times, *Geophys. J. Int.*, *121*(2), 427–434, doi:10.1111/j.1365-246X.1995.tb05723.x.
Holliger, K., and J. Bühnemann (1996), Attenuation of broad-band (50–1500 Hz) seismic waves in granitic rocks near the Earth' surface, *Geophys. Res. Lett.*, *23*, 1981–1984, doi:10.1029/96GL01855.
Hudson, J. A. (1981), Wave speeds and attenuation of elastic waves in material containing cracks, *Geophys. J. Int.*, *64*(1), 133–150.
Johnston, D., M. Toksöz, and A. Timur (1979), Attenuation of seismic waves in dry and saturated rocks: II. Mechanisms, *Geophysics*, *44*(4), 691–711, doi:10.1190/1.1440970.
Juhlin, C. (1990), Seismic attenuation, shear wave anisotropy and some aspect of fracturing in the crystalline rock of the Siljan Ring area, central Sweden, Uppsala dissertations from the Faculty of Science ISSN 0346–6485, Doctoral thesis., Acta Universitatis Upsaliensis, Uppsala.
Juhlin, C. (1995a), Finite-difference elastic wave propagation in 2D heterogeneous transversely isotropic media, *Geophys. Prospect.*, *43*(6), 843–858, doi:10.1111/j.1365-2478.1995.tb00284.x.
Juhlin, C. (1995b), Imaging of fracture zones in the Finnsjon area, central Sweden, using the seismic reflection method, *Geophysics*, *60*(1), 66–75, doi:10.1190/1.1443764.
Juhlin, C., E. Sturkell, J. O. R. Ebbestad, O. Lehnert, A. E. S. Högström, and G. Meinhold (2012), A new interpretation of the sedimentary cover in the western Siljan Ring area, central Sweden, based on seismic data, *Tectonophysics*, *580*, 88–99, doi:10.1016/j.tecto.2012.08.040.
Kjartansson, E. (1979), Constant *Q*-wave propagation and attenuation, *J. Geophys. Res.*, *84*, 4737–4748, doi:10.1029/JB084iB09p04737.
Knopoff, L. (1964), Q, *Rev. Geophys.*, *2*, 625–660, doi:10.1029/RG002i004p00625.
Kong, L., B. Gurevich, T. M. Muller, Y. Wang, and H. Yang (2013), Effect of fracture fill on seismic attenuation and dispersion in fractured porous rocks, *Geophys. J. Int.*, *195*(3), 1679–1688, doi:10.1093/gji/ggt354.
Kornfält, K.-A., and H. Wikman (1988), *The Rocks of the Äspö Island. Description to the Detailed Maps of Solid Rocks Including Maps of Uncovered Trenches*, 280 pp., PR, Swedish Nuclear Waste Management Co. - SKB, Stockholm.
Kornfält, K.-A., P.-O. Persson, and H. Wikman (1997) *Granitoids from the Äspö Area, Southeastern Sweden—Geochemical and Geochronological Data*, 330 pp., GFF, Swedish Nuclear Waste Management Co. - SKB, Stockholm.
Liu, E., and A. Martinez (2013), *Seismic Fracture Characterization: Concepts and Practical Applications*, 279 pp., EAGE Education Tour EET 8, EAGE Publications bv, Houten, Nederlands.
Lundberg, E. (2014), *2D and 3D Reflection Seismic Studies over Scandinavian Deformation Zones*, 57 pp., Acta Universitatis Upsaliensis, Uppsala.
Lundberg, E., and C. Juhlin (2011), High resolution reflection seismic imaging of the Ullared deformation zone, southern Sweden, *Precambrian Res.*, *190*(1–4), 25–34, doi:10.1016/j.precamres.2011.07.012.

Lundberg, E., C. Juhlin, and A. Nasuti (2012), High resolution reflection seismic profiling over the Tjellefonna fault in the Møre-Trøndelag fault complex, Norway, *Solid Earth*, *3*(1), 175–188, doi:10.5194/se-3-175-2012.

Lüth, S., R. Giese, P. Otto, K. Krüger, S. Mielitz, T. Bohlen, and T. Dickmann (2008), Seismic investigations of the Piora Basin using *S*-wave conversions at the tunnel face of the Piora adit (Gotthard Base Tunnel), *Int. J. Rock Mech. Min. Sci.*, *45*(1), 86–93, doi:10.1016/j.ijrmms.2007.03.003.

Mair, J. A., and A. G. Green (1981), High-resolution seismic reflection profiles reveal fracture zones within a "homogeneous" granite batholith, *Nature*, *294*(5840), 439–442, doi:10.1038/294439a0.

Malehmir, A., and G. Bellefleur (2010), Reflection seismic imaging and physical properties of base-metal and associated iron deposits in the Bathurst mining camp, New Brunswick, Canada, *Ore Geol. Rev.*, *38*(4), 319–333, doi:10.1016/j.oregeorev.2010.08.002.

Malehmir, A., S. Wang, J. Lamminen, B. Brodic, M. Bastani, K. Vaittinen, C. Juhlin, and J. Place (2015a), Delineating structures controlling sandstone-hosted base-metal deposits using high-resolution multicomponent seismic and radio-magnetotelluric methods: A case study from northern Sweden, *Geophys. Prospect.*, *63*(4), 774–797, doi:10.1111/1365-2478.12238.

Malehmir, A., F. Zhang, M. Dehghannejad, E. Lundberg, C. Döse, O. Friberg, B. Brodic, J. Place, M. Svensson, and H. Möller (2015b), Planning of urban underground infrastructure using a broadband seismic landstreamer—Tomography results and uncertainty quantifications from a case study in southwestern Sweden, *Geophysics*, *80*(6), B177–B192, doi:10.1190/geo2015-0052.1.

Malehmir, A., S. Heinonen, M. Dehghannejad, P. Heino, G. Maries, F. Karell, M. Suikkanen, and A. Salo (2017), Landstreamer seismics and physical property measurements in the Siilinjärvi open-pit apatite (phosphate) mine, central Finland, *Geophysics*, *82*(2), B29–B48, doi:10.1190/geo2016-0443.1.

Martínez, K., and J. A. Mendoza (2011), Urban seismic site investigations for a new metro in central Copenhagen: Near surface imaging using reflection, refraction and VSP methods, *Phys. Chem. Earth Parts ABC*, *36*(16), 1228–1236, doi:10.1016/j.pce.2011.01.003.

Maurer, H., and A. G. Green (1997), Potential coordinate mislocations in crosshole tomography: Results from the Grimsel test site, Switzerland, *Geophysics*, *62*(6), 1696–1709, doi:10.1190/1.1444269.

Mavko, G., and A. Nur (1979), Wave attenuation in partially saturated rocks, *Geophysics*, *44*(2), 161–178, doi:10.1190/1.1440958.

Mavko, G., T. Mukerji, and J. Dvorkin (2009), *The Rock Physics Handbook: Tools for Seismic Analysis of Porous Media*, 511 pp., Cambridge Univ. Press, New York.

Melanson, D. M., D. J. White, C. Samson, G. Bellefleur, E. Schetselaar, and D. R. Schmitt (2015), Mode-converted volcanogenic massive sulphide ore lens reflections in vertical seismic profiles from Flin Flon, Manitoba, Canada: Mode-converted VMS ore lens reflections, *Geophys. Prospect.*, *63*(4), 849–860, doi:10.1111/1365-2478.12267.

Meléndez-Martínez, J., and D. R. Schmitt (2016), A comparative study of the anisotropic dynamic and static elastic moduli of unconventional reservoir shales: Implication for geomechanical investigations, *Geophysics*, *81*(3), D245–D261, doi:10.1190/geo2015-0427.1.

Mukerji, T., and G. Mavko (1994), Pore fluid effects on seismic velocity in anisotropic rocks, *Geophysics*, *59*(2), 233–244, doi:10.1190/1.1443585.

O'Connell, R. J., and B. Budiansky (1974), Seismic velocities in dry and saturated cracked solids, *J. Geophys. Res.*, *79*, 5412–5426, doi:10.1029/JB079i035p05412.

Paulsson, B., N. Cook, and T. McEvilly (1985), Elastic-wave velocities and attenuation in an underground granitic repository for nuclear waste, *Geophysics*, *50*(4), 551–570, doi:10.1190/1.1441932.

Place, J., A. Malehmir, K. Högdahl, C. Juhlin, and K. P. Nilsson (2015), Seismic characterization of the Grängesberg iron deposit and its mining-induced structures, central Sweden, *Interpretation*, *3*(3), SY41–SY56, doi:10.1190/INT-2014-0212.1.

Podvin, P., and I. Lecomte (1991), Finite difference computation of traveltimes in very contrasted velocity models: A massively parallel approach and its associated tools, *Geophys. J. Int.*, *105*(1), 271–284, doi:10.1111/j.1365-246X.1991.tb03461.x.

Pyrak-Nolte, L. J., L. R. Myer, and N. G. W. Cook (1990), Transmission of seismic waves across single natural fractures, *J. Geophys. Res.*, *95*, 8617–8638, doi:10.1029/JB095iB06p08617.

Rhén, I., G. Gustafson, R. Stanfors, and P. Wikberg (1997), *Äspö HRL–Geoscientific Evaluation 1997/5. Models Based on Site Characterization 1986–1995*, 428 pp., TR, Swedish Nuclear Waste Management Co. - SKB, Stockholm.

Ronczka, M., K. Hellman, T. Günther, R. Wisen, and T. Dahlin (2016), Electric resistivity and seismic refraction tomography, a challenging joint underwater survey at Äspö Hard Rock Laboratory, *Solid Earth Discuss.*, *1–22*, doi:10.5194/se-2016-157.

Rubino, J. G., and K. Holliger (2012), Seismic attenuation and velocity dispersion in heterogeneous partially saturated porous rocks: Mesoscopic effects and partial saturation, *Geophys. J. Int.*, *188*(3), 1088–1102, doi:10.1111/j.1365-246X.2011.05291.x.

Rydström, H., and L. Gereben (1989), *Seismic Refraction Survey on Äspö and Hålö*, 243 pp., PR, Swedish Nuclear Waste Management Co. - SKB, Stockholm.

Rønning, J. H. S., O. Kihle, J. O. Mogaard, and P. Walker (2003), *Simpevarp Site Investigation. Helicopter Borne Geophysics at Simpevarp, Oskarshamn, Sweden*, 287 pp., P, Swedish Nuclear Waste Management Co. - SKB, Stockholm.

Sheriff, R. (2002), *Encyclopedic Dictionary of Exploration Geophysics*, *Geophys. Ref. Ser.*, No. 1, 384 pp. Soc. of Explor. Geophys., Tulsa, Okla.

Siggins, A. F., and D. N. Dewhurst (2003), Saturation, pore pressure and effective stress from sandstone acoustic properties: Pore pressure and saturation in sandstones, *Geophys. Res. Lett.*, *30*(2), 1089, doi:10.1029/2002GL016143.

Sopher, D., C. Juhlin, F. Huang, M. Ivandic, and S. Lüth (2014), Quantitative assessment of seismic source performance: Feasibility of small and affordable seismic sources for long term monitoring at the Ketzin CO_2 storage site, Germany, *J. Appl. Geophys.*, *107*, 171–186, doi:10.1016/j.jappgeo.2014.05.016.

Stanfors, R., I. Rhén, E.-L. Tullborg, and P. Wikberg (1999), Overview of geological and hydrogeological conditions of the Äspö Hard Rock Laboratory site, *Appl. Geochem.*, *14*(7), 819–834.

Stephens, M. B. (2009), Synthesis of the bedrock geology in the Bergslagen region, Fennoscandian shield, south-central Sweden, Sveriges Geologiska Undersökning (SGU).

Stockwell, J. (1997), Free software in education: A case study of CWP/SU: Seismic Un*x, *Lead. Edge*, *16*(7), 1045–1050, doi:10.1190/1.1437723.

Thomsen, L. (1986), Weak elastic anisotropy, *Geophysics*, *51*(10), 1954–1966, doi:10.1190/1.1442051.

Thomsen, L. (2002), *Understanding Seismic Anisotropy in Exploration and Exploitation*, *Distinguished Instruct. Ser.*, No. 5, 252 pp., Soc. of Explor. Geophys. and Eur. Assoc. of Geosci. and Eng., Tulsa, Okla.

Toksöz, M., D. Johnston, and A. Timur (1979), Attenuation of seismic waves in dry and saturated rocks: I. Laboratory measurements, *Geophysics*, *44*(4), 681–690, doi:10.1190/1.1440969.

Tonn, R. (1991), The determination of the seismic quality factor Q from VSP data: A comparison of different computational methods, *Geophys. Prospect.*, *39*(1), 1–27.

Toverud, T., and B. Ursin (2005), Comparison of seismic attenuation models using zero-offset vertical seismic profiling (VSP) data, *Geophysics*, *70*(2), F17–F25, doi:10.1190/1.1884827.

Tryggvason, A., and N. Linde (2006), Local earthquake (LE) tomography with joint inversion for *P*- and *S*-wave velocities using structural constraints, *Geophys. Res. Lett.*, *33*, L07303, doi:10.1029/2005GL025485.

Tryggvason, A., S. T. Rögnvaldsson, and Ó. G. Flóvenz (2002), Three-dimensional imaging of the *P*- and *S*-wave velocity structure and earthquake locations beneath Southwest Iceland, *Geophys. J. Int.*, *151*(3), 848–866, doi:10.1046/j.1365-246X.2002.01812.x.

Wahlgren, C.-H., J. Hermanson, O. Forssberg, P. Curtis, H. Drake, and E.-L. Tullborg (2006), *Geological Description of Rock Domains and Deformation Zones in the Simpevarp and Laxemar Subareas*, 271 pp., R, Swedish Nuclear Waste Management Co. - SKB, Stockholm.

Wang, Y. (2008), *Seismic Inverse Q Filtering*, 248 pp., Blackwell, Malden, Mass.

Wang, X.-Q., A. Schubnel, J. Fortin, E. C. David, Y. Guéguen, and H.-K. Ge (2012), High Vp/Vs ratio: Saturated cracks or anisotropy effects?, *Geophys. Res. Lett.*, *39*, L11307, doi:10.1029/2012GL051742.

Worthington, M. H., and J. A. Hudson (2000), Fault properties from seismic *Q*, *Geophys. J. Int.*, *143*(3), 937–944, doi:10.1046/j.1365-246X.2000.00315.x.

Xu, C., and R. Stewart (2006), Seismic attenuation (*Q*) estimation from VSP data, CSEG National Convention, Extended Abstracts, pp. 268–277, Citeseer.

Yardley, G. S., and S. Crampin (1991), Extensive-dilatancy anisotropy: Relative information in VSPs and reflection surveys1, *Geophys. Prospect.*, *39*(3), 337–355.

Yordkayhun, S., A. Tryggvason, B. Norden, C. Juhlin, and B. Bergman (2009), 3D seismic traveltime tomography imaging of the shallow subsurface at the CO_2 SINK project site, Ketzin, Germany, *Geophysics*, *74*(1), G1–G15, doi:10.1190/1.3026553.

BeFo

Box 5501
SE-114 85 Stockholm

info@befoonline.org • www.befoonline.org
Visiting address: Storgatan 19, Stockholm

ISSN 1104-1773